2003

Resonance Two Photon Ionization Study of Binary Clusters of Styrene with Polar Molecules

Hatem Ahmed Mahmoud
Virginia Commonwealth University

Colleague of Humanities and Science
Virginia Commonwealth University

This is to certify that the Dissertation prepared by Hatem Ahmed Mahmoud entitled RESONANCE TWO PHOTON IONIZATION STUDY OF BINARY CLUSTERS OF STYRENE WITH POLAR MOLECULES has been approved by his committee as satisfactory completion of the dissertation requirement for the degree of Doctor of Philosophy

M. Samy El-Shall, Ph. D., Professor, Chemistry, VCU

Jim Terner, Ph. D., Professor, Chemistry, VCU

Raphael M. Ottenbrite, Ph. D., Professor, Chemistry, VCU

Purusottam Jena, Ph. D., Professor, Physics, VCU

Fred M. Hawkridge, Ph. D., Professor, Chemistry, VCU

Stephen D. Gottfredson, Ph. D., Dean of Humanities and Science, VCU

Dr. F. Douglas Boudinot, Dean of the School of Graduate Studies

Date

RESONANCE TWO PHOTON IONIZATION STUDY OF BINARY CLUSTERS OF STYRENE WITH POLAR MOLECULES

A Dissertation submitted in partial fulfillment of the requirements for the degree of doctor of philosophy at Virginia Commonwealth University.

by

HATEM AHMED MAHMOUD
Bachelor of Science, South Valley University, Sohag, Egypt, 1989
Master of Science, South Valley University, Sohag, Egypt, 1994

Director: M. SAMY EL-SHALL
Professor, Department of Chemistry

Virginia Commonwealth University
Richmond, Virginia
May 2004

Table of Contents

List of Tables

Page

List of Figures

Page

Abstract

RESONANCE TWO PHOTON IONIZATION STUDY OF BINARY CLUSTERS OF STYRENE WITH POLAR MOLECULES

By Hatem Ahmed Mahmoud, Ph. D.

A Dissertation submitted in partial fulfillment of the requirements for the degree of Doctor of Philosophy at Virginia Commonwealth University.

Virginia Commonwealth University, 2004

Major Director: M. Samy El-Shall
Professor, Department of Chemistry

One-color resonance two-photo ionization (R2PI) spectra of mixed clusters of styrene molecule (S) with polar molecules [water (W), methanol (M), ethanol (E), and trifuoroethanol (T)] were measured through the $S_1 \leftarrow S_0$ transition of the styrene molecule. The spectra reveal a rapid increase in complexity with the number of polar molecules in the cluster, associated with van der Waal modes and isomeric forms. The spectral shifts of the cluster origins from the S_1-S_0 transition of the bare styrene molecule reflect the nature of the intermolecular interactions within the binary clusters. The obtained R2PI spectra

were compared with the spectra of the analogous benzene containing clusters. The styrene-water and the styrene-methanol complexes exhibited very different spectral shifts and structures as compared to the benzene-water and benzene-methanol complexes, respectively. The favorable interactions of polar molecules with the olefin group of styrene may explain the strong inhibition effects of exerted by small concentrations of water and alcohols on the cationic polymerization of styrene. Size-specified intracluster proton transfer reactions were observed for mixed clusters of styrene dimer with water, methanol and ethanol molecules. It was proposed that the polar molecules tend to aggregate around the olefin center, which promotes the transfer of the charge from the propagating chain to the hydrogen-bonded polar molecules subcluster. The minimum number of polar molecules required for a proton transfer to take place exothermically depends on the proton affinity of the polar molecules subcluster. The estimated upper limit value for the proton affinity of styrene dimer radical was evaluated based on the energetic of the proton transfer reaction to be ≤ 220.4 kcal/mol. No intracluster reaction was observed for styrene-trifluoroethanol (ST_n) system. In order to provide a comparison between the styrene and benzene systems, the benzene-ethanol (BE_n) and benzene-trifluoroethanol (BT_n) clusters were studied by using the R2PI technique via the 6_0^1 transition of the benzene molecule. Both dissociative electron transfer and dissociative proton transfer reactions were observed within the BE_n clusters, where n = 2 and 3, respectively. Proton transfer reactions were observed following dissociative electron transfer reactions within the (BT_n) clusters, where n = 4, to generate the protonated clusters (H^+T_n).

Chapter 1 Introduction

A molecular level understanding of the solvent effects in chemical reactions requires detailed knowledge of solute-solvent interactions including the size dependence of the spectral shifts and the evolution of intermolecular mode frequencies.[1-4] Gas phase molecular clusters provide models for such interactions since the size effect and the degree of complexity of the interaction potentials can be systematically varied in well-defined systems.[5-10] The influence of stepwise solvation on both the ground and the excited electronic states of a solute molecule can be probed by studying molecular clusters composed of a single ”solute” molecule and selected numbers of “solvent” molecules. The solvent molecules can be chosen in such a way to present a wide range of intermolecular interactions which may result in small perturbations of the electronic states of the solute molecule or in large changes in the structure and electronic properties such as those associated with charge-transfer and excimer interactions. Such studies have been advanced by the development of powerful techniques, which enables one to isolate ultracold clusters containing a “solute” chromophore and selected numbers of “solvent” molecules. Among these techniques, Resonant Two- Photon Ionization (R2PI) has been extensively used as a selective spectroscopic tool for the study of molecular clusters of various sizes and compositions.[6-26]

The study of molecular clusters of varying sizes and compositions constitutes an active and fascinating area of research. These clusters provide microscopic models for a molecular level understanding of a variety of important condensed phase phenomena such as solvation, phase transitions, nucleation, microphase separation, polymerization reactions, protein folding, and molecular recognition.[2, 3, 5-10, 27]

Binary clusters composed of a non-polar aromatic center and polar or hydrogen-bonded solvent molecules represent an important class of molecular clusters. Several examples of these clusters have been investigated in recent years using combinations of spectroscopic and theoretical techniques.[6-10] The majority of the work has been focused on benzene in the presence of various polar and hydrogen bonding molecules.[6-10, 20-23, 25, 28-32] For example, extensive studies have been conducted on the benzene-water (BW_n) and benzene-methanol (BM_n) clusters using spectroscopic techniques such as Resonant Two- Photon Ionization (R2PI), hole burning, and resonant ion-dip infrared spectroscopy. [10, 20-23, 25, 28, 29, 33, 34] These studies have established several characteristic features of the intermolecular interactions between aromatic π-systems and hydrogen bonded solvent molecules. Among these features are (a) the blue spectral shifts in small clusters, which seem to increase with increasing hydrogen bonding ability of the solvent molecules, (b) the gradual switch to red shifts in larger clusters, (c) the tendency of the solvent molecules to form a hydrogen bonding network in a one-sided structural type with the benzene ring, and (d) the very efficient fragmentation of the photoionized clusters, which has been interpreted as a direct consequence of the hydrogen bonding to the benzene

ring.[10] For a complete understanding of these systems, it is desirable to study other aromatic systems, including in which an additional π-interaction site is available.

Styrene is the simplest molecule that contains an unsaturated group covalently linked to an aromatic ring, and therefore represents a model system for studying the interactions between different π-systems with H-bonded molecules such as water and methanol. The unsaturated side chain provides an additional site for π-interaction with polar molecules that competes with the aromatic ring. These interactions are relevant to a wide variety of chemical, photochemical and biological processes in several fields such as photoconductivity, light induced charge and electron transfer reactions, and polymer chemistry.[1-3, 27, 35, 36] Styrene polymerization is among the most extensively studied polymerization process and continues to attract interest. The molecule is known to undergo polymerization in bulk monomer or in solution by free radical, cationic and anionic mechanisms.[37, 38] The thermally-initiated gas phase polymerization has been demonstrated and efforts to achieve a molecular level understanding of the various processes taking place during the polymerization continue to increase the potential of designing novel polymeric materials with unusual advanced properties.

In condensed phases, the crucial role played by trace amounts of water and other protic impurities on the mechanism and rate of polymerization in styrene is widely recognized. Under very dry conditions, radiation-induced polymerization of the bulk monomer proceeds rapidly [38, 39], but under "wet" conditions ($[H_2O] > 10^{-3}$ M) polymerization proceeds more slowly.[39] Small amounts of methanol are also known to suppress polymerization and enhance dimerization in styrene.[40]

The particular systems of interest in the present study consist of a single styrene molecule (S) and several solvent molecules: water (W), methanol (M), ethanol (E), and trifuoroethanol (T). These systems have never been studied before. The study of styrene-water (SW_n), styrene-methanol (SM_n), styrene-ethanol (SE_n), and styrene-trifluoroethanol (ST_n) clusters can provide information on the interactions involved in these systems and a greater a molecular level understanding of the retardation and inhibition effects of water and alcohols on the polymerization of styrene. The addition of the first few solvent molecules to the styrene molecule provides information on the preferred solvent sites and their relative strengths. The addition of further molecules yields information on solvent cooperative effects, coordination, and formation of solvent shells around the reactive monomer species. Like water, alcohol can participate in relatively weak hydrogen bonding to the π-system of styrene. However, the presences of the alkyl and fluoroalkyl groups provide favorable sites for hydrophobic interactions with the π-system of styrene. Detailed knowledge of these interactions is a prerequisite for a molecular level understanding of the retardation, inhibition and solvation effects of water and alcohols on the polymerization of styrene.

In order to provide a comparison between the styrene and benzene systems, we also study the benzene-ethanol, BE_n, and benzene-trifluoroethanol, BT_n, clusters. Again, these cluster systems have not been studied before.

The work described in this thesis is presented in five chapters. In chapter 2, a review of the spectroscopy of benzene and benzene-containing clusters is provided. In addition, the spectroscopy of the styrene molecule is presented and discussed. Chapter 3

deals with the experimental methods used in this research, which include cluster beam, time-of-flight mass spectrometry (TOF), resonant enhanced multiphoton ionization (REMPI) and non-resonance multiphoton ionization (MPI). Chapter 4 includes the results of the REMPI studies of the SW_n, SM_n, SE_n, ST_n , BE_n and BT_n clusters. These results include both the spectroscopy of the neutral clusters and the reactions observed following the ionization of the clusters. In Chapter 5, we present the overall conclusions from these studies.

Chapter 2 Literature Survey

2.1 The Spectroscopy of Styrene and Styrene Containing Clusters

The 288 nm $\tilde{A} - \tilde{X}$ absorption spectra of styrene and styrene-β-D_2 were recorded by Hollas et al.[41] The spectra resembled that of $\tilde{A} - \tilde{X}$ systems of aniline, phenol, chlorobenzene and ethynylbenezene and indicated that the $\tilde{A} - \tilde{X}$ excitation involved primarily the benzene ring with some participation from the ethylene group. They reported that no vibrational evidence was found to support the proposal by Hui and Rice[42] that the CH_2-group is perpendicular to the plane of the rest of the molecule (see Figure 1). The C(1)-C(α) torsional vibration (ν_{42}) was found to be strongly mixed in the $\tilde{A}$ state with ν_{41}, out-of-plane vibration. The 0_0^0 band of styrene-β-D_2 exhibited a small blue shift of $+19\ cm^{-1}$ from that of styrene, which is incompatible with such configuration. The cross-sequence $41_0^1 42_1^0$, $41_0^2 42_2^0$, … in the X state was stronger than the sequence 42_1^1, 42_2^2, … The values for the separation of the first three levels of ν_{42} in X state was deduced and were in disagreement with those obtained from Raman spectrum in the liquid phase.[43] The problem of torsional potential function for ν_{42} remained unsolved until the single vibronic level (SVL) spectra of styrene following laser excitation into 0_0^0 band were recorded by Hollas and Ridley[44]. Also, they were recorded SVL spectra following laser excitation

into more bands of the styrene $\tilde{A}-\tilde{X}$ system.[45] Interpretation of those spectra led to many new assignments and reassignment of $41_0^1\,42_0^1$ which was previously assigned to 40_0^2. The normal coordinates of ν_{41} and ν_{42} were found to be heavily mixed in the excited state A. Again no spectroscopic evidence was found to support the configuration of Hui and Rice.[42]

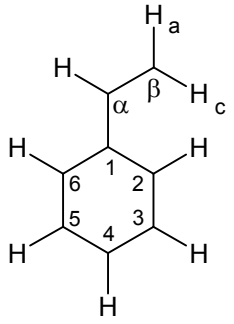

Figure 1: The atom numbering convention for styrene.

Zewail et al[46] were studied the excitation and dispersed fluorescence spectra for the $\tilde{A}^1A'\leftarrow\tilde{X}^1A'$ transition of jet-cooled styrene. Although the obtained frequencies were in good agreement with Hollas and co-workers[41], their studies revealed new features of the mode structure and coupling for styrene in the absence of spectral congestion and sequence bands present in the previous bulb work. The excess energy and intramolecular vibrational redistribution were discussed in relevance to the dynamics of photoisomerization. The results of these studies were in support of planner configuration with significant rate of isomerization at low excess energies. The barrier to isomerization in the excited state $\tilde{A}$ was estimated to be larger than that of t-stilbene (≈ 1200 cm^{-1}).

The binding energy of jet-cooled styrene-Ar cluster was determined by using resonant two-photon ionization.[47] The spectral shift of STY-Ar relative to the 0_0^0 band of $^1B_2 \leftarrow ^1A_1$ of bare styrene was found to be -30 cm^{-1}. The main feature in the R2PI spectra of STY-Ar was the disappearance of electronic vibrational transitions at excess vibrational energy E_v>410 cm^{-1} with respect to the 0_0^0 origin of styrene. This result was attributed to the vibrational predissociation on the $^1B_2$ potential surface. The lower and upper limits for the dissociation energy in the excited state were determined from the R2PI spectra of STY-Ar. The dissociation energy D($^1B_2$) of STY-Ar was estimated to be 426±16 cm^{-1}. Since the spectral shift δν corresponded to the extra stabilization of STY-Ar, the value of the dissociation energy in the ground state was thus; D($^1A_2$) = D($^1B_2$) - δν = 396±16 cm^{-1}. This value was in good agreement with the calculated value of benzene-Ar complex [48] (D = 366± cm^{-1}). The first adiabatic ionization energies of styrene (STY), phenylacetylene (PA), styrene-argon (STY-Ar) and phenylacetylene-argon (PA-Ar) were measured using (1+1') resonance enhanced multiphoton ionization (REMPI) threshold photoelectron spectroscopy (TES) technique as 68,267± 5, 71,175±5, 68,151±5, and 71,027±5 cm^{-1}, respectively[49]. By this technique a specific molecule can be selected by tuning the excitation laser (frequency ω_1) to a resonant excited state and then ionizing from that state with a second laser (frequency ω_2). The threshold electrons were collected by applying a delayed pulsed field extraction as ω_2 was scanned. So, the photoelectron spectrum was obtained for the molecule in a chosen vibrational level of its excited state and the sum of the laser frequencies ($\omega_1+\omega_2$) represents the energy axis of the spectrum. Ionization from a

particular S_1 mode enhanced the intensity of the photoelectron spectrum and vibrational assignment of this structure could be achieved if the assignment of the vibronic level was already known. This was done for three modes in both styrene and phenylacetylene and the obtained ionic vibrational frequencies were compared with those known for S_0 and S_1 states.

RE2PI spectra were recorded for styrene-Ar_n clusters (n = 2,3) and for 4-fluorostyrene-Ar_n clusters (n = 2-5).[50] The 0_0^0 electronic origins of STY-Ar, STY-Ar_2 and STY-Ar_3 were red shifted by 30, 63 and 33 cm^{-1}, respectively, with respect to the 0_0^0 band of styrene. It was important to notice that the additive rule governs for STY-Ar_n clusters. Therefore, the structure of STY-Ar_2 was believed to be (1+1) adduct. On the other hand, two possible structures could explain the red shifted origin for STY-Ar_3 by 33 cm^{-1} which was nearly the same for STY-Ar; the first was a (3+0) adduct and the second was a (2+1) adduct with the argon atom that caused the blue shift attached to the other side of the styrene molecule. The trend in the R2PI spectra for 4-FSTY-Ar_n clusters was very similar to that for STY-Ar_n clusters. Broad-band and multi-structured spectra were observed starting from 4FSTY-Ar_2. These observations were attributed to different isomeric structures, with argon atom tied to one or both sides of the aromatic ring. The quantum calculations of the van der Waals vibrational frequencies for mono-Ar complexes matched with the observed spectrum for 4-FSTY-Ar.

In a recent study[51], the one-color REMPI of styrene-Ar_n, n = 4-12, were reported. The spectra of these clusters exhibited a single band, red shifted from the styrene origin transition by 24-37 cm^{-1}.

2.2 The spectroscopy of Benzene and Benzene Containing Clusters

The vibronic spectroscopy of benzene has received comprehensive studies. Moreover, the electronic structure of benzene is one of the most important polyatomic structures in the modern structural chemistry. The recent developed in the experimental techniques has resolved many of outstanding problems in benzene spectroscopy such as; the mechanism of vibronic coupling in π E_{2g} singlet state, the absence of $\sigma \rightarrow \pi^*$ or $\pi \rightarrow \sigma^*$ transitions, the absence of *n*s Rydberg transitions and, the nature of rapid radiationless process above the origin of the first transition "channel three".

The vibrational pattern of an electronic excitation consists of two components; the vibronically induced component and the Frank-Condon component. Frank-Condon component forms progressions added to the vibronic inducing modes and possibly to the vibrationless origin. The analyses of vibrational pattern gave more information about the structure of the molecule in the excited state.[52]

2.2.1 The Spectroscopy of Benzene

Spears and Rice[53] were studied the lifetime of 22 vibronic states of benzene and the relative quantum yield of SVL fluorescence for transitions from these states. The data showed the dependence of radiative and nonradiative lifetimes on excess vibrational energy and on vibrational symmetry type. The nonradiative lifetime τ_{nr} decreased as the

number of vibrational quanta increases in the prepared stats. The rate of change of τ_{nr} per quantum of vibrational energy was almost the same for all vibrational modes. They found that the nonradiative rate constants increased linearly with increasing vibrational energy for the 6^n1^m and 1^n levels. They found a pressure dependence of the observed lifetime to a lower pressure limit of 0.006 torr, which was due to hard-core collision of benzene.

Schuyler et al[54, 55] analyzed the SVL fluorescence spectra of benzene vapor in the $^1B_{2u}$ state. The fluorescence spectra were found to be in good agreement with Herzberg-Teller description of the $^1B_{2u}$-$^1A_{1g}$ vibronically induced transition. A single first-order Herzberg-Teller selection rule described the dominant feature in every obtained SVL spectrum. Higher order Herzberg-Teller selection rules provided a consistent account for minor fluorescence structure. Qualitative agreement was found between observed and Herzberg-Teller predicted fluorescence band intensities. The relative intensities in ν_1 progressions of the types 1_n^o, 1_n^1 and 1_n^2 were qualitatively different, and each matches the approximate Frank-Condon calculations. Four new vibrational frequencies in the $^1B_{2u}$ state were located: $\nu_{4'} = 365$ cm^{-1}, $\nu_{5'} = 749$ cm^{-1}, $\nu_{9'} = 1148$ cm^{-1} and $\nu_{17'} = 712$ cm^{-1}. Six bands were found among the prominent structure in $^1B_{2u}$-$^1A_{1g}$ absorption spectrum.[55] The absorption spectrum and SVL fluorescence spectra showed that a set of 12 vibrations was responsible for most the structure in $^1B_{2u}$-$^1A_{1g}$ radiative transitions. The “active” vibrations encompassed six of the ten vibrational symmetry species. Each vibration in these six species was “active”.

The MPI spectrum of benzene was first reported by Johnson.[56, 57] A low-lying state of benzene was observed at 391 nm, which had not been previously seen, in the three-photon ionization spectrum. This new state was an allowed two-photon state of probable symmetry $^1E_{1g}$ or $^1E_{2g}$. The three-photon Rydberg structure was found to be similar to the one-photon absorption spectrum. This similarity indicated a strong $^1A_{1g}$ component in the two-photon virtual state in agreement with the two-photon vibronic structure of the $^1B_{2u}$ state, which was also strongly $^1A_{1g}$.

Schlag et al[58] reported the two-photon excitation spectra of benzene and benzene-d_6 in the gas phase with a high power tunable laser. The two-photon inducing modes ν_{14}, ν_{15} (b_{2u} symmetry) and ν_{18} (e_{1u} symmetry) were determined experimentally by new technique based on the zero point level of S_1 state of benzene. The hot band spectrum was assigned from these transitions. The two strongest inducing modes in the excited state were found to be the ν_{14} mode (b_{2u} symmetry) and the ν_{18} mode (e_{1u} symmetry). The frequency of the ν_{14} showed a strong blue shift by 257 cm^{-1} in the excited state. The ν_{19} was found to be extremely weak or absent in disagreement with the theoretical predictions.

The absorption spectra of benzene-h_6 and benzene-d_6 were measured photoelectrically.[59] The data were in consistent with Frank-Condon factors predicted on the basis of Herzberg-Teller theory for a C-C change in the range 0.032 to 0.035 Å. The relative intensities for a large number of progressions showed small deviations from prediction and not all of which could be assigned to Fermi resonance.

The resonance enhanced multiphoton ionization and fragmentation of benzene beam in mass spectrometer were reported by Bernstein et al.[60, 61] The fragmentation

pattern of benzene ion, corresponding to m-photon ionization and two-photon excitation, were measured near 391 nm. Increasing the laser pulse peak energy increased the average number of photon absorbed per molecule and thus the extent of fragmentation. However, the ionization and the fragmentation were found to be wavelength dependence even at the highest laser peak power intensities. Under strong focusing conditions, C^+ ion was the most abundant ion indicating the absorption of at least 9 photons per molecule during the 6 ns laser pulse.

Atkinson and Parmenter studied the 260 nm absorption of benzene. They were re-measured the positions and intensities of most band maxima in the $^1B_{2u}$-$^1A_{1g}$ transition of benzene vapor[62] at 300 K. They examined the role of vibrational angular momentum, vibrational degeneracies and the selection rules in the 260 nm absorption spectrum of benzene[63]. They developed a new parameter, χ, which can be used to obtain the rotational band contour of any vibronic component transition. Maxima were sorted into ν_1 progressions and then most of these progressions assigned to first-, second-, and third order Herzberg-Teller transitions[64]. Third-order transitions were found to be few in number with intensities that comparable to those of second-order transitions. New nine fundamentals in the $^1B_{2u}$ state and two in the $^1A_{1g}$ state were specified.

The FL spectrum of free jet benzene at a rotational temperature of 0.3 K was studied.[65] The band contour of rotationally cooled benzene displayed well-resolved single rovibronic transitions in contrast with the band contour obtained for a room temperature sample.[66] The derived rotational and Coriolis constants were in agreement

with those derived from room temperature band contour analyses. It was found that more than 95% of all benzene molecules were in the lowest possible rovibronic level.

Two time delayed laser pulses of different frequencies were used to study the mechanism of multiphoton ionization and fragmentation of jet cooled benzene.[67] Data showed that the mechanism of multiphoton ionization of benzene includes two different energy states. First, the neutral molecules absorbed photons until the ionization potential was reached. Then ions were formed with little excess energy. Photoexcitation of these cold ions to states with higher excess energy produced fragmentation.

Johnson et al[68] studied R2PI of benzene-h_6 and benzene-d_6 The effect of channel three[69], which was the increase in the radiationless rates in the S_1 state of benzene when the vibrational excess energy exceeded about 3000 cm^{-1}, was followed 3000 cm^{-1} past the fluorescence region. Under rotationally cooled conditions, a new progression in C_6H_6 spectrum was revealed next to the $14_0^1 1_0^n$ progression (n = 1-5). Also, new and well-resolved structure was obtained for C_6D_6 as the $14_0^1 1_0^n$ progression was followed.

Benzene, aniline, N,N-dimethyl and 2,4-dimethyl aniline were studied by resonance enhanced laser ionization mass spectrometry under collision free conditions.[70] At lower laser intensities, these molecules showed efficient R2PI producing entirely the parent ion. At higher laser intensities, extensive fragmentation was produced by R3PI or R4PI. For benzene, the fragmentation pattern showed $C_3H_3^+$, $C_4H_2^+$, $C_5H_3^+$ and $C_6H_6^+$ peaks. All of these ionic fragments were observed in conventional electron impact spectra.

The cross section for ionization of $^1B_2$ excited state in benzene and aniline were found to be equal and independent of the wavelength in the range 250-300 nm.

The $^1B_{2u}$ transition of benzene at room temperature was very congested. The rotational envelopes were broad and it was hard to resolve the rotational band because of Doppler broadening. Using Doppler free two-photon FL spectroscopy Schlag and co-workers[71] resolved a part of one rotational band. In this study, it was difficult to determine the band origin. By using supersonic molecular beam, most of the rotational envelope was eliminated providing accurate assignment of band origins. Johnson et al[72] obtained the $^1B_{2u}$-$^1A_{1g}$ two-photon spectra of several isotopes of benzene using supersonic beam-multiphoton ionization spectroscopy. New assignments and reassignments were introduced especially in transitions concerning the ν_{12} vibration. Also, they measured the isotope shifts due to naturally occurring C^{13} in benzene and perdeuterated benzene. New feature due to benzene dimmers was revealed in all the deuterium isotopes.

An extensive investigation of the single vibronic level fluorescence spectroscopy of jet-cooled benzene was carried out by Rice co-workers.[73] The intramolecular energy transfer in the $^1B_{2u}$ of benzene was investigated. The most important result was the assignment of the 8^1_0 transition. The assignment for ν_8 in the $^1B_{2u}$ state led to new assignments involving the activity in ν_{18} and ν_4; one-photon transitions involving the e_{1u} mode ν_{18} were observed and, two new progressions involving activity of the b_{2g} mode ν_4 were recognized. Several spectroscopic controversies of the $^1B_{2u}$-$^1A_{1g}$ spectra of benzene were resolved. The spectral simplification accomplished by using supersonic expansion

allowed measurements of the lifetimes of several vibrational levels in $^1B_{2u}$ benzene.[74] Non-exponential fluorescence decays were observed from vibrational levels near the "channel three" region.

Smalley et al[16] obtained the $S_1 \leftarrow S_o$ spectrum of $(benzene)_n$, where n=2-4, in a supersonic beam using 2C-R2PI technique. Weakly induced 0_0^0 transitions red shifted from the forbidden 0_0^0 of benzene were observed for all clusters. The red shifts were –40, -115, and –149 cm^{-1} from the monomer origin for the dimer, trimer, and the tetramer, respectively. The splitting of the 0_0^0 band was found to be less than 6 cm^{-1} for all the clusters. The trimer and teramer showed strong vdW progressions. The fluorescence measurement data showed that the dimer rearrange from the T-shaped structure into sandwich excimer with net D_{6h} symmetry within several picosecond after laser excitation.

Levy et al[75] reported the $^1B_{2u}$-$^1A_{1g}$ ultraviolet spectra of benzene clusters. Sharp features were observed in the fluorescence excitation spectrum for dimers, trimers and tetramers. The dispersed fluorescence spectra of the trimer showed identical structures from excitation of 6^1 and 0^0 levels.

2.2.2 Spectroscopy of Benzene Containing Clusters:

The spectral shift of the cluster's origin with respect to the rare benzene gives a direct measure of the relative binding energies of the cluster in the ground and excited states, S_0 and S_1 respectively. This shift is known as solvent shift. The electronic frequency shifts for most benzene-$(solvent)_n$ clusters are on the order of a few hundred wavenumber. The solvent can induce transitions that are forbidden in the bare benzene molecule. For

example, the 0_0^0 transition is electronic dipole forbidden in the absence of external perturbations. If the solvent bounds to benzene in such a way to reduce the sixfold symmetry of benzene to lower than threefold symmetric, the 0_0^0 transition becomes allowed. Therefore, studying of the vibrations that gain intensity upon clustering can be used as a probe for the symmetry and structure of benzene-X complexes.

2.2.2.1 Benzene-Rare Gas Clusters:

The benzene-rare gas clusters have been the subject of numerous experiments and several theoretical studies. Shown in Table 1 are the spectral shifts of benzene-rare gas clusters relative to the 6_0^1 transition of bare benzene molecule. Illustrated in Figure 2 is the dependence of the spectral shift of benzene-rare gas clusters on the polarizability of the rare gas. One-sided benzene-Ar_n clusters (n=1-7) showed ideal size dependence on the spectral shift as shown in Figure 3.

Table 1: Collective data for benzene-rare gas binary clusters.

Bz-R	Shift, cm^{-1}, 6_0^1	Ionization potential, ev	References
He	2.30	21.56454	[65]
Ar	-21.0	15.759	[76]
Kr	-33.397	13.99961	[77]
Xe	-53.666	12.12987	[77]

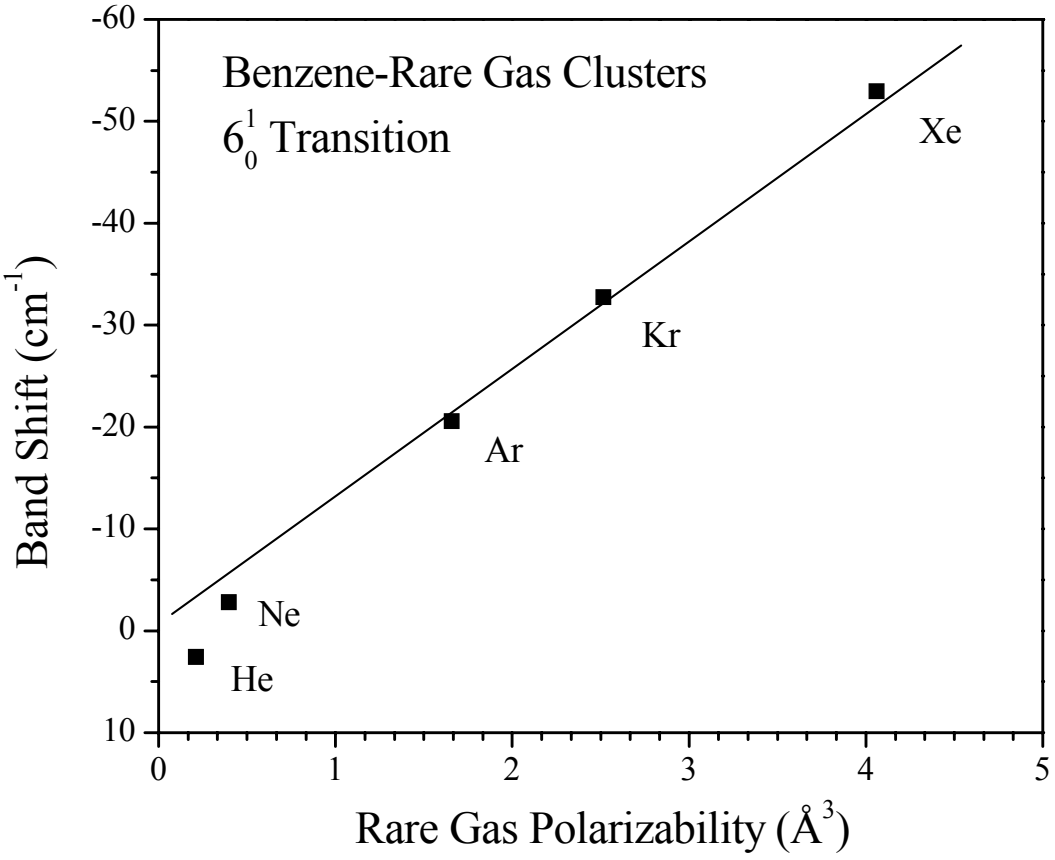

Figure 2: Spectral shift of the band as a function of the rare gas polarizability of the measured benzene-rare gas complexes. (Adapted from reference [77])

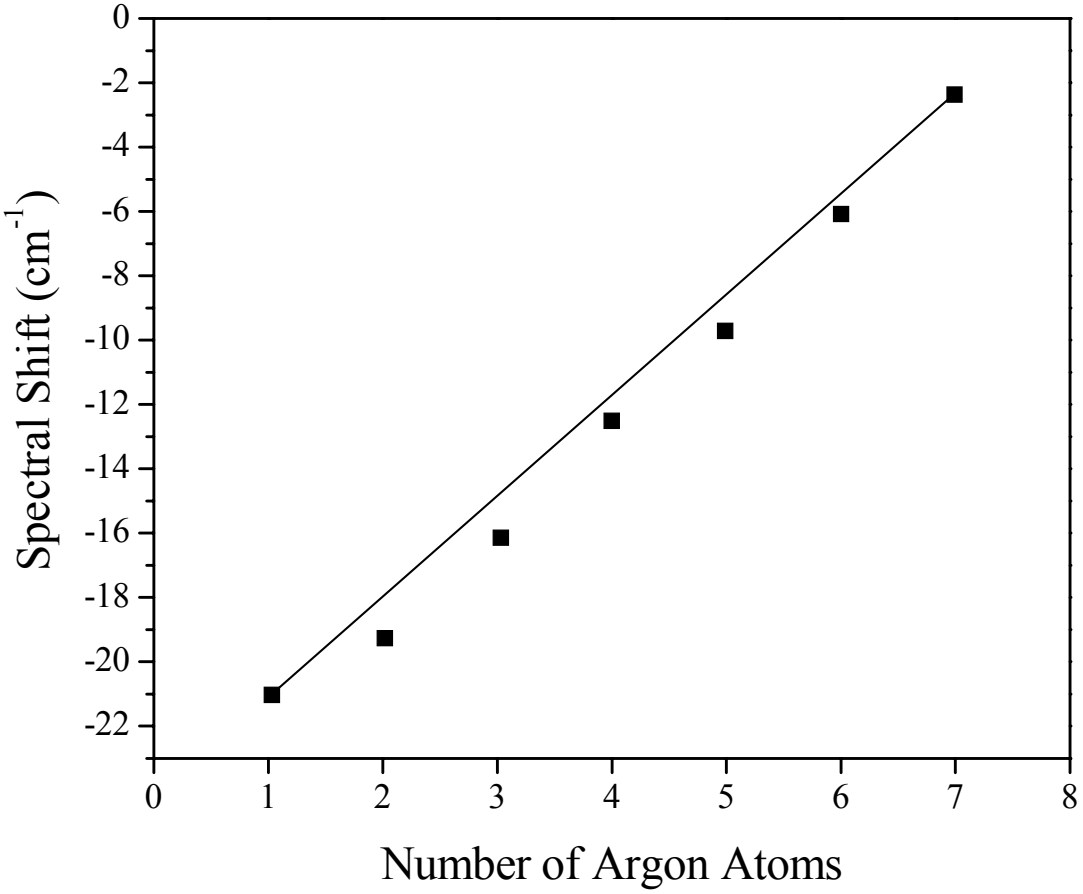

Figure 3: Size dependence of the spectral shift of the one-sided Bz-Ar_n clusters (where n=1-7). (Adapted from reference [76])

2.2.2.2 Benzene-Nonpolar Molecule and Benzene-Polar Molecules Clusters

The collective data for benzene-nonpolar molecule and benzene-polar molecule binary clusters are given in Table 2 and Table 3, respectively.

Table 2: Collective data for benzene-nonpolar molecule binary clusters.

Bz-X	Shift, cm^{-1} 6_0^1	Binding energy, cm^{-1}	Dipole moment[78], Debye	Ionization potential, ev	Polarizability 10^{-25} cm^3	References
C_2H_2	-127		0	11.40		[79]
C_3H_8	-72.0	1044	0.084	10.94		[80]
CCl_4	-68	839-1119	0	8.11	105	[21], [81],[82]
C_2H_6	-57(I) - 51(II)	778	0	11.52		[80]
Cyclohexane	-47		0	9.88		[83]
C_6H_6	-43/-39		0	9.24	103	[31]
CD_4	-41.2	540	0	10.53		[26]
CH_4	-41	599	0	12.61	26.0	[84]
SF_6	-11.5		0	15.32		[85], [86]
N_2	-6.8	-501	0	15.581	17.6	[87], [88]
CO_2	4	-868	0	13.78	26.5	[87], [88]
CF_4	6.1		0	10.14		[26]

Table 3: Collective data for benzene-polar molecule binary clusters.

Bz-X	Shift, cm^{-1} 6_0^1	Binding energy, cm^{-1}	Dipole moment, Debye	Ionization potential, ev	Polarizability 10^{-25} cm^3	References
NH_3	-25	-677	1.47	10.07	23.0	[89], [15]
CO	-16	-612	0.112	14.01	19.5	[87], [88]
CH_3Cl	8	524-1189	1.87	11.37	45.3	[21],[81],[82]
CH_3CN	37.6	559.4	3.9	12.20		[90], [31]
CH_3OH	44		1.70	10.84	32.0	[25], [91]
H_2O	52	559-1468	1.85	12.62	14.8	[21], [81],[82]
HCl	125.1	629-1329	1.08	12.74	26.0	[21], [81],[82]
DCl	132.5		1.084	12.76		[20]
CH_3COOH	152		1.74	10.65		[30]
$HCCl_3$	179	699-1608	1.01	11.37	85.0	[21], [81],[82]

Chapter 3 Experimental

3.1 Cluster Beam Apparatus

The generation of clusters involved the expansion of a gas from a high-pressure source (stagnant pressure) through a narrow hole into an expansion chamber of lower pressure. The thermal energy in the high-pressure source is converted into a directed velocity u as the gas expands. If Cp is the heat capacity of the expanding gas at source temperature T_S, the energy balance of an ideal gas of molecular weight m is given by:

$$C_P T_S = C_P T_B + mu^2/2 \qquad \text{Eq. 3-1}$$

Where T_B is the beam temperature. Since $mu^2/2$ is positive, T_B is lower than the source temperature T_S. So the adiabatic gas expansion provides cooling of gas molecules, which promotes clustering. The expansion of the gas into a collision free region (a few nozzle diameters) creates a directed motion of the gas. This directed motion provides cooling in the vibrational, rotational and translational temperatures. The quenched temperatures are in the order $T_{vib}>T_{rot}>T_{trans}$. The liberation of latent heat of condensation during the clustering increases the internal temperature of the clusters. However, collisions with an inert gas provide cooling of the internal temperature of the clusters.[92]

The cluster beam apparatus consists of two cubic chambers connected by a tube (Figure 5). The chambers are isolated through a conical skimmer orifice (1 mm or 3 mm). The first chamber (expansion or jet chamber) is used mainly for the generation of clusters

and the second chamber (beam chamber) houses the TOF mass spectrometer. The expansion chamber is pumped by a diffusion pump (Varian VHS-6, pumping speed = 3000 l/s in He), achieving a background pressure of 10^{-7}-10^{-8} Torr, and a working pressure of ≈ $5x10^{-5}$ Torr when the nozzle is operated with a backing pressure of 10^{2}-$5x10^{3}$ Torr. The beam chamber is pumping by a diffusion pump (Varian VHS-6) equipped with nitrogen trap to condense the background gas, hence lowering the ultimate vacuum that can achieved (low 10^{-8} Torr). The background pressure of the beam chamber rises to ≈10^{-7} Torr when the nozzle is operated.

3.2 TOF Mass Spectrometry

The common configuration in TOFMS is the two-stage Wiley-McLaren configuration.[93] The principle of mass separation in this design relies on the ions being created at the same time and location within an electrostatic field. Then the ions are accelerated in an electrostatic field. The two-stage accelerating field consists of three parallel plates (Figure 5). The electrostatic field accelerates all ions into a field-free drift region with a kinetic energy of zV, where z is the ion charge and V is the applied voltage. Since the ion kinetic energy is $½mv^2$, lighter ions reach the detector at the end of drift region sooner than the heavier ions.

Focused laser beams are ideal for TOF ionization sources due to their short pulse width and small beam waist. The placement and overlap of the cluster and laser beams within the repeller and accelerator fields define the ionization region. However, since both laser and cluster beams have finite temporal and spatial widths, broadening occurs in the measured ion flight time distribution. The laser plus width is less than 10 ns, and therefore

the spatial effects are more significant than the temporal effects. The spatial distribution of ions results in a spread of ion kinetic energies since the ions are created with different potential energies (determined by the ion distance from the field). The space focus design reduces the broadening by creating ions within a differential positive field, and hence, focusing the ions. The focusing region is defined by the differential voltage between the repeller and accelerator fields ($\Delta V \approx 500$ V). The focused ions enter the second stage and are accelerated ($\Delta V \approx 4000$ V) and proceed to travel a field free region (≈ 110 cm) until detected by two-stage microchannel-plate detector. Two deflection plates (0-350 V) are placed in the free field region to correct the trajectories of ions.

The current output of the detector is amplified and then digitized by 500 MHz (LeCroy 9350A). In principle, a complete TOF mass spectrum can be obtained from a single ionization event, but in practice an average mass spectrum is from 50-1000 ionization events.

Pulsed adiabatic expansion of a sample seeded into an inert carrier gas was employed to generate the neutral clusters. A vapor of mixture sample was expanded through a conical nozzle (200 or 500 μm diameter) in pulses of 300-550 μs duration at a repetition rate of 8-20 Hz into an evacuated chamber at $\approx 10^{-5}$ Torr. The jet was skimmed and passed into a high vacuum chamber, which is maintained at $2x10^{-7}$-$8x10^{-8}$ Torr. The collimated cluster beam passed into the ionization region of the TOF mass spectrometer where it intersects the laser beam. A XeCl excimer pumped dye laser combination (Lambda Physik LPX-101 and FL3002) was used to provide tunable light for

photoionization of clusters. Coumarin 540A (Exciton; λ_{range}= 513-612 nm) and coumarin 307 (Lambda Physik; λ_{range}= 485-546 nm) were used with β-BaB_2O_4 crystal (CSK Co.) to generate a tunable frequency-doubled output of 10^{-8} s pulses for styrene and benzene clusters systems, respectively. The spatially ultraviolet radiation (using a set of four quartz Pellin-Broca prisms) of average pulse energies 0.1-0.3 mj per pulse was shaped with a 3 cm lens to provide 1-2 mm^2 beam in the ionization region.

3.3 Resonant Enhanced Multiphoton Ionization REMPI

In the REMPI process, the neutral molecule or cluster in the ground electronic state is excited to an intermediate state by absorbing a resonant *m*-photon. The presence of a resonant intermediate state enhances the probability of ionization. Absorbing of one or more *n*-photon ionizes the molecule. This resonant ionization process is labeled (*m*+*n*)R(*m*+*n*)PI or 1C-R(*m*+*n*)PI for one-color photoionization scheme and (*m*+*n*′)R(*m*+*n*′)PI or 2C-R(*m*+*n*′)PI for two-color photoionization scheme (Figure 4). The combination of REMPI, supersonic beam and mass-selective TOF spectrometry provides a powerful spectroscopic technique.

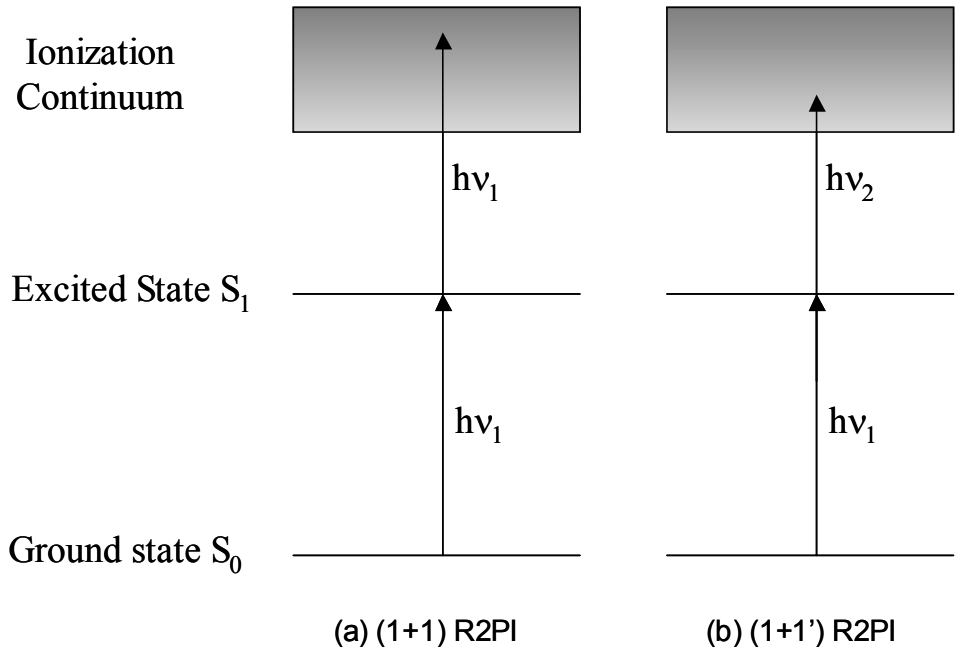

Figure 4: (a) One-color photoinoization scheme or (1+1)R2PI or 1C-R2PI. (b) two-color photoionization shceme or (1+1´)R2PI or 2C-R2PI.

3.4 Multiphoton Ionization MPI

The process at which two or more photons are absorbed in concerted interaction with individual atoms or molecules is called "multiphoton". The cluster beam was prepared as previously described above. The ionization was accomplished by absorbing photons of monochromatic light. The MPI was achieved by one of the folllowing laser: ArF (193 nm) provided by excimer laser (Lambda Physik COMPex 102).

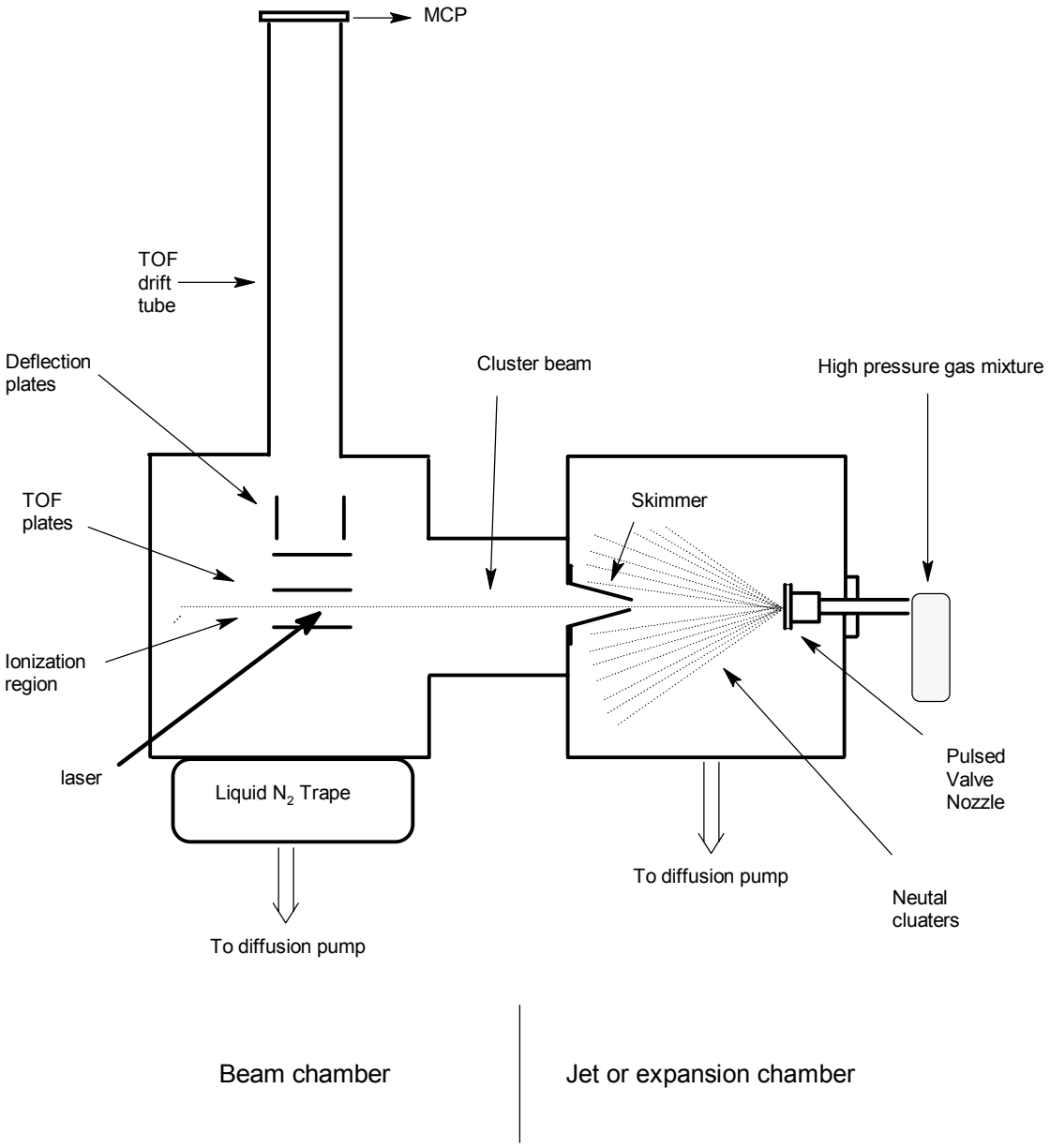

Figure 5: Schematic representation of the cluster beam apparatus combined with the TOF mass spectrometer.

Chapter 4 Results and Discussion

4.1 Styrene Spectroscopy of Clusters

Displayed in Figure 6 are the R2PI spectra obtained by monitoring the mass channel corresponding to styrene (S) in the 0_0^0 region between 34,730 and 35,820 cm^{-1}. The spectrum in the bottom panel shows the 0_0^0 origin, the overtone band 41_0^2 and the vibronic band 29_0^1 as well as the cross sequence bands $41_0^1 42_0^1$ between the ν_{42} and ν_{41} modes (ethylene group torsional rotation and out-of-plane bend, respectively) and $40_0^1 41_0^1$. The middle panel shows strong activities of three vibronic bands (28_0^1, 27_0^1 and 26_0^1), two overtone bands (42_0^2 and 40_0^2) and three cross-sequence bands ($29_0^1 41_0^1 42_0^1$, $41_0^2 42_0^2$ and $28_0^1 29_0^1$). The spectrum region in the top panel shows seven fundamental vibrations (ν_{19}-ν_{25}). The vibration modes ν_{19}, ν_{20}, ν_{21} and ν_{23} were attributed to in plane C-H bending vibrations, while the vibration mode ν_{19} corresponds to $-CH_2$ rocking vibration. The spectrum is in good agreement ($\pm$ 0.7 cm^{-1}) with previous fluorescence excitation study by Zewail et al.[46] The relative frequencies and intensities obtained from this work together with data obtained by Zewail et al [46] are tabulated in Table 4.

The styrene 0_0^0 band obtained by monitoring the mass channels corresponding to C_8H_8, $^{13}CC_7H_8$ and $^{13}C_2C_6H_8$ [zero, one and two ^{13}C isotopes in C_8H_8, m/z = 104, 105 and

106; respectively] (Figure 7). The replacement of one and two ^{12}C with ^{13}C atoms results in small blue shifts of the 0_0^0 band by 2.5 and 5 cm^{-1} in the spectra, respectively. Similarly, the shift of the 0_0^0 can also be induced by the clustering of atoms or molecules around the styrene molecule.

Shown in Figure 8 is the R2PI spectra of $(styrene)_n$ clusters, where n = 1-4, in the $S_1 \leftarrow S_0$ 0_0^0 band region of styrene monomer. The R2PI excitation spectrum of styrene dimer, S_2, exhibits a broad red-shifted band with several spectral features on the base line. These features are reproducible under various expansion conditions and tabulated in Table 5. The red-most peak at –252.4 cm^{-1} may be the origin of S_2. The fragmentations from higher styrene clusters greatly contribute to the broadening in the R2PI spectrum of styrene dimer. The spectra of trimer, S_3, and tetramer, S_4, show unresolvable and broad bands with maximum red shifted by –107 cm^{-1} ahead from the origin of styrene monomer. The obtained mass spectrum at this maximum is displayed in Figure 9. The red spectral shifts by the styrene clusters are due the intramolecular dispersion forces within these clusters.

A typical mass spectrum obtained following the multiphoton ionization of styrene clusters produced by 193 nm is displayed in Figure 10. The MPI mass spectrum of styrene clusters illustrates an enhanced intensity for S_2 with a distinguished even/odd alternation in the ion intensities, up to n = 10. Similar findings have been reported by our group using different laser wavelength (248 nm).[94] The styrene dimer cation ($C_{16}H_{16}^{+\cdot}$) is believed to possess covalently bonded structure.[37, 38, 94-96]

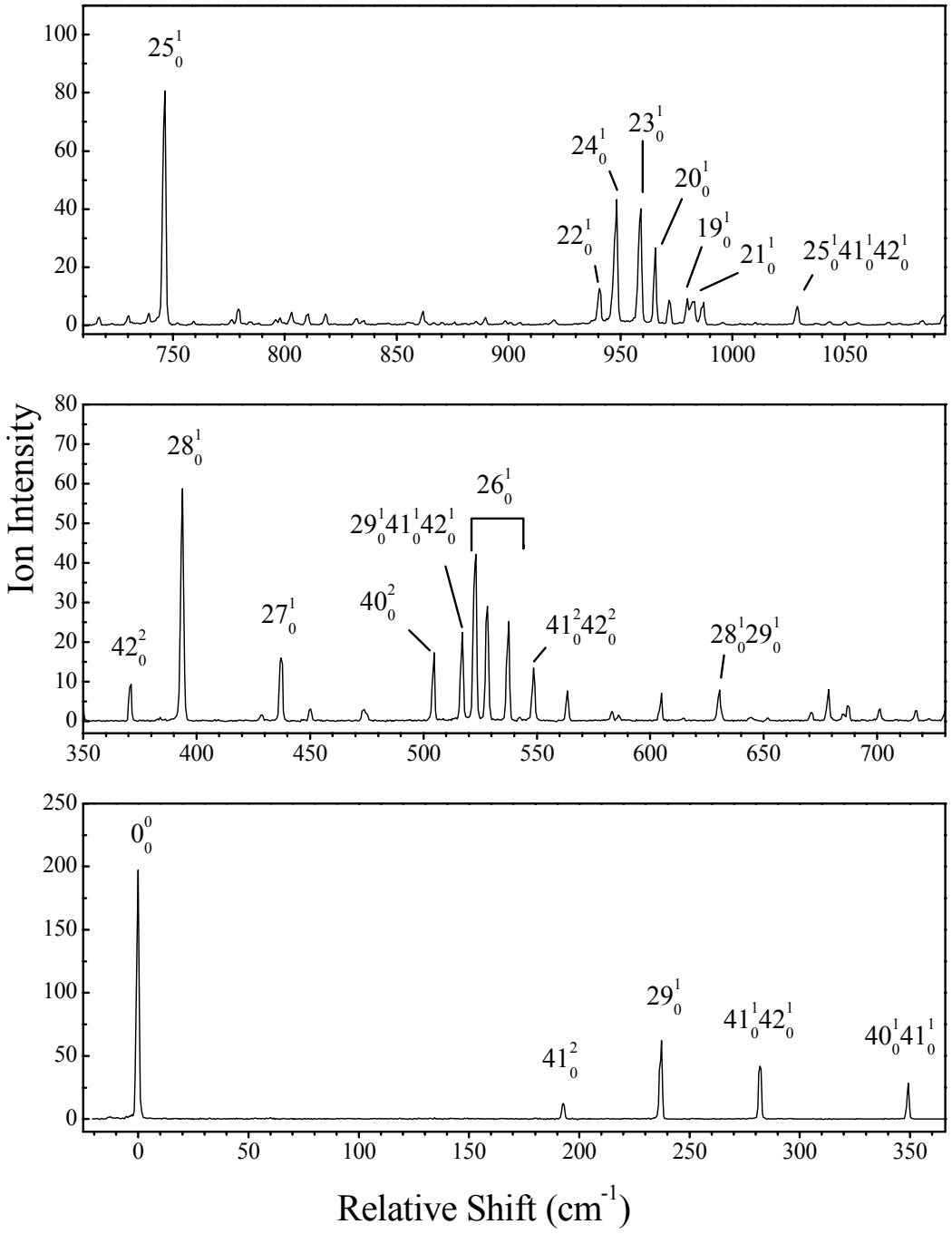

Figure 6: Three successive panels of the one-color R2PI spectrum of the jet-cooled styrene molecule in the supersonic expansion at He carrier gas (P = 100 psi). The relative shift is scaled with respect to the 0_0^0 transition at 34,758.79 cm^{-1}.

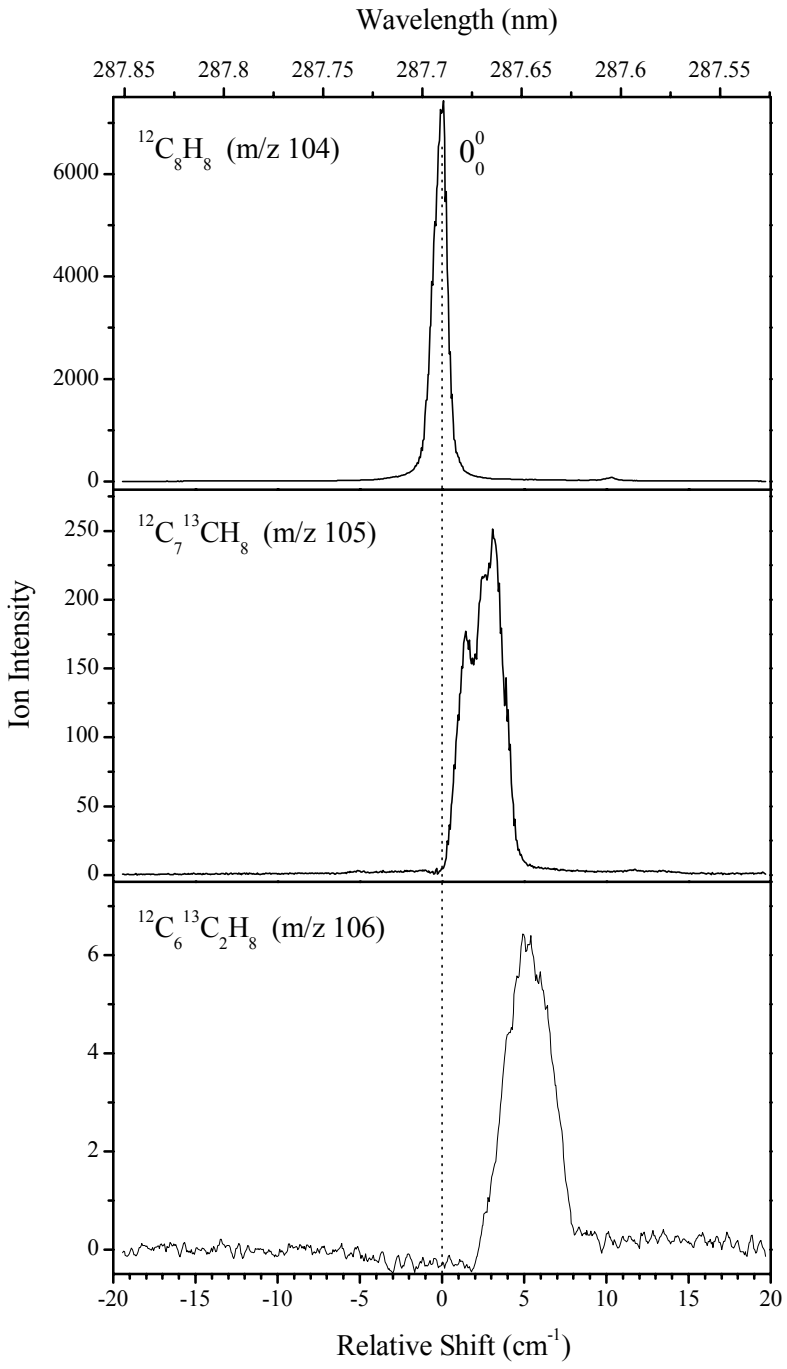

Figure 7: The effect of ^{13}C isotope substitution on the 0_0^0 band of styrene molecule.

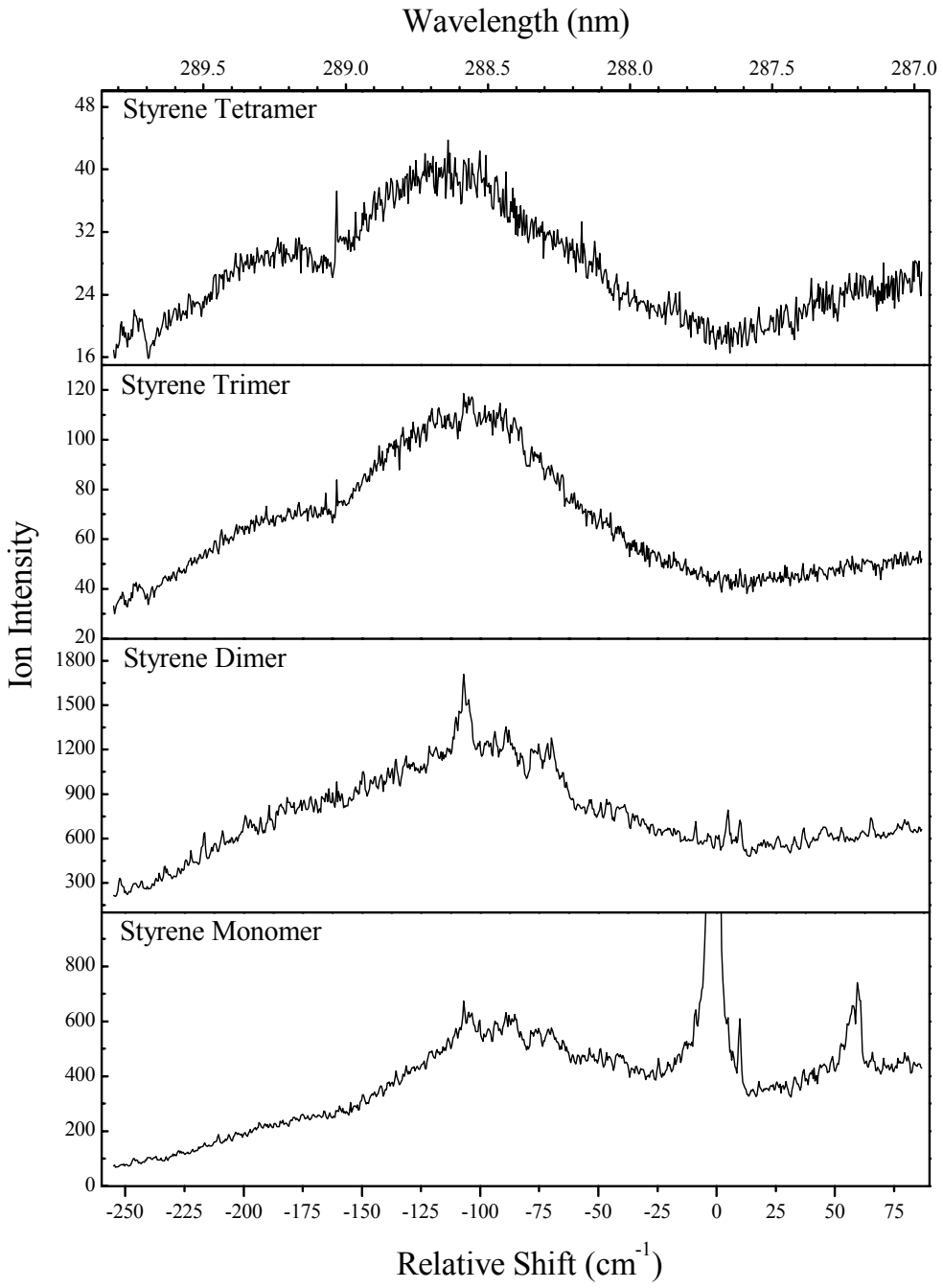

Figure 8: One-color R2PI measured in the $(styrene)_n$ mass channels, with (n = 1-4), [S, S_2, S_3 and S_4] relative to the electronic origin band of the $S_1 \leftarrow S_0$ transition of the styrene molecule at 34,758.79 cm^{-1}.

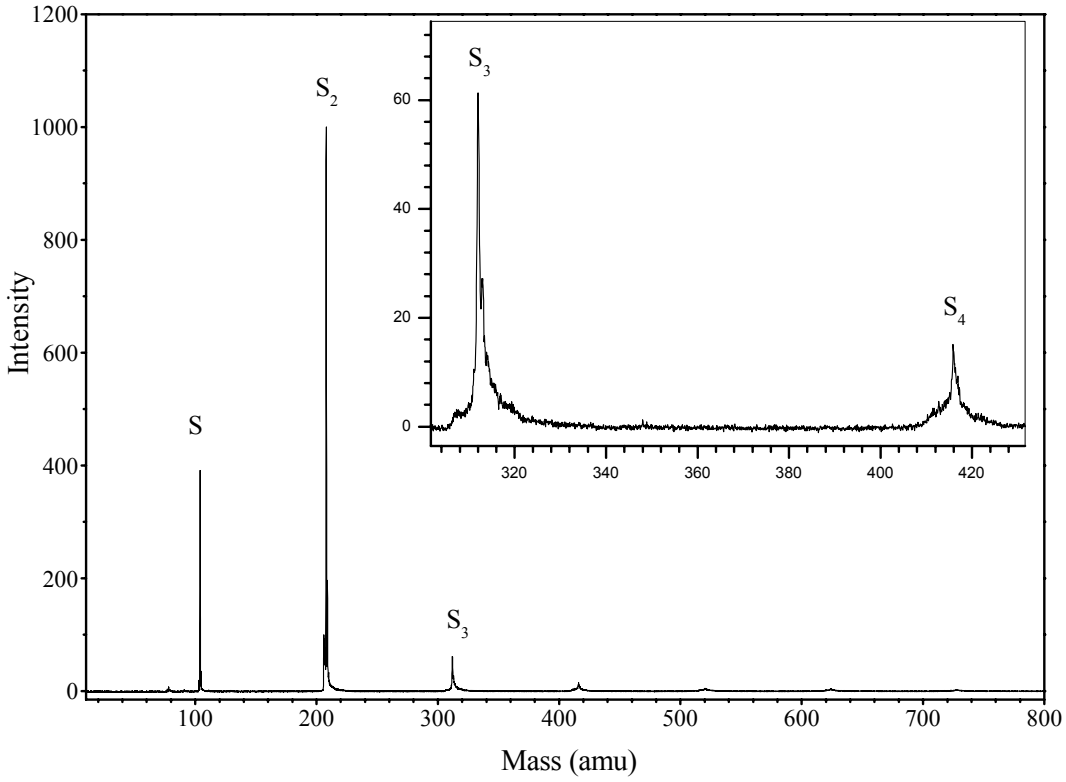

Figure 9: R2PI mass spectrum of the styrene cluster beam obtained at 288.577 nm.

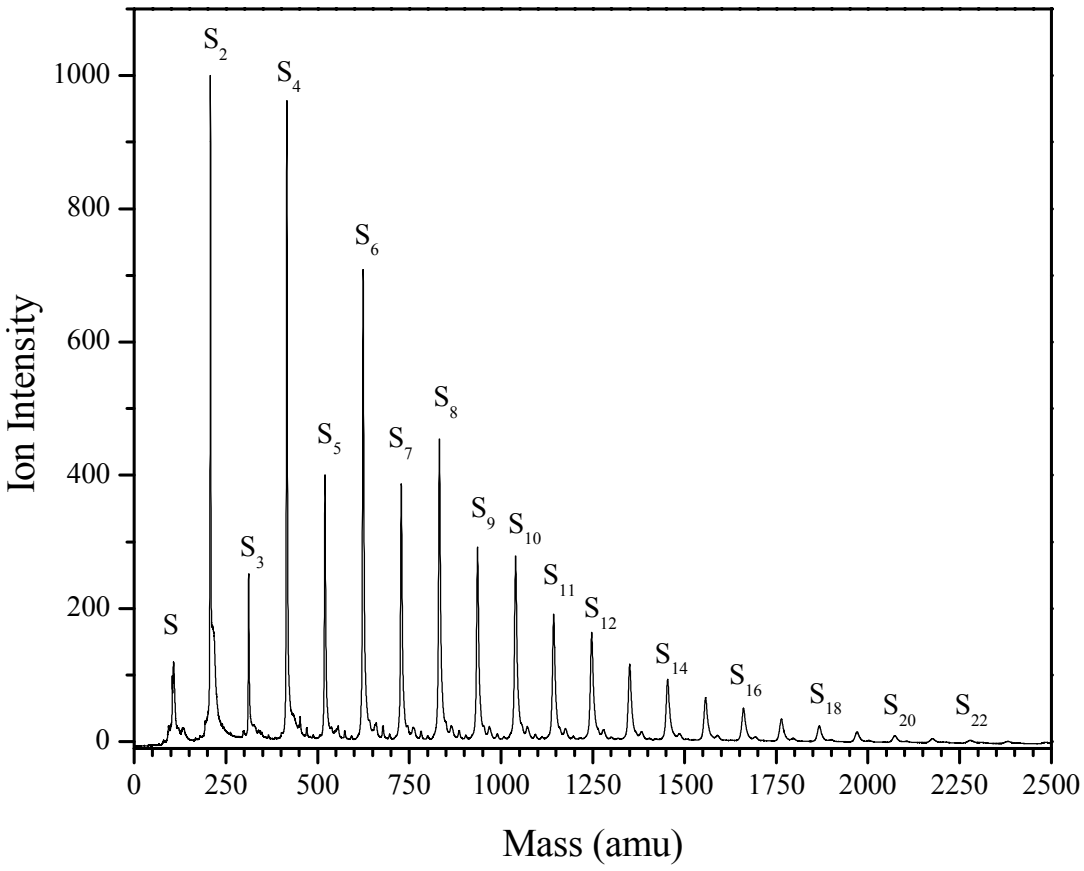

Figure 10: Multiphoton ionization mass spectrum of styrene cluster beam (S_n), n up to 22, obtained by using 193 nm excitation wavelength.

Table 4: Assignment of the R2PI spectrum of the jet-cooled styrene molecule.

Relative Shift (this work)	Relative Intensity (this work)	Relative Shift (Ref [46])	Relative Intensity (Ref [46])	Assignment (Ref [46])
0.0	100.0	0.0	100	0_0^0
60.0	0.6	59.5	0.6	$41_0^1 42_1^0$
192.8	6.3	193.2	0.9	41_0^2
237.3	31.4	237.2	8.9	29_0^1
282.0	21.2	282.4	9.3	$41_0^1 42_0^1$
349.3	14.4	349.1	4.0	$40_0^1 41_0^1$
371.0	4.7	371.0	0.8	42_0^2
393.7	29.8	394.5	9.6	28_0^1
437.3	8.1	437.1	2.0	27_0^1
504.8	8.8	505.5	0.6	40_0^2
517.2	11.4	517.5	0.6	$29_0^1 41_0^1 42_0^1$
523.2	21.4	523.2	4.6	
528.1	14.7	528.2	2.9	26_0^1
537.6	12.8	537.3	2.0	
563.5	3.9	563.6	0.2	$41_0^2 42_0^2$
630.5	4.0	630.0	0.3	$28_0^1 29_0^1$
678.6	4.0	678.7	0.3	$28_0^1 41_0^1 42_0^1$, $27_0^1 29_0^1$(?)
746.5	40.9	745.8	23.6	25_0^1
861.8	2.4	862.2	0.2	27_0^2, $28_0^1 29_0^2$(?)
940.6	6.5	940.4	3.4	22_0^1
948.3	21.9	947.8	22.6	24_0^1
959.0	20.4	959.1	22.8	23_0^1
965.6	13.5	965.1	8.3	20_0^1
979.9	4.7	980.7	3.1	19_0^1
982.0	4.2	983.0	3.0	21_0^1(?)

987.1	4.0	987.3	1.9	$25_0^1 29_0^1$(?)
1029.0	3.3	1029.2	1.7	$25_0^1 41_0^1 42_0^1$

Table 5: Spectral features observed in S_2 mass channel (S = styrene)

Relative Shift	Relative Intensity	Relative Shift	Relative Intensity
65.1	738	-141.8	1031
52.7	674	-144.3	1018
37.0	670	-149.4	1050
9.8	725	160.7	983
4.7	792	-164.0	935
-8.8	716	-169.5	863
-35.5	766	-171.6	882
-69.8	1280	-174.5	858
-71.5	1241	-181.7	878
-75.2	1240	-189.2	825
-82.8	1178	-193.0	743
-89.2	1354	-197.2	727
-93.8	1322	-199.3	755
-106.9	1709	-208.9	651
-110.3	1421	-216.5	639
-118.7	1217	-222.3	519
-121.6	1224	-224.4	456
-123.7	1104	-233.6	410
-131.3	1158	-252.4	330
-135.5	1136		

4.2 R2PI of Styrene-Water Clusters

4.2.1 R2PI spectra of styrene (water)$_n$ clusters, n=1-2

The R2PI spectra obtained by monitoring the mass channels corresponding to S, SW and SW_2 in the 0_0^0 region of the styrene monomer between 34,700 cm^{-1} and 34,900 cm^{-1} are presented in Figure 11. The electronic origin band of the $S_1 \leftarrow S_0$ transition of styrene is located at 34,758.79 cm^{-1}.[46, 97] The excitation spectrum obtained in the S mass channel shows the 0_0^0 origin and the vibronic band 42_0^2 as well as the cross–sequence band $41_0^1 42_0^1$ between the ν_{42} and ν_{41} modes (ethylene group torsional rotation and out-of-plane bend, respectively). The other small features shown in the spectrum of Figure 11 are due to hot bands (29_1^1 and 42_1^1). The spectrum is in very good agreement with previous fluorescence excitation and REMPI studies.[46, 98]

The SW mass channel has several strong features identical to the features that appear in the SW_2 channel. These features were assigned to the SW_2 cluster with a sharp origin peak blue shifted relative to the 0_0^0 of the styrene by 45.7 cm^{-1}. In addition, a week peak at 21.5 cm^{-1} was assigned to the origin of the SW complex. Two other small peaks at 25 and 35 were assigned to low frequency van der Waals (vdW) intermolecular vibrations of the SW complex. The SW^+ cluster ion fragments efficiently into the styrene channel as indicated by the significant intensity of the 21.5 cm^{-1} peak found in the S channel shown in Figure 11.

In contrast to the simplicity of the spectral features assigned to the SW complex, a very rich spectrum is observed in the SW_2 mass channel with all the features appearing in the SW channel as a result of efficient loss of a water molecule from the SW_2 cluster upon photoionization. The origin of the SW_2 cluster possesses two long progressions of bands assigned to the excitation of the intermolecular vibrational modes [the first progression appears at 73, 100, 125 and 148 cm^{-1} and the second progression corresponds to peaks at 80, 107, 133 and 156 cm^{-1}. The very rich intermolecular Franck-Condon activity of the SW_2 cluster indicates a large change in the geometry of the cluster following the electronic excitation of the cluster.

The tentative assignments of the SW and SW_2 origins are complicated by the efficient fragmentation of the ionized clusters as a direct result of the structural change between the neutral and the ionized cluster. As the cluster ion relaxed to a more stable structure, the relaxation energy released promotes fast evaporation of water molecules from the cluster. The effect of fast ion fragmentation can be clearly seen in Figure 12 and Figure 13, which display the mass spectra of the styrene/water clusters obtained at the resonance features assigned the SW and SW_2 cluster origins, respectively. It is clear that the ion intensity of the SW complex obtained at the origin of the SW_2 cluster is much higher than that obtained at the SW origin. Fragmentation probabilities for the SW^+ and SW_2^+ cluster ions were measured by comparing the absolute integrated intensities I_n at various mass channels (parent and daughter) at the same wavelength of an identified spectral resonance and normalizing to the sum over I_n. The results expressed as a percent of the parent ion intensity are shown in Table 7. Within the two photon's energy limit,

93% of the SW complex fragments into the styrene mass channel (S^+) upon photoionization. The fragmentation efficiency of the $SW_2^+ \rightarrow SW^+$ process is estimated as 63% from the origin peak and between 67%-73% from the vdW progressions. The SW_2^+ cluster ion also fragments into the S^+ mass channel by the loss of two water molecules (29% at the SW_2 origin at 45.7 cm^{-1}).

In order to support the assignments of the cluster origins, the dependence of the intensities of the spectral features assigned to the origins of the SW and SW_2 clusters on the water vapor concentration in the pre-expansion mixture was investigated. The results, shown in Figure 14, indicate that the peak at 45.7 cm^{-1} (assigned to the SW_2 origin) decreases much more rapidly with decreasing the water concentration as compared to the peak at 21.5 cm^{-1} (assigned to the SW origin). This behavior indicates that the two peaks must be due to different water containing clusters. The very weak dependence of the peak at 21.5 cm^{-1} and the strong dependence of the peak at 45.7 cm^{-1} on the water concentration support the assignments of these peaks to the SW and SW_2 clusters, respectively.

4.2.2 R2PI spectra of styrene (water)$_n$ clusters, n=3-5

The spectra detected at the mass channels of SW_3, SW_4 and SW_5 clusters are displayed in Figure 15. The origin of SW_3 is blue shifted by 64.2 cm^{-1} with respect to the 0_0^0 of styrene at 34,758.79 cm^{-1}. Two peaks at 84.7 and 106.1 cm^{-1} from the 0_0^0 of styrene were assigned the vdW progressions developed on the SW_3 origin. There are several other features present in the R2PI scan of the SW_3 mass channel as well as the main peaks described. The peaks at 31.8 and 77.3 cm^{-1} appear to be coming from the features of SW_5

mass channels. The other features in the SW_3 mass channels are not assigned. The R2PI mass spectrum obtained at the resonance wavelength of the SW_3 origin at 287.165 nm is shown in Figure 16.

The spectral shift reverses its direction for the origin band of SW_4 at 20.7 cm^{-1} as shown in the SW_4 mass channel in Figure 15. This observation suggests that the structure of SW_4 incorporates dispersion interaction between styrene molecule and water tetramer subcluster. Furthermore, this assumption is supported by the low fragmentation probability of SW_4^+ cluster ion into SW_3 mass channel (Table 7). Two van der Waals progressions were assigned to SW_4 at 39.7 and 58.1 cm^{-1} relative to the 0_0^0 band of styrene molecule (Table 6). The other spectral features at 31.8, 62.3 and 77.3 cm^{-1} in SW_4 mass channel have the same fingerprints of SW_5 cluster (Figure 15).

In SW_5 mass channel, three major spectral features were assigned to SW_5 neutral cluster. The 0_0^0 origin band of SW_5 was blue shifted at 31.8 cm^{-1} with respect to the $S_1 \leftarrow S_0$ transition of styrene molecule as shown in Figure 15. The built-in progressions of van der Waals modes are located at 62.3 and 77.3 cm^{-1}. The SW_5^+ cluster ion experiences considerable fragmentation efficiencies into SW_4 mass channel as shown in Table 7. The tentative assignments of the R2PI spectra of SW_n (n=1-5) clusters are listed in Table 6

The overall R2PI scan of styrene-$(water)_n$ clusters, where n = 1-5, is displayed on Figure 17. Figure 18 presents the observed spectral shifts of the styrene$(water)_n$ cluster origins, with respect to the 0_0^0 band of styrene molecule, as a function of of water molecules. The first three clusters of SW_n (n=1-3) showed linear increases in the direction

of spectral blue shift, with a maximum of 64.2 cm^{-1} for the SW_3 cluster. The shifts of SW_n (n = 1-3) clusters are consistent with H-bonding to the π-system of styrene.

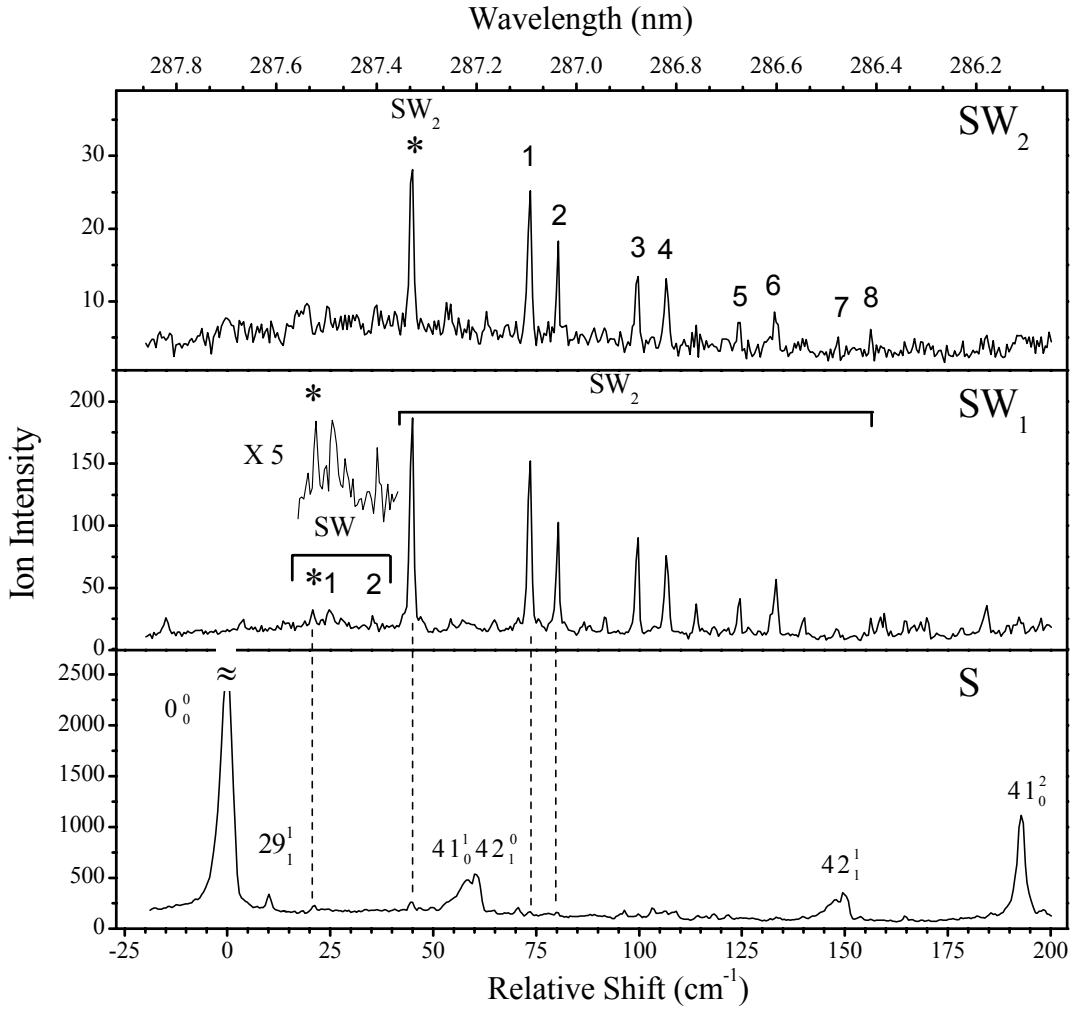

Figure 11: One-color R2PI spectra measured in the styrene mass channel [S] and styrene(water)$_n$ mass channels, with n = 1 and 2, [SW_1 and SW_2] relative to the electronic origin band of the $S_1 \leftarrow S_0$ transition of styrene at 34,758.79 cm^{-1}. In SW_1 and SW_2 mass channels, the origin of each cluster isomer is marked with (*) and the peaks labeled with numbers following each cluster's origin represent vdW bands associated with the cluster origin (see Table 6).

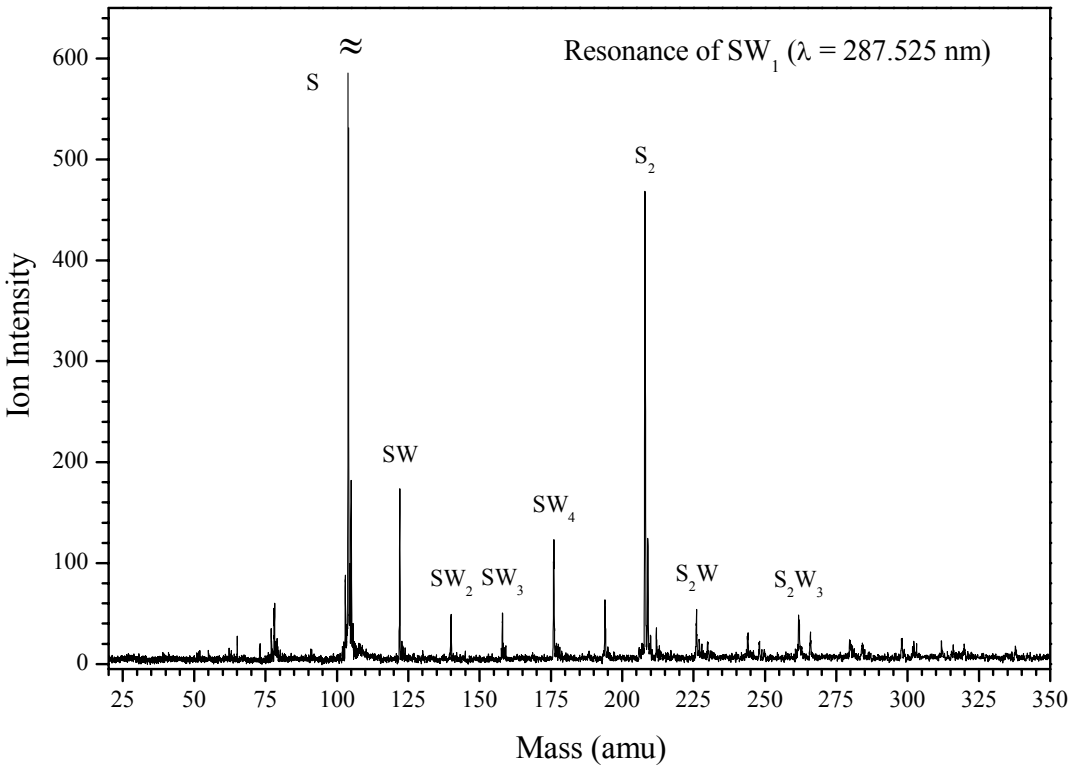

Figure 12: R2PI mass spectra of the styrene-water (SW_n) cluster beam obtained at the resonance ionization assigned to the origin of SW_1.

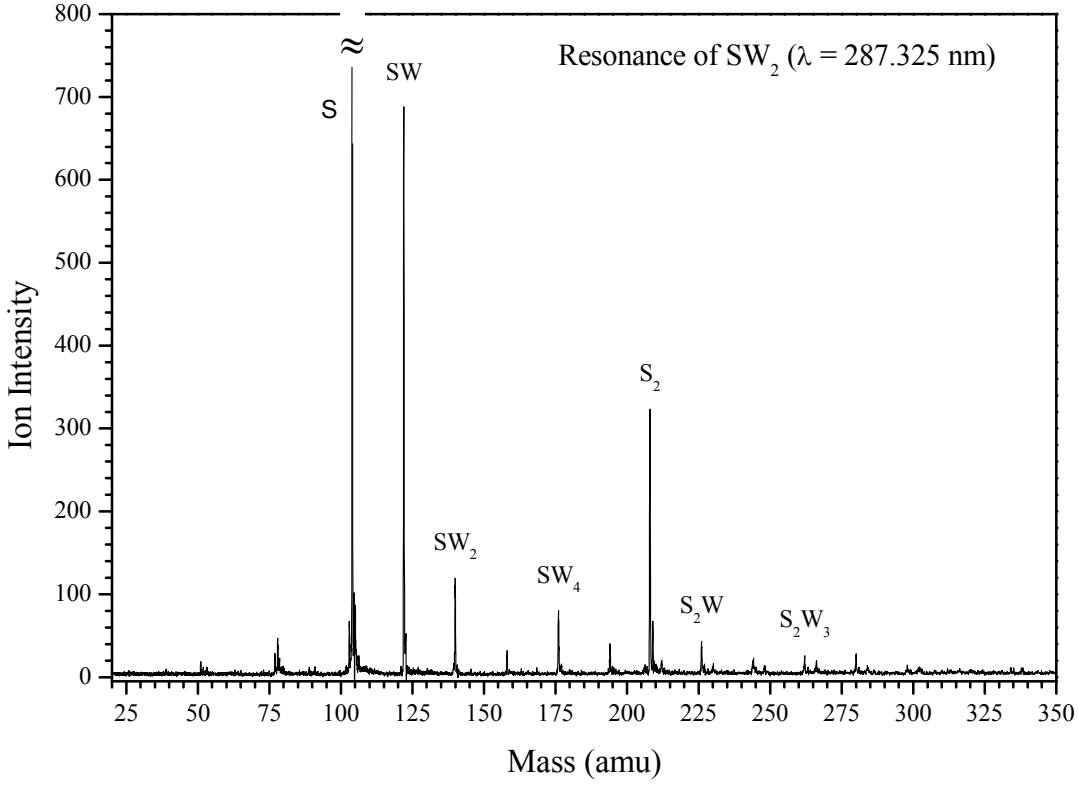

Figure 13: R2PI mass spectra of the styrene-water (SW_n) cluster beam obtained at the resonance ionization assigned to the origin of SW_2.

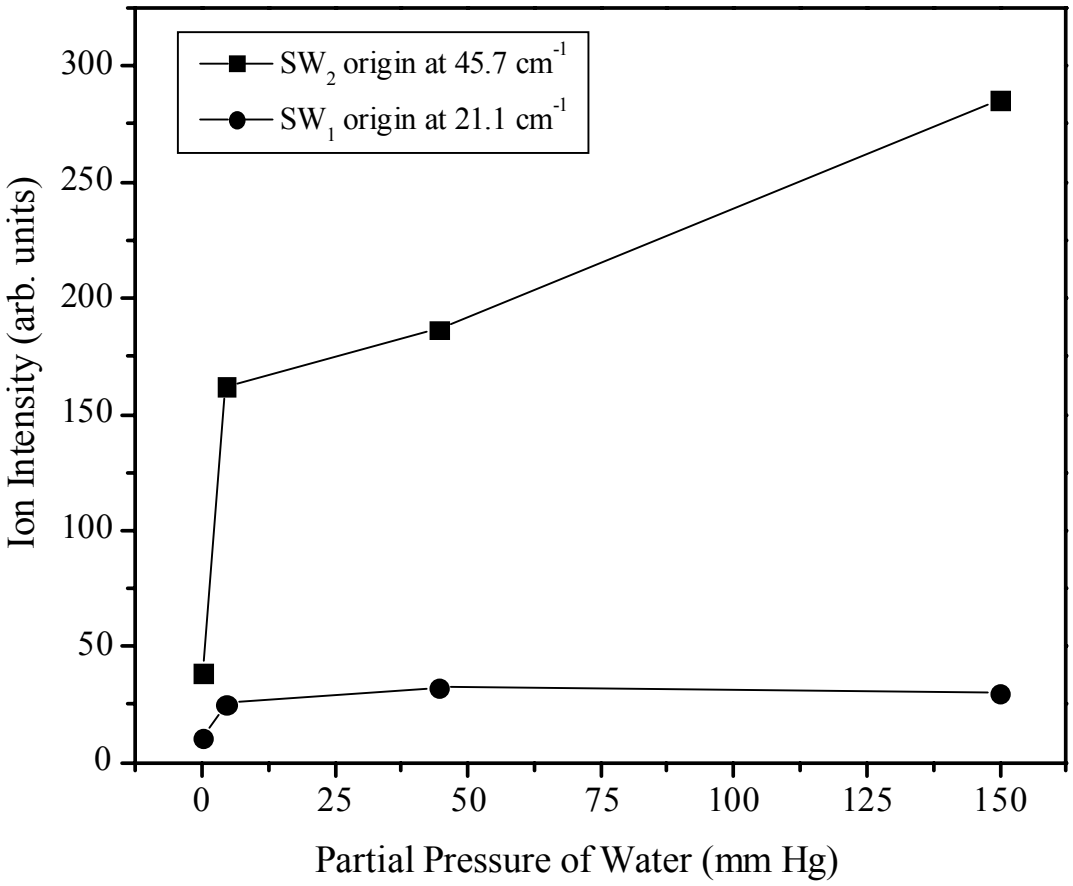

Figure 14: The dependence of the ion intensity assigned to the SW and SW_2 clusters on the water vapor pressure in the pre-expansion mixture. The plot points represent water vapor pressures of 0.005, 4.43, 44.56 and 149.97 mm Hg.

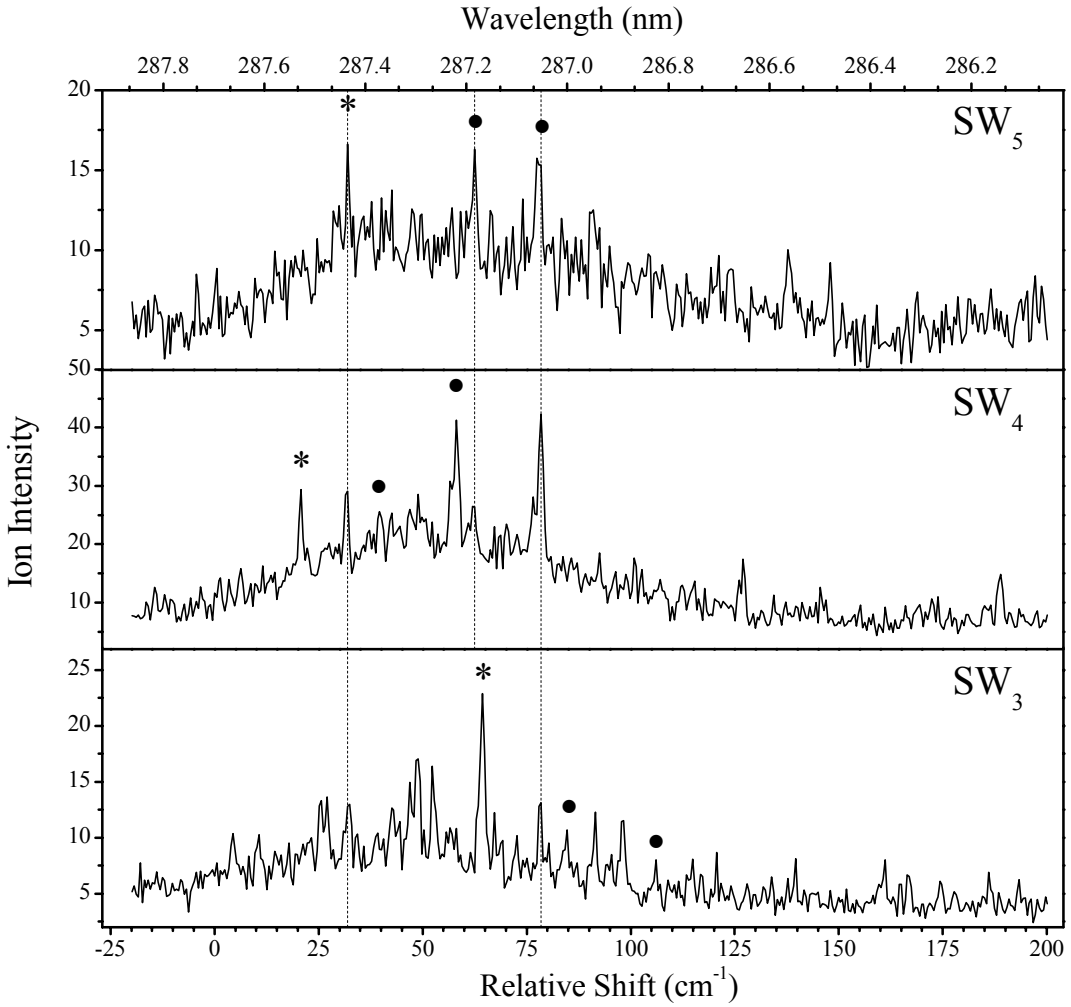

Figure 15: One-color R2PI spectra measured in the styrene(water)$_n$ mass channels, with n = 3-5, [SW_3, SW_4 and SW_5] relative to the electronic origin band of the $S_1 \leftarrow S_0$ transition of styrene at 34,758.79 cm^{-1}. The origin of each cluster isomer is marked with (*). The peaks labeled with symbols following each cluster's origin represent vdW bands associated with the cluster origin (see Table 6).

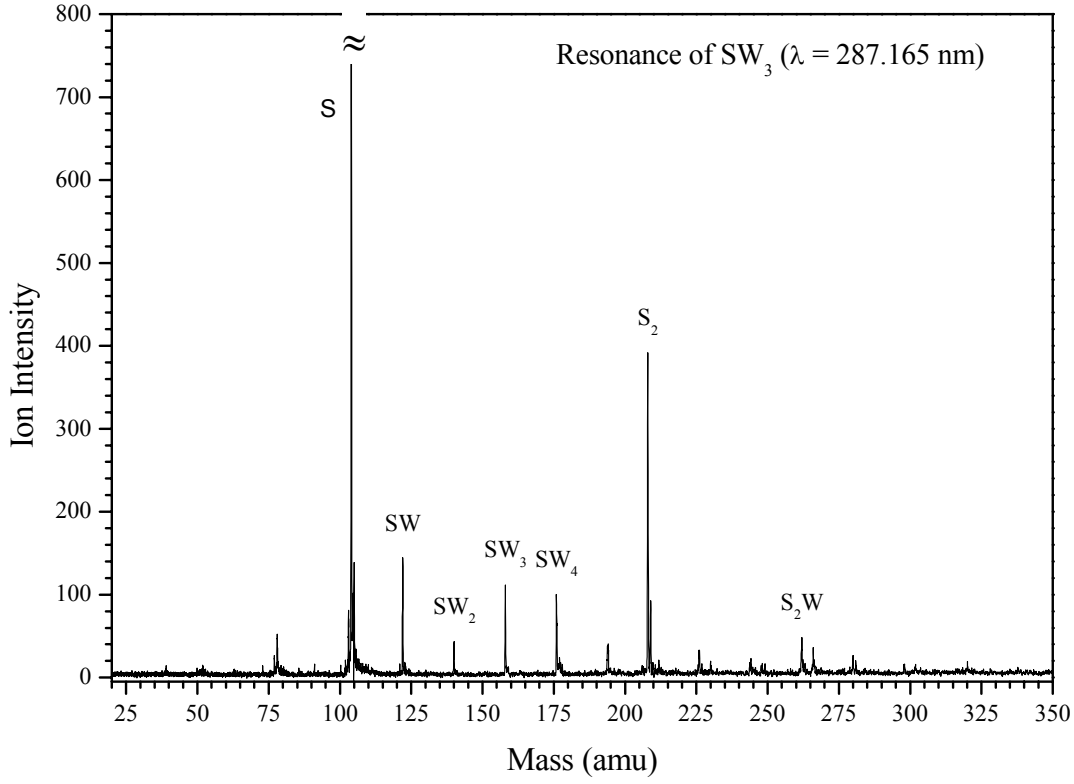

Figure 16: R2PI mass spectra of the styrene-water (SW_n) cluster beam obtained at the resonance ionization assigned to the origin of SW_3.

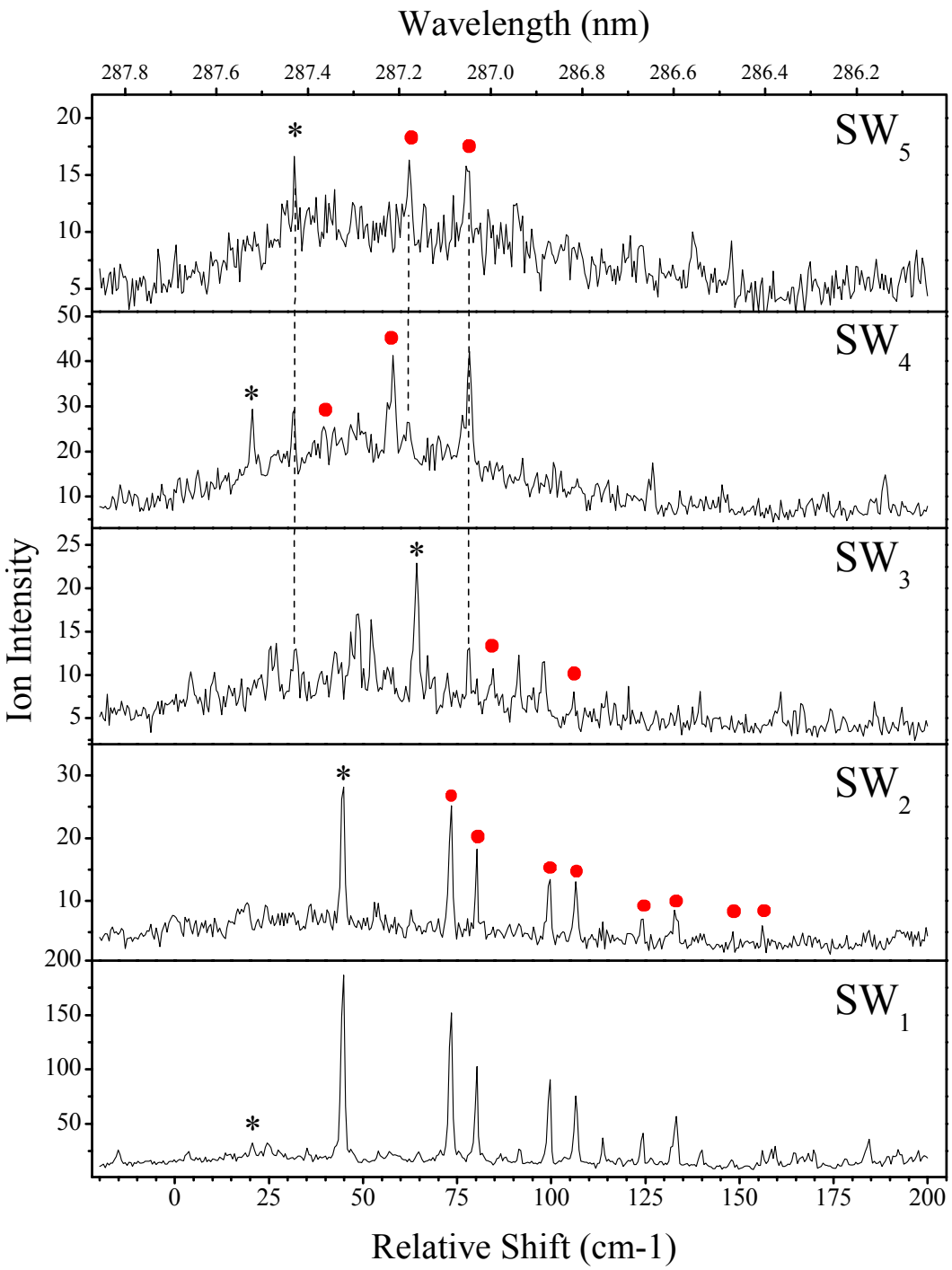

Figure 17: Overall R2PI spectra measured in the styrene(water)$_n$ mass channels, with n = 1-5, relative to the electronic origin band of the $S_1 \leftarrow S_0$ transition of styrene at 34,758.79 cm^{-1}. The origin of each cluster isomer is marked with (*). The peaks labeled with symbols following each cluster's origin represent vdW bands associated with the cluster origin (see Table 6).

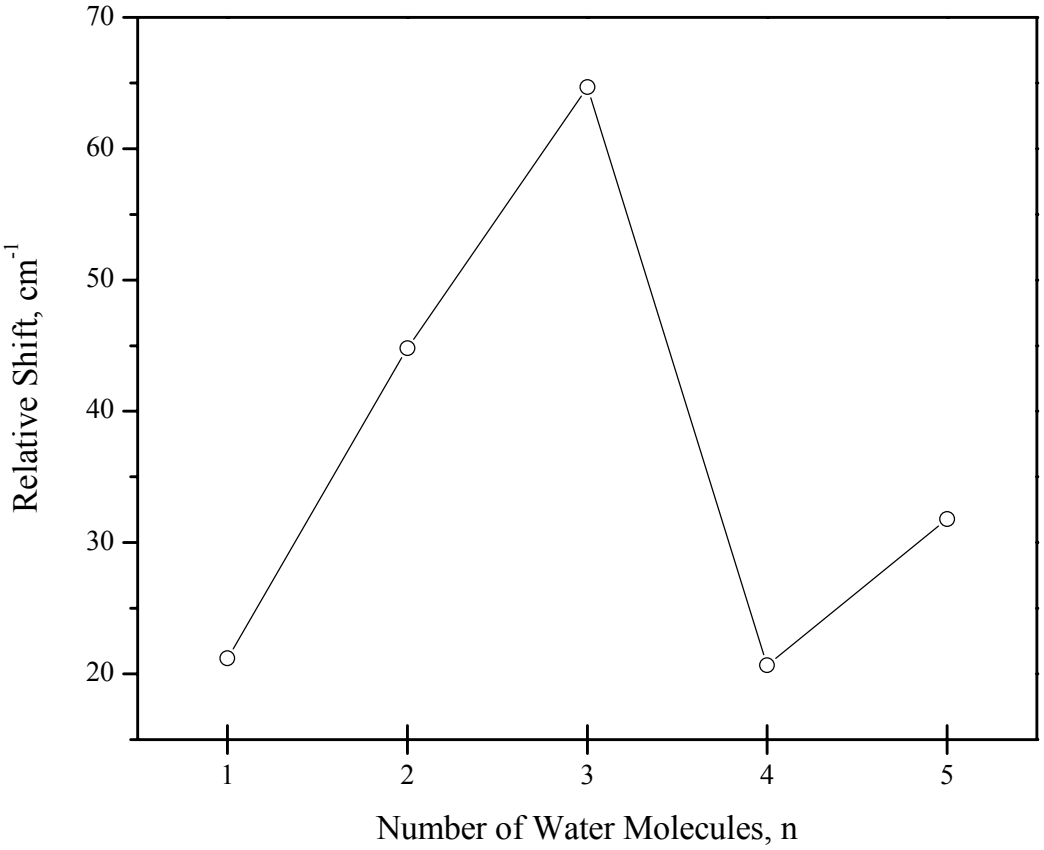

Figure 18: Spectral shifts of the origins of the SW_n clusters, relative to the 0_0^0 band of styrene, as a function of number of water molecules, n.

Table 6: Spectral features observed in the SW_n mass channels (S = Styrene, W = Water, vdW = van der Waals Mode)

Cluster	Shift (cm^{-1}) from the 0_0^0 of styrene	Observed mass channel	Relative intensity	Assignments	Shift (cm^{-1}) from cluster's origin
SW	21.2	SW	30.4	SW origin	0
SW_2	44.8	SW	285.7	SW_2 origin	0
	44.8	SW_2	40.3	SW_2 origin	0
	73.4	SW	220.8	vdW	28.6
	73.4	SW_2	30.7	vdW	28.6
	99.6	SW	171.3	vdW	54.8
	99.6	SW_2	23.7	vdW	54.8
	106.7	SW	149.8	vdW	61.9
	106.7	SW_2	18.8	vdW	61.9
	124.3	SW	103.5	vdW	79.5
	124.3	SW_2	15.4	vdW	79.5
	133.1	SW	155.5	vdW	88.3
	133.1	SW_2	18.0	vdW	88.3
	148.1	SW	43.3	vdW	103.3
	147.6	SW_2	7.8	vdW	102.8
	156.2	SW	49.8	vdW	111.4
	156.0	SW_2	7.6	vdW	111.2
SW_3	64.2	SW_3	22.6	SW_3 origin	0
	84.7	SW_3	107	vdW	20.5
	106.1	SW_3	8.0	vdW	41.9
SW_4	20.7	SW_4	29.4	SW_4 origin	0
	39.7	SW_4	25.6	vdW	19.0
	58.1	SW_4	41.3	vdW	37.4
SW_5	31.8	SW_3	12.8	SW_5 origin	0
	31.8	SW_4	29.1	SW_5 origin	0
	31.8	SW_5	16.6	SW_5 origin	0
	62.3	SW_4	26.4	vdW	305
	62.3	SW_5	16.3	vdW	30.5
	77.3	SW_3	13.1	vdW	45.5
	77.3	SW_4	42.2	vdW	45.5
	77.3	SW_5	15.8	vdW	45.5

Table 7: Fragmentations probabilities of the SW_n cluster ions

Fragmentation channel	Parent, shift (cm^{-1})	%
$SW^+ \rightarrow S^+$	SW origin (21.2)	93.2
$SW_2^+ \rightarrow SW^+$	SW_2 origin (44.8)	62.6
	vdW 1 (73.4)	67.5
	vdW 2 (80.2)	67.7
	vdW 3 (99.6)	66.5
	vdW 4 (106.6)	63.0
$SW_2^+ \rightarrow S^+$	SW_2 origin (44.8)	29.3
	vdW 1 (73.4)	21.6
	vdW 2 (80.2)	21.6
	vdW 3 (99.6)	24.6
	vdW 4 (106.6)	24.6
$SW_3^+ \rightarrow SW_2^+$	SW_3 origin (64.7)	39.3
$SW_4^+ \rightarrow SW_3^+$	SW_4 origin (20.7)	19.6
$SW_5^+ \rightarrow SW_4^+$	SW_5 origin (31.8)	43.9

4.3 R2PI of Styrene-Methanol Clusters

Shown in Figure 19 are the R2PI spectra obtained by monitoring the mass channel corresponding to styrene (S) in the 0_0^0 region between 34,700 cm^{-1} and 35,000 cm^{-1}. The spectrum has the 0_0^0 origin and the vibronic bands 41_0^2 and 29_0^1 as well as the cross – sequence bands $41_0^1 42_0^1$ between the ν_{42} and ν_{41} modes (ethylene group torsional rotation and out-of-plane bend, respectively), $41_0^1 42_1^0$ and $41_0^3 42_1^0$. The spectrum is in good agreement with previous fluorescence excitation and REMPI studies.[46, 97, 98] The other small features observable in Figure 19 are hot bands (29_1^1 and 42_1^1) and some minor features (marked with asterisks) correspond to SM_n clusters that fragment to the S mass channel. These features will be discussed in the next section.

4.3.1 Spectra of Small SM_n Clusters, n = 1-3

Displayed in Figure 20 are the spectra obtained by monitoring the mass channels corresponding to SM, SM_2 and SM_3 clusters. The SM channel shows several strong features, which appear in the SM_2 channel with very small intensities. The peak at 63.5 cm^{-1} relative to the 0_0^0 of styrene (not present in the SM_2 mass channel) was assigned to the 0_0^0 of the SM complex with a small peak at 78 cm^{-1} assigned to a vdW vibration of the complex. Several other peaks at 95, 106, 116 and 126.5 cm^{-1} from the 0_0^0 of styrene were assigned to a vdW progression built on the SM origin.

The stronger peak at 83.8 cm^{-1} accompanied by two rich vdW progressions was assigned to one isomer of the SM_2 cluster (SM_2-I). The SM_2-I cluster possesses two long

progressions of bands assigned to the excitation of intermolecular vibrational modes. The first progression appears at 102, 121, 140.6, 157 and 176.6 cm^{-1} (corresponding to peaks 1-5, respectively in the SM channel in Figure 20). The second progression corresponds to peaks a, b, c, d and e shown in the SM channel at frequencies 96, 106, 116, 126.5 and 136 cm^{-1}, respectively. It should be noted that the peaks a, b, c and d are relatively broad and they overlap with the vdW progression assigned to the SM cluster. Therefore, it appears that the series of peaks a-e contain contributions from both the vdW progressions of the SM and SM_2 clusters. The appearance of strong vibronic intensities away from the origin of the SM and SM_2-I clusters indicates that Franck-Condon factors do not favor the cluster origin intensity, thus the ground state and excited state geometries of the SM and SM_2-I isomer are quite different.

The SM_2 mass channel shows three sets of peaks. The small red-shifted peaks, relative to the 0_0^0 of the styrene, are due to larger clusters containing the styrene dimer S_2. These features were found in the mass channels corresponding to S_2M_2 and S_2M_3 clusters at the same frequencies as they appear in the SM_2 channel. The second group consists of a strong peak that blue shifted by 3.4 cm^{-1} from the 0_0^0 of styrene. This peak was assigned to a second isomer of the SM_2 cluster (SM_2-II) with a vdW progression at 32, 49, 60 and 72 cm^{-1} (corresponding to peaks 1-4 following the SM_2-II origin in the SM_2 channel in Figure 20). It is interesting that the second isomer SM_2-II does not show significant fragmentation upon photoionization. This suggests that the SM_2-II isomer possesses a structure distinct

from that of the SM_2-I isomer, and that this structure does not appear to undergo major changes upon photoionization.

The third group of peaks observed in the SM_2 mass channel starts with a sharp peak at 182 cm^{-1} followed by a vdW progression of very low frequency modes at 189, 199, 204, 213, 232 and 341 cm^{-1} (corresponding to peaks 1-6 following the SM_3-I origin in the SM_2 channel in Figure 20). Some of these peaks appear with very small intensities in the SM_3 mass channel, and they may be tentatively assigned to one isomer of the SM_3 cluster (SM_3-I).

The most prominent features in the SM_3 mass channel in Figure 20 could be assigned to a second isomer of the SM_3 cluster with a strong origin peak blue shifted from the styrene origin by 16.5 cm^{-1}. This origin is accompanied by a strong vibronic intensity with a well-defined vdW progression of doublets at 24, 33, 43, 52, 62, 70 and 80 cm^{-1}. In addition, two other weaker peaks appear at 28 and 36 cm^{-1}. Several weaker features to the red of the SM_3-II isomer are due to fragmentation from the SM_4 cluster.

The blue shift observed for the SM cluster (63 cm^{-1}) is consistent with a weak hydrogen bonding interaction between the OH group of methanol and the styrene π-system. For example, benzene complexes with H_2O, CH_3OH, CH_3COOH, HCl and $CHCl_3$ exhibit blue shifts of 52, 44, 152, 125 and 179 cm^{-1}, respectively.[20-23, 25, 30] It is interesting to note that the addition of a second methanol molecule to styrene resulted in a greater blue shift in the SM_2-I cluster (84 cm^{-1}). This is very similar to the benzene $(methanol)_n$ clusters, BM_n, where the spectral shifts of BM and BM_2 clusters relative to the

6_0^1 origin of the isolated benzene molecule are 44 and 80 cm^{-1}, respectively.[25] Also, the spectrum of the SM_2 cluster exhibits several vdW transitions indicating that the 1:2 clusters undergo major changes in geometries upon the electronic excitation of styrene. This is exactly the same trend found in the BM_2 clusters.[25] Furthermore, in both the benzene and styrene systems extensive fragmentation was observed following photoionization of the neutral clusters. The high fragmentation probability of the ionized clusters is consistent with the hydrogen bonding interaction with the π-system in benzene or styrene.

A noticeable difference between the benzene and styrene systems is the assignment of two structural isomers to the SM_2 cluster with quite different spectral shifts (84 and 3.4 cm^{-1} relative to the 0_0^0 transition of styrene). This is in contrast to the BM_2 cluster, where only one isomer was assigned.[25] The interactions between the ethylene group of styrene and the methyl group for methanol are considered to be purely dispersive. This suggests that the SM_2-II isomer may represent a structure that maximizes induced dipole-induced dipole forces between the ethylene group of styrene and the methyl groups of the two methanol molecules. This interaction is known to lead to red spectral shifts, and, therefore, one expects the SM_2-II isomer to exhibit a significant red shift relative to the SM complex ($\Delta\nu$ = -60 cm^{-1}). The dominance of the dispersion interaction and the small π-hydrogen bonding interaction in the SM_2-II isomer is consistent with the low fragmentation probability observed for this isomer following photoionization.

The blue-shifted isomer assigned to the SM_3 cluster (SM_3-I) may have a hydrogen-bonded methanol chain structure H-bonded to the styrene π-system. This structure is

compatible with the strong blue shift observed (182 cm^{-1} with respect to the styrene origin). The second isomer (SM_3-II) may reflect a cyclic methanol structure with no hydrogen bonding to styrene since all the OH groups would be used in the formation of the methanol trimer ring. This isomer has a smaller blue shift of 16 cm^{-1}, which is consistent with the absence of hydrogen bonding interaction to the styrene π-system. The calculated structures for the SM_n clusters are consistent with the structural predictions presented here based on the observed spectral shifts and the degree of cluster's fragmentation following ionization.[99]

4.3.2 Spectra of SM_n Clusters, n = 4-6

The R2PI spectra obtained by monitoring the mass channels corresponding to the SM_4, SM_5 and SM_6 clusters in the region of the styrene 0_0^0 transition are displayed in Figure 21. A remarkable shift in the spectra from blue to red, with respect to the styrene origin, is observable at the start of the SM_4 cluster. In additions, ion fragmentations from the S^+M_5 and S^+M_6 clusters to the S^+M_4 channel appear to be pronounced since several features belonging to the SM_5 and SM_6 clusters are present in the S^+M_4 mass channel. The set of strong peaks in the -98 to -60 cm^{-1} region were assigned to the SM_4 cluster with the origin assigned to the singlet at -94 cm^{-1}. A vdW progression associated with the cluster origin also appears at -88, -79, -72, -66 and -62 cm^{-1} (corresponding to peaks 1-5 following the SM_4 origin in the SM_2 channel in Figure 21). The cluster origin and the vdW modes also appear in the SM_3 channel as a result of the ion fragmentation process $S^+M_4 \rightarrow S^+M_3$.

Other features present in the S^+M_4 mass channel, as a result of dissociation of the ionized clusters, include two isomers of each of the SM_5 and SM_6 clusters.

The red shifted spectrum of the SM_4 cluster, unlike the SM, SM_2 and SM_3 clusters, may indicate a major departure from the structure that allows hydrogen bonding interaction between the OH group of methanol and the styrene π-system. A possible structure may involve a cyclic methanol tetramer placed above the styrene molecular plane. This structure is expected to enhance the dispersion and induction interactions, which typically result in red spectral shifts. The calculated lowest energy structures of the SM_4 cluster[99] are consistent with the proposed cyclic methanol tetramer above the styrene plane.

Two geometrical isomers are assigned to the SM_5 cluster, which appear in both the SM_5 and SM_4 mass channels. The first isomer (SM_5-I) has a strong origin at -59 cm^{-1} and possesses two vdW peaks at -41 and -25 cm^{-1} (corresponding to peaks 1 and 2 following the SM_5-I origin in the SM_5 channel in Figure 21). The second isomer (SM_5-II) displays a weak low energy origin at -119 cm^{-1} followed by a stronger vdW mutiplet at -115, -110, -105 and -103 cm^{-1} (corresponding to peaks 1-4 following the SM_5-II origin in the SM_5 channel in Figure 21). Other weak vdW peaks appear at -108 and -98 cm^{-1} and possess significant intensities in the SM_4 mass channel. The origins of both isomers and their vdW features also appear in the S^+M_4 mass channel as a result of ion fragmentation.

The SM_6 mass channel contains features belonging to both the SM_6 and SM_7 clusters. Two isomers SM_6-I and SM_6-II can be assigned to the SM_6 cluster with origins at -46 and -113 cm^{-1}, respectively. Several weaker features with a long progression are

assigned to vdW modes associated with the SM_6-I isomer and they appear at -31, -14, -2, 10 and 21 cm^{-1} from the styrene origin (corresponding to peaks 1-5 following the SM_6-I origin in the SM_6 channel in Figure 21). The SM_6-I isomer undergoes extensive fragmentation to both the SM_5 and the SM_4 mass channels following photoionization of the cluster. The fragmentation also proceeds through the associated vdW modes as evident in the SM_4 and SM_5 mass channels. The SM_6-II origin (-113 cm^{-1}) has two vdW peaks at -100 and -96 cm^{-1} and both fragment to the SM_5 mass channel.

4.3.3 Spectra of SM_n Clusters, n = 7-9

Displayed in Figure 22 are the R2PI spectra obtained by monitoring the mass channels corresponding to the SM_7, SM_8 and SM_9 clusters. The SM_7 cluster shows two distinct isomers (SM_7-I and SM_7-II) with origins at +54 and -89 cm^{-1}, respectively. Both clusters fragment efficiently upon photoionization into the SM_6 mass channel. The SM_7-I isomer exhibits a small vdW multiplet at 64, 66, 70, 73 and 79 cm^{-1} with greater intensity in the SM_6 mass channel due to ion fragmentation (corresponding to peaks 2-6 following the SM_7-I origin in the SM_6 channel in Figure 21). The second isomer SM_7-II shows small vdW peaks at -80/-79, -75 and -73 cm^{-1}. The remaining features in the SM_7 mass channel belong to the SM_8 and SM_9 clusters. The SM_8 cluster origin appears in the SM_8 mass channel at -36/-34 cm^{-1}. A vdW progression associated with the SM_8 cluster appears at -28, -23, -14, -8 and -3 cm^{-1}, corresponding to peaks 1-5, respectively following the SM_8 origin in the SM_8 channel in Figure 22. The SM_8 cluster has a doublet origin and shows strong

fragmentation into the SM_7 mass channel through the vdW modes which appear at -34, -28, -23, -14, -8 and -5 cm^{-1}. The other features in the SM_8 mass channel can be assigned to the SM_9 cluster as shown in Figure 22. Based on the comparison of the spectral features in the SM_8 and SM_9 mass channels, we assign the peak at -120 cm^{-1} to one isomer of the SM_9 cluster (SM_9-II). This isomer shows several vdW peaks at -111, -105, -100, -94, -87, -78, -74, -68 and -63 cm^{-1} corresponding to peaks 1-9, respectively following the SM_9–II origin in the SM_9 channel in Figure 22. Another origin in the SM_9 mass channel at +24 cm^{-1} followed by a doublet at +29/30 cm^{-1} and a vdW peak at +46 cm^{-1} is assigned to a second isomer of the SM_9 cluster (SM_9-I). It is interesting to note that all the assigned isomers of the SM_n clusters with n = 4-9 exhibit red spectral shifts, relative to the styrene origin, except for the SM_7-I and SM_9-I isomers which display blue shifts. Figure 23 exhibits the overall R2PI spectra recorded in the SM_n mass channels with n=1-9, displayed relative to the 0_0^0 origin of styrene. The relative frequencies and tentative assignments of the SM_n cluster isomers are listed in Table 8.

4.3.4 Spectral Shifts

The spectral shifts relative to the 0_0^0 origin of the isolated styrene molecule imposed by methanol clusters provide information on the nature of the intermolecular interactions within the binary clusters. Spectral shifts are due to different cluster binding energies in the ground and excited states. A red shift implies that the excited state is more tightly bound than the ground state, and a blue shift is associated with stronger interaction in the ground state. A

red shift is usually observed in clusters where the dispersion energy is dominant due to the increase in the molecular polarizability in the excited state relative to the ground state.[100-102] For example, ring-ring interactions result in red shifts since dispersive forces are stronger for the more delocalized excited states, as in benzene and other aromatic clusters.[17, 103] On the other hand, hydrogen-bonding to the π-system results in a blue shift, which tends to increase with increasing the H-bond donating capacity of the solvent molecules.[10]

In contrast to benzene, few studies of clusters containing styrene have been reported.[49-51, 104-111] Clusters of styrene with Ar, N_2, CO_2, NH_3 and trimethylamine were studied by laser-induced fluorescence (LIF) and REMPI.[47, 49-51, 105, 106, 108, 110, 112] The origin bands of these clusters are shifted by -31 cm^{-1}, -25.5 cm^{-1}, +51 cm^{-1}, +52 cm^{-1}, and -24 cm^{-1} relative to the 0_0^0 band of the bare styrene molecule. The spectra of the styrene-TMA 1:1 cluster were assigned to two isomeric forms, both capable of forming a charge transfer complex upon excitation to the locally excited state.[105, 106] We recently reported the REMPI spectra of styrene $(water)_n$ clusters, SW_n, with n = 1-2, which indicate that the origin of the SW complex is blue shifted by -22 cm^{-1} relative to the 0_0^0 band of the bare styrene molecule.[104]

In the case of methanol clusters, the binding energy is mainly due to hydrogen bonding. Monte Carlo, molecular dynamics, density functional and *ab initio* calculations have shown that the intermolecular interactions in small methanol clusters (n = 4-9) are dominated by configurations in which hydrogen-bonded chains are formed with cyclic structures starting at n = 3.[113-117] If it is assumed that the styrene molecule does not significantly affect

hydrogen bonding in methanol clusters, then shifts of the electronic origin of SM_n clusters can be related to the styrene ↔ (methanol subcluster) interaction.

Displayed in Figure 24 are the observed spectral shifts of the SM_n cluster origins, relative to the 0_0^0 transition of styrene, as a function of n. The observed pattern reveals some interesting correlation with the proposed structures of the clusters. Figure 23 and Figure 24 show that the first isomers of SM_n (n=1-3) exhibit successively greater increases in blue shift, which reaches a maximum of 182 cm^{-1} for the SM_3-I isomer. The shifts of these isomers are consistent with H-bonding to the π-system of styrene. The SM_2-II and SM_3-II isomers exhibit smaller blue shifts, which may reflect more dispersive interactions suggesting structures with no directional hydrogen bonding to the π-system of styrene.[99]

The spectral shift reverses direction in the single isomer observed for SM_4. The successive addition of methanol molecules to the SM complex leads to a stable cyclic methanol tetramer in SM_4 that is unable to H-bond to the styrene π-system, consistent with the observed red shift.[99]

The two isomers assigned to each of the SM_5 and SM_6 clusters may contain cyclic methanol subclusters. Similarly, the two SM_7 cluster isomers could have cyclic five- or six-member rings with the other molecule(s) as ring branches. The single isomer assigned to the SM_8 cluster could involve a bicyclic methanol ring structure. Also, the two SM_9 isomers could represent a larger bicyclic ring containing nine methanol molecules, and a bicyclic eight-member ring on one side of styrene and a free methanol molecule on the other side of the styrene plane. Interestingly, the addition of the red shift of -36 cm^{-1} imposed by the SM_8

cluster and the blue shift of +63 cm^{-1} of the SM cluster results in a +27 cm^{-1} shift, which is similar to the observed shift of the SM_9-I isomer. This may suggest that the SM_9-I isomer consists of a M_8 subcluster on one side of styrene and a single methanol molecule on the other. The arrangement of the methanol molecules with respect to the styrene plane has been investigated using pair potentials.[99]

4.3.5 Fragmentation of the Ionized Clusters

The ionization potential of the styrene molecule is 68,267 cm^{-1}.[49] Since the 0_0^0 transition is located at 34,758.79 cm^{-1}, two photons resonant with the origin transition suffice to ionize styrene in a one-color REMPI experiments. The ionic state of the styrene molecule in the SM_n cluster is prepared according to the Franck-Condon distribution, while the rest of the cluster relaxes structurally in a time-dependent manner about the styrene ion. This relaxation releases energy and thus lowers the cluster ionization threshold relative to that of the isolated styrene molecule, and the additional energy imparted to the S^+M_n cluster ion promotes fragmentation via solvent evaporation from the cluster. However, since a large fraction of the energy usually goes to the electron, some cluster ions are formed with little internal energy and may not dissociate while in the acceleration zone of the TOF (typically 1-2 μs in these experiments). If the time scales for the post-ionization fragmentation processes [$S^+M_n \rightarrow S^+M_{n-m}$] are faster than the time of acceleration in the mass spectrometer, then the resonant intensity of cluster n will contribute to the observed intensity of cluster n-m. These time scales will in general depend on the cluster's internal energy prior to excitation, the final

energy state produced by ionization, and the timescale of energy relaxation into the intermolecular modes.

Fragmentation probabilities are measured by comparing the absolute integrated intensities I_n at various mass channels (parent I_n and daughters I_{n-1}, I_{n-2}, etc.) at the laser wavelength of a specific spectral resonance and normalizing to the sum over $I_n + I_{n-1} + \ldots$etc. The results expressed as a percent of the parent ion intensity are shown in Table 9.

The relatively efficient fragmentation observed for the S^+M complex following photoionization is a direct consequence of the π-hydrogen-bonded geometry of the neutral complex. The structural change in going from the π-hydrogen-bonding geometry in the neutral species to the predominantly ion-dipole interaction in the ionized species involves a great strain, which leads to efficient fragmentation. However, the fragmentation of the S^+M complex is significantly less than that of the B^+M complex (where almost 100% fragmentation was observed). This is consistent with the methanol interacting with both the ethylene double bond and the aromatic ring.

Displayed in Figure 25 are the examples of the mass spectra obtained at some selected resonance features assigned to the SM_n cluster origins. In the two examples displayed in Figure 25, the S^+M_4 and S^+M_5-I clusters show little fragmentation following photoionization, and the mass peaks corresponding to the parent resonance cluster show enhanced intensity. However, when fast ion fragmentation is predominant, significant intensity of the SM_{n-1} ions are observed following the resonant ionization of the SM_n clusters. This was clearly observed in the SM_2-I, SM_3-I and SM_7-I cluster isomers. The small fragmentation probability of the

SM_4 cluster ion supports the assumption of a ring structure of the methanol tetramer placed above the plane of the styrene molecule.[99]

4.3.6 Intracluster Reactions following Photoionization

Mass spectra of the SM_n clusters obtained at selected resonance ionization energies reveal the generation of protonated methanol clusters H^+M_n starting at $n \geq 2$. Since pure methanol clusters (in the absence of styrene) could not be ionized with the same laser power used in the R2PI experiments, the origin of the protonated clusters must be attributed to the SM_n clusters. The H^+M_n clusters could be produced by either dissociative electron transfer (DET) or dissociative proton transfer (DPT), or combination of both mechanisms. The small intensity of the H^+M_n ions (due to the necessity of low laser power in order to stay within the two photon process) prevented correlation of their spectral features with those of the parent SM_n clusters and the unambiguous determination the origin of the protonated methanol clusters.

Shown in Figure 26 are the mass spectra obtained at wavelengths corresponding to the assigned SM_3-I and SM_3-II cluster origins. It was noted that the protonated methanol clusters are formed exclusively at the resonance for the SM_3-I isomer (286.202 nm) and not at the SM_3-II resonance. However, it should be noted that at this wavelength the mass spectrum contains significant contributions from the styrene dimer ($S_2^{+\cdot}$) and the $S_2M_n^+$ series. The styrene dimer cation has been a subject of several studies that have established it to be covalently bonded ($C_{16}H_{16}^{+\cdot}$) and probably cyclic in structure.[37, 38, 94-96] The correlation between the generation of the $S_2M_n^+$ series and the protonated methanol clusters suggests that

DPT takes place from the styrene dimer cation $C_{16}H_{16}^{+}$ to the methanol sub-cluster M_n within the $S_2M_n^{+}$ cluster to generate the $H^{+}M_n$ species, as shown in Eq. 4-1. At lower laser power, the protonated methanol clusters are generated starting at n = 3. This suggests that the protonated methanol dimer is produced by evaporation from larger $H^{+}M_n$ clusters with $n \geq 3$ as shown in Eq. 4-2.

$$C_{16}H_{16}^{+}(CH_3OH)_n \rightarrow H^{+}(CH_3OH)_n + C_{16}H_{15} \cdots n \geq 3 \qquad \text{Eq. 4-1}$$

$$H^{+}(CH_3OH)_n \rightarrow H^{+}(CH_3OH)_{n-1} + CH_3OH \qquad \text{Eq. 4-2}$$

The proposed mechanism involves structural changes following the ionization of the styrene dimer resulting in the formation of a covalent bonded styrene dimer cation ($C_{16}H_{16}^{+}$) solvated by methanol molecules in the cluster. DPT between $C_{16}H_{16}^{+}$ and methanol sub-cluster then, results in the generation of protonated methanol clusters $[H^{+}(CH_3OH)_n]$ and the $C_{16}H_{15}$ radical. It should be noted the DPT channel becomes exothermic in the $S_2M_3^{+}$ cluster if the proton affinity (PA) of $C_{16}H_{15}$ $[C_{16}H_{16}^{+} \rightarrow C_{16}H_{15} + H^{+}]$ is less than that of the methanol trimer $[H^{+}M_3 \rightarrow M_3 + H^{+}]$. Based on the estimation of the PA of M_3 as 224 kcal/mol, [82] the upper limit of the PA of the styrene dimer radical ($C_{16}H_{15}$) can be estimated as ≤ 224 kcal/mol.

The DPT mechanism suggested for the generation of the protonated methanol clusters is consistent with the study of the styrene/water binary clusters, where isotopic experiments involving D_2O have revealed that the protonated water clusters $H^{+}(H_2O)_n$ were produced via a DPT mechanism involving the styrene dimer series $[C_{16}H_{16}^{+}(D_2O)_n]$ with n≥3.

The observed intracluster DPT reactions in $S_2M_n^+$ series are consistent with the detrimental effect of methanol on the bulk cationic polymerization of methanol. For example, it is well established that radiation-induced polymerization of styrene proceeds via a cationic mechanism in pure, dry bulk styrene.[38-40, 118, 119] The presence of a small amount of methanol suppresses the cationic polymerization and enhances both the dimerization and the radical polymerization. It has been shown that methanol reacts with the dimer radical cation and converts it to a neutral radical that initiates the radical polymerization.[39] This is exactly the result obtained in the present work via the DPT mechanism within the $S_2M_n^+$ clusters. The similarity between the cluster and the bulk phase results provides strong evidence for the validity of the cluster approach in elucidating the mechanisms of initiation, propagation and inhibition of cationic polymerization.

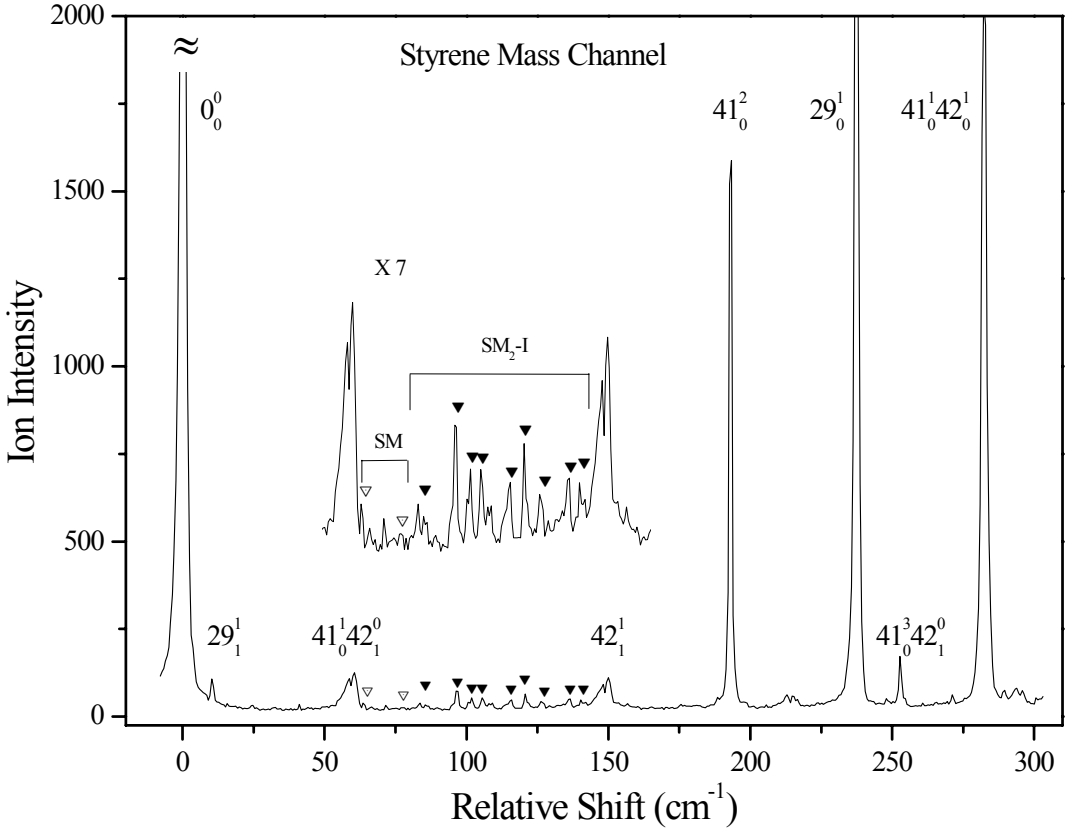

Figure 19: One-color R2PI spectra of styrene (S) mass in the region of $S_1 \leftarrow S_0$ transition of the styrene molecule at 34,758.79 cm^{-1}.

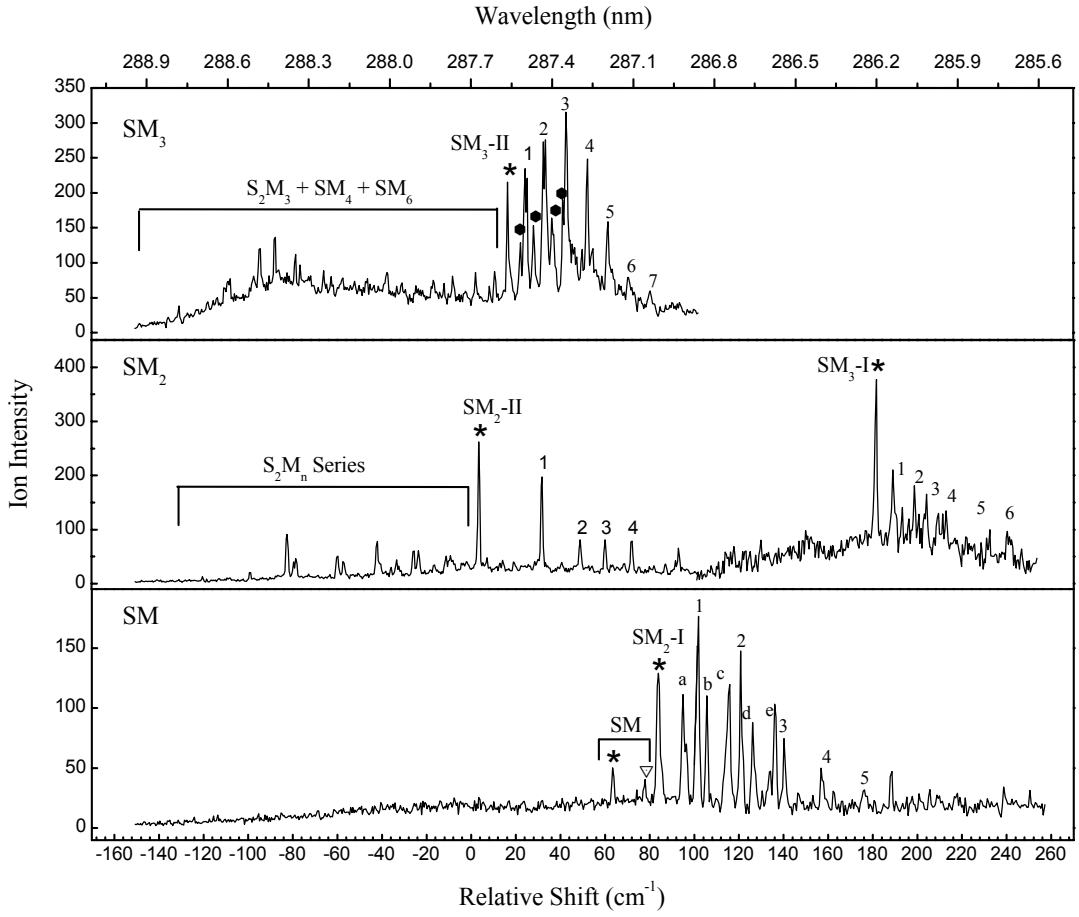

Figure 20: One-color R2PI spectra measured in the styrene (methanol)$_n$ mass channels with n = 1-3, [SM, SM_3 and SM_3] relative to the electronic origin band of the $S_1 \leftarrow S_0$ transition of the styrene molecule at 34,758.79 cm^{-1}. The origin of each cluster isomer is marked with a (*). The peaks labeled with numbers, letters or symbols following each cluster's origin represent vdW bands associated with the cluster origin (see Table 8).

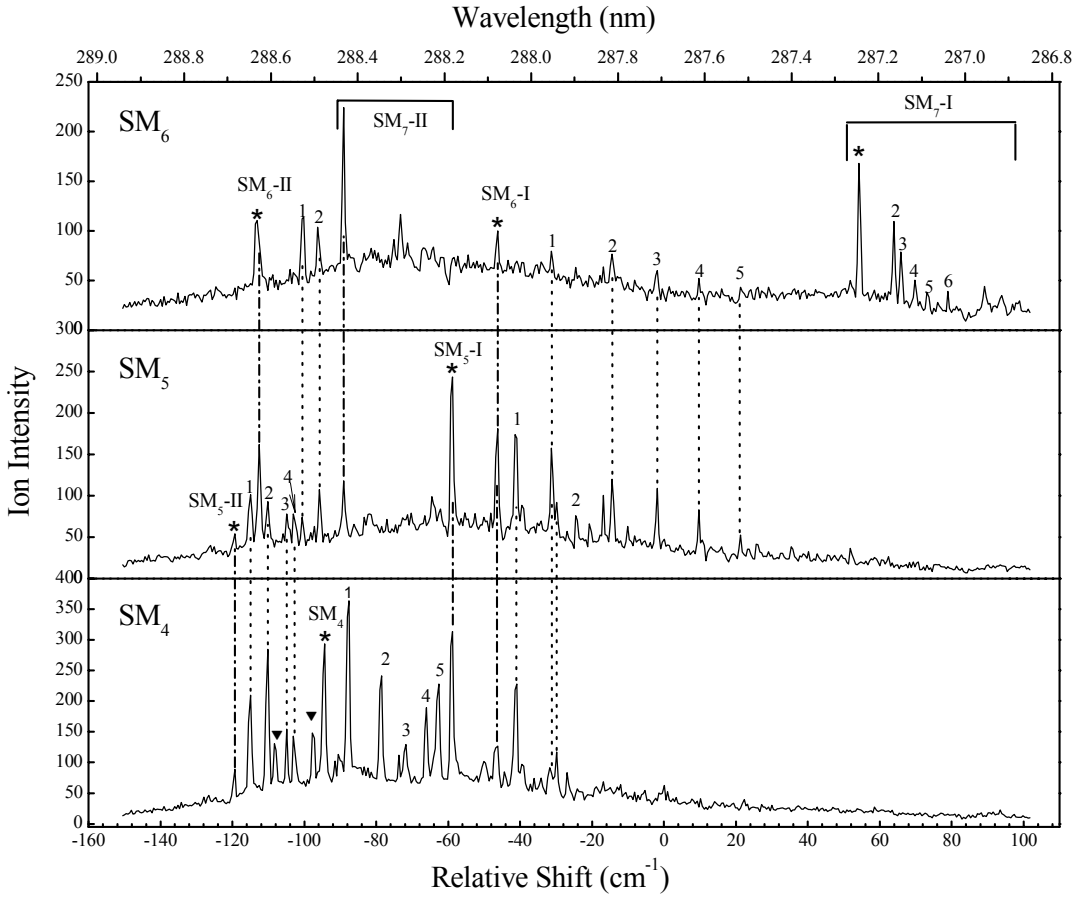

Figure 21: One-color R2PI spectra measured in the styrene $(methanol)_n$ mass channels with n = 4-6, [SM_4, SM_5 and SM_6] relative to the electronic origin band of the $S_1 \leftarrow S_0$ transition of the styrene molecule at 34,758.79 cm^{-1}. The origin of each cluster isomer is marked with a (*). The peaks labeled with numbers following each cluster's origin represent vdW bands associated with the cluster origin (see Table 1). The two peaks labeled with ▼ at –108 cm^{-1} and –98 cm^{-1} from the styrene origin in the SM_4 mass channel are unassigned.

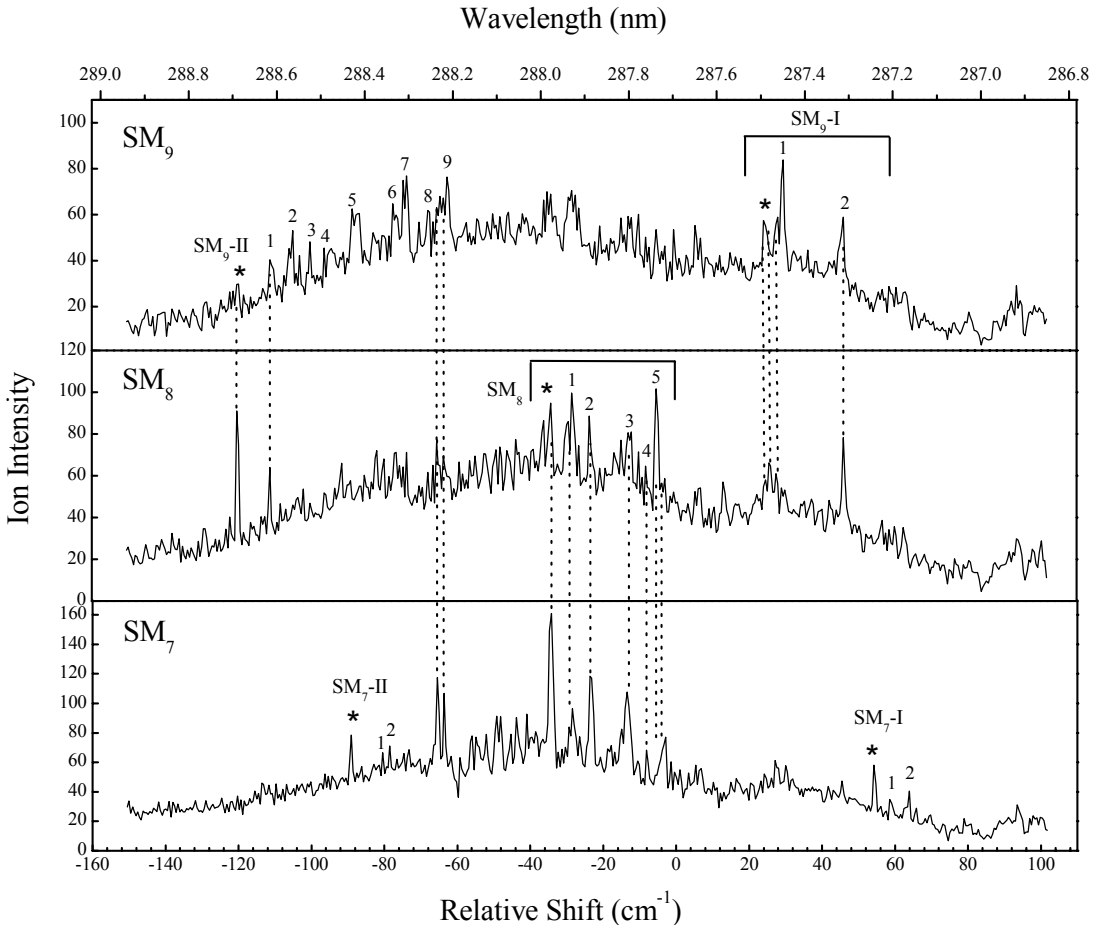

Figure 22: One-color R2PI spectra measured in the styrene (methanol)$_n$ mass channels with n = 7-9, [SM_7, SM_8 and SM_9] relative to the electronic origin band of the $S_1 \leftarrow S_0$ transition of the styrene molecule at 34,758.79 cm-1. The origin of each cluster isomer is marked with a (*). The peaks labeled with numbers following each cluster's origin represent vdW bands associated with the cluster origin (see Table 8).

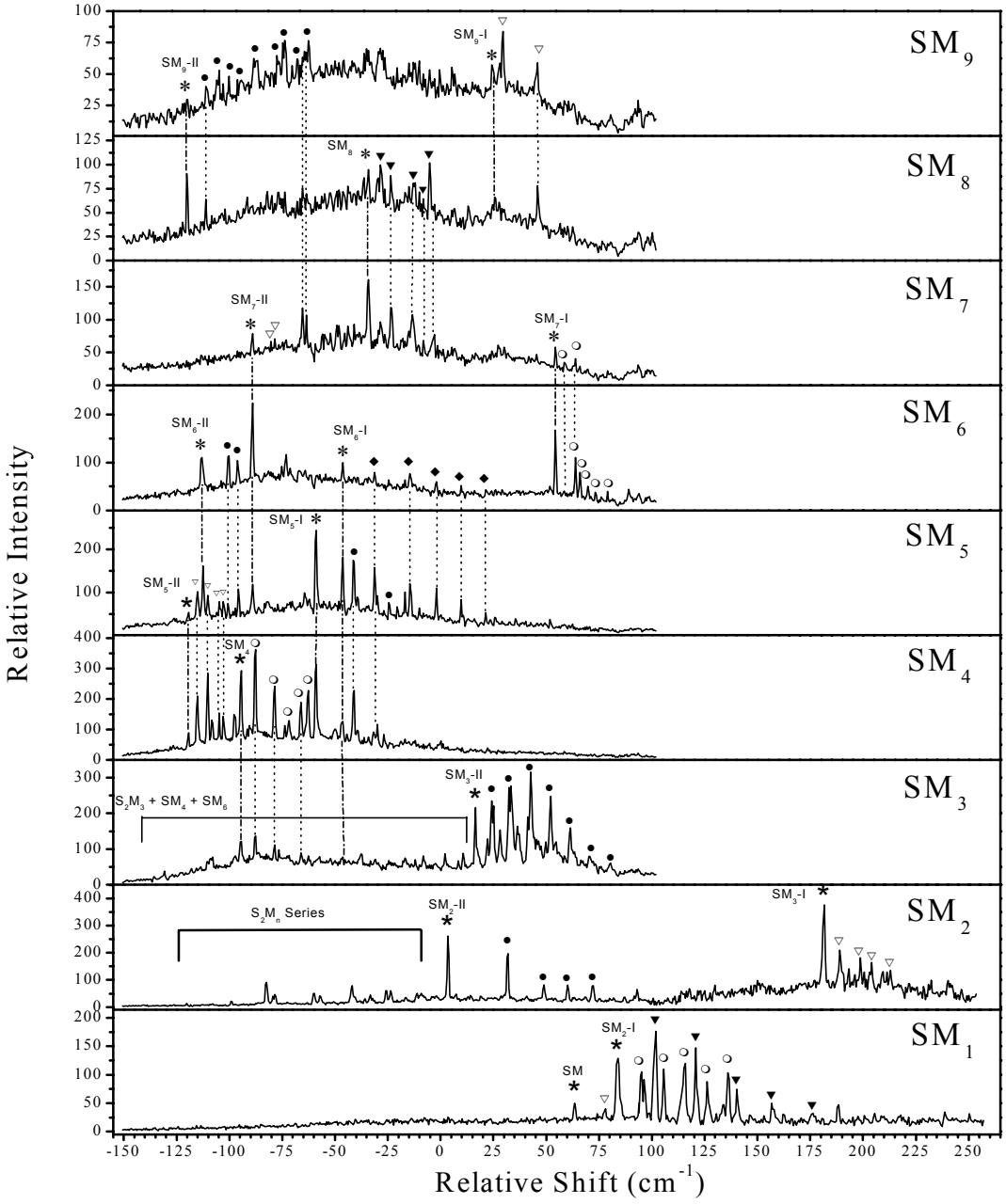

Figure 23: Overall R2PI spectra measured in the styrene $(methanol)_n$ mass channels (SM_n), n = 1-9, relative to the electronic origin band of the $S_1 \leftarrow S_0$ transition of the styrene molecule at 34,758.79cm^{-1}. The origin of each cluster isomer is marked with a (*). The peaks labeled with symbols following each cluster's origin represent vdW bands associated with the cluster origin (see Table 8).

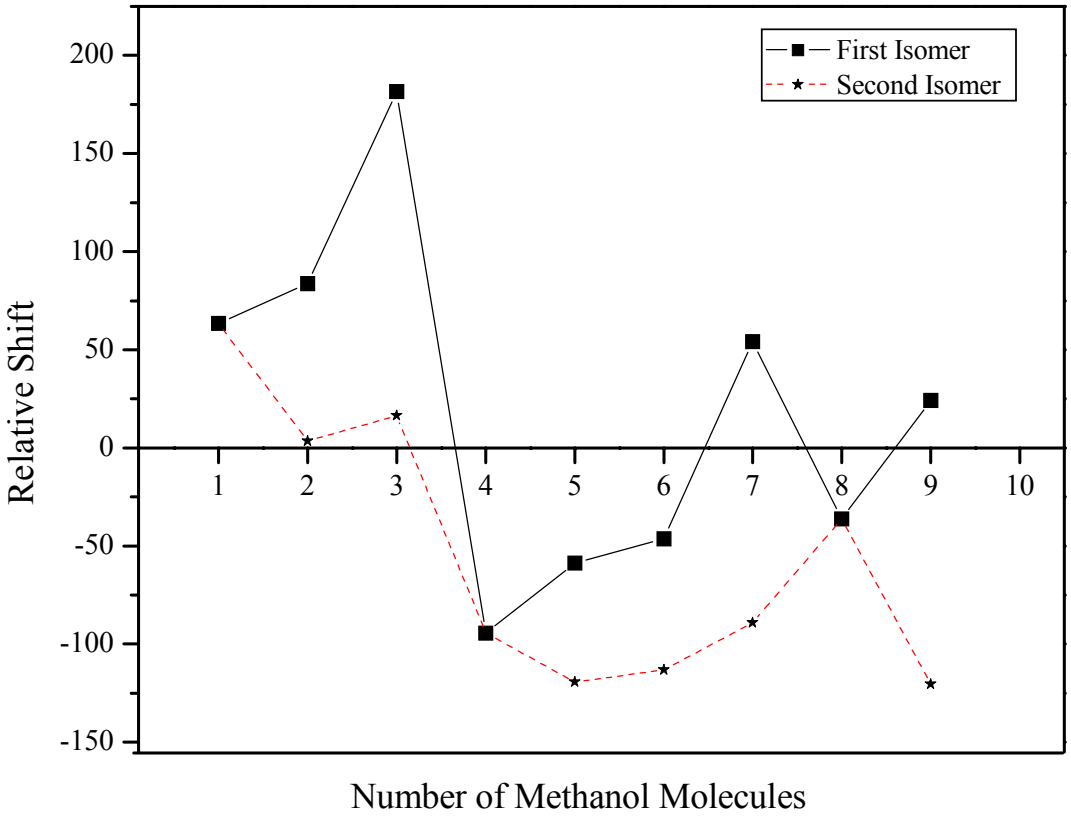

Figure 24: Spectral shifts of the origins of the SMn clusters, relative to the 0_0^0 band of styrene, as a function of n.

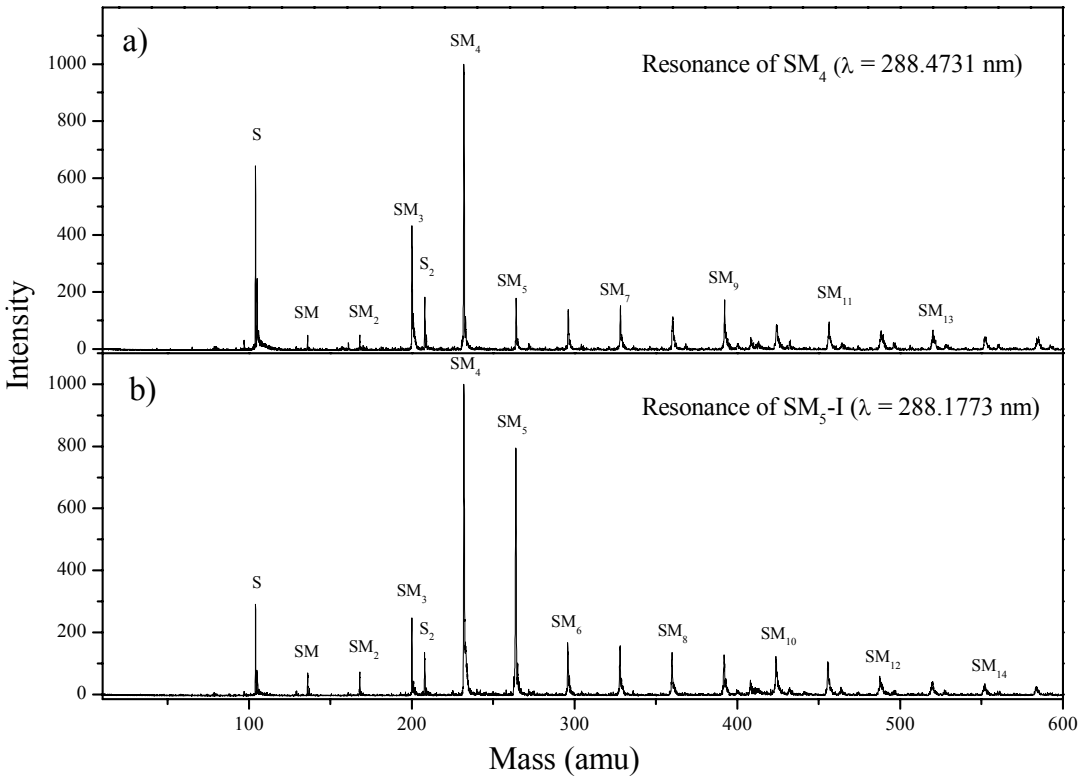

Figure 25: R2PI mass spectra of the styrene-methanol (SM_n) cluster beam obtained at the resonance ionizations assigned to the origins of (a) SM_4 and (b) SM_5–I clusters.

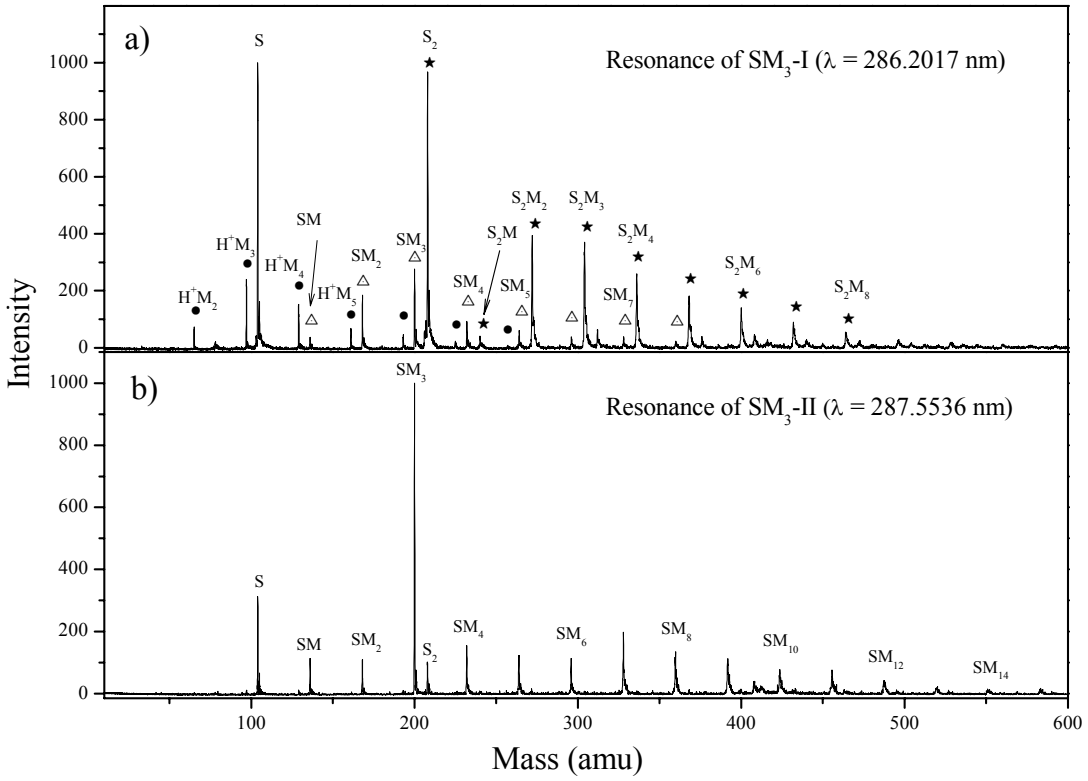

Figure 26: R2PI mass spectra of the styrene-methanol (SM_n) cluster beam obtained at the resonance ionizations assigned to the origins of (a) SM_3–I and (b) SM_3–II clusters. The SM_n series is labeled as △. Note the correlation between the generations of the protonated methanol clusters H^+M_n (labeled as ●) and the styrene dimer series S_2M_n (labeled as ★) as shown in (a).

Table 8: Spectral features observed in the SM_n mass channels (S = styrene, M = methanol, vdW = van der Waals mode).

Cluster	Shift (cm^{-1}) from the 0_0^0 of Styrene	Observed Mass Channel	Relative Intensity	Assignment	Shift (cm^{-1}) from Cluster's Origin
SM	63.4	SM	50	SM origin	0
	78.0	,,	41	vdW	14.6
SM_2-I	83.8	SM	128	SM_2–I origin	0
	95.2/96.4	,,	104/92	vdW-a	11.4/12.6
	102.2	,,	176	vdW-1	18.4
	105.8	,,	110	vdW-b	22.0
	116.2	,,	120	vdW-c	32.4
	121.1	,,	147	vdW-2	37.3
	126.5	,,	88	vdW-d	42.7
	136.3	,,	103	vdW-e	52.6
	140.6	,,	75	vdW-3	56.8
	157.0	,,	50	vdW-4	73.2
	176.6	,,	32	vdW-5	92.6
SM_2-II	3.4	SM_2	262	SM_2–II origin	0
	32.0	,,	197	vdW-1	28.6
	48.9	,,	81	vdW-2	45.5
	60.1	,,	91	vdW-3	56.7
	72.2	,,	79	vdW-4	68.8
SM_3-I	181.6	SM_2	377	SM_3–I origin	0
	188.9	,,	210	vdW-1	7.3
	198.7	,,	181	vdW-2	17.1
	204.1	,,	165	vdW-3	22.5
	212.9	,,	135	vdW-4	31.3
	232.4	,,	100	VdW-5	50.8
	241.2	,,	86	VdW-6	59.6
SM_3–II	16.5	SM_3	216	SM_3–II origin	0
	24.2	,,	235	vdW-1	7.7
	28.1	,,	153	vdW	11.6
	33.4	,,	276	vdW-2	16.9
	36.3	,,	164	vdW	19.8
	42.6	,,	315	vdW-3	26.1

	52.3	,,	248	vdW-4	35.8
	61.5	,,	158	vdW-5	45
	70.2	,,	79	vdW-6	53.7
	80.4	,,	60	vdW-7	63.9
SM_4	-94.4	SM_3	121	SM_4 origin	0
	,,	SM_4	293	,,	,,
	-87.6	SM_3	137	vdW-1	6.8
	,,	SM_4	363	,,	,,
	-78.5	SM_3	112	vdW-2	15.9
	,,	SM_4	241	,,	,,
	-71.8	SM_3	81	vdW-3	22.6
	,,	SM_4	130	,,	,,
	-66.0	SM_3	88	vdW-4	28.4
	,,	SM_4	189	,,	,,
	-62.6	SM_3	81	vdW-5	31.8
	,,	SM_4	228	,,	,,
SM_5–I	-58.8	SM_4	314	SM_5–I origin	0
	,,	SM_5	244	,,	,,
	-41.4	SM_3	66	vdW-1	17.4
	,,	SM_4	228	,,	,,
	,,	SM_5	174	,,	,,
	-24.6	SM_3	67	VdW-2	34.2
	,,	SM_5	76	,,	,,
SM_5–II	-119.3	SM_4	89	SM_5–II origin	0
	,,	SM_5	54	,,	,,
	-115.5	SM_3	47	vdW-1	4.0
	,,	SM_4	210	,,	,,
	,,	SM_5	102	,,	,,
	-110.2	SM_3	64	vdW-2	9.1
	,,	SM_4	284	,,	,,
	,,	SM_5	93	,,	,,
	-108.3	SM_4	131	vdW	11.0
	-104.9	,,	155	vdW-3	14.4
	,,	SM_5	78	,,	,,
	-103.1	SM_4	143	vdW-4	16.2
	,,	SM_5	78	,,	,,
	-97.7	SM_4	148	vdW	21.6
SM_6-I	-46.2	SM_3	77	(SM_6–I) origin	0
	,,	SM_4	127	,,	,,

	,,	SM_5	181	,,	,,
	,,	SM_6	100	,,	,,
	-30.8	SM_3	71	vdW-1	15.4
	,,	SM_4	92	,,	,,
	,,	SM_5	157	,,	,,
	,,	SM_6	80	,,	,,
	-14.4	SM_5	120	vdW-2	31.8
	,,	SM_6	77	,,	,,
	-1.9	SM_5	109	vdW-3	44.3
	,,	SM_6	60	,,	,,
	9.7	SM_5	83	vdW-4	55.9
	,,	SM_6	52	,,	,,
	21.3	SM_5	52	vdW-5	67.5
	,,	SM_6	44	,,	,,
SM_6-II	-112.6	SM_5	162	SM_6–II origin	0
	,,	SM_6	110	,,	,,
	-100.6	SM_5	74	vdW-1	12.0
	,,	SM_6	114	,,	,,
	-95.8	SM_5	107	vdW-2	16.8
	,,	SM_6	104	,,	,,
SM_7-I	54.2	SM_6	168	SM_7–I origin	0
	,,	SM_7	58	,,	,,
	58.6	SM_6	41	vdW-1	4.4
	,,	SM_7	35	,,	,,
	63.9	SM_6	110	vdW-2	9.7
	,,	SM_7	41	,,	,,
	65.9	SM_6	79	vdW-3	11.7
	69.8	,,	50	vdW-4	15.6
	73.1	,,	38	vdW-5	18.9
	79.0	,,	39	vdW-6	24.8
SM_7–II	-89.1	SM_5	118	SM_7–II origin	0
	,,	SM_6	224	,,	,,
	,,	SM_7	78	,,	,,
	-80.4	SM_6	81	vdW	8.7
	,,	SM_7	67	,,	,,
	-78.5	,,	71	vdW-2	10.6
	-73.2	SM_6	117	vdW	15.9
	,,	SM_7	69	,,	,,
SM_8	36.1/34.2	SM_8	86/95	SM_8 origin	-

	-34.2	SM_7	161	,,	0
	-28.4	,,	96	VdW-1	7.7
	,,	SM_8	100	,,	,,
	-23.1	SM_7	117	VdW-2	13
	,,	SM_8	89	,,	,,
	-13.5	SM_7	108	VdW-3	22.6
	,,	SM_8	81	,,	,,
	-8.2	SM_7	68	VdW-4	27.9
	,,	SM_8	65	,,	,,
	-2.84	SM_7	77	VdW-5	33.26
SM_9-I	24.2/25.7	SM_8	66	SM_9-I origin	-
	24.2	SM_9	58	,,	0
	29.5	,,	84	VdW-1	5.3
	46.0	SM_8	78	VdW-2	20.3
	,,	SM_9	59	,,	,,
SM_9-II	-120.3	SM_8	91	SM_9–II origin	0
	,,	SM_9	30	,,	,,
	-111.2	SM_8	64	VdW-1	9.1
	,,	SM_9	40	,,	,,
	-104.9	,,	53	vdW-2	15.4
	-100.1	,,	48	vdW-3	20.2
	-94.4	,,	45	vdW-4	25.9
	-86.7	,,	61	vdW-5	33.6
	-77.5	,,	65	vdW-6	42.8
	-73.7	,,	77	vdW-7	46.6
	-67.9	,,	61	vdW-8	52.4
	-62.6	,,	77	vdW-9	57.7

Table 9: Fragmentations probabilities of the SM_n cluster ions.

Fragmentation channel	Parent, shift (cm^{-1})	%
$SM \rightarrow S$	63.4	65
SM_2-I$\rightarrow SM$	83.8	96
SM_2-II$\rightarrow SM$	3.4	4
SM_3-I$\rightarrow SM_2$	181.6	82
SM_3-II$\rightarrow SM_2$	16.5	2
$SM_4 \rightarrow SM_3$	-94.4	20
SM_5-I$\rightarrow SM_4$	-58.8	55
SM_5-II$\rightarrow SM_4$	-119.3	67
SM_6-I$\rightarrow SM_5$	-46.2	48
SM_6-II$\rightarrow SM_5$	-113.1	63
SM_7-I$\rightarrow SM_6$	54.2	81
SM_7-II$\rightarrow SM_6$	-89.1	61
SM_7-II$\rightarrow SM_5$	-89.1	26
$SM_8 \rightarrow SM_7$	-36.1	11
SM_9-I$\rightarrow SM_8$	24.2	27
SM_9-II$\rightarrow SM_8$	-120.3	74

.

4.4 R2PI of Styrene-Ethanol Clusters

4.4.1 Spectra of SE_n Clusters, n = 1-2

The R2PI absorption spectra obtained by monitoring the styrene, S, and styrene-$(C_2H_5OH)_n$, SE_n, (n = 1 and 2) mass channels are represented in Figure 27. In each mass channel, the assignments have been carefully designated to the observed spectral features taking into account the possible fragmentations from higher mass channels. The R2PI spectrum obtained for SE mass channel exhibits very rich spectral features starting form 37 cm^{-1} to 104 cm^{-1}. Several peaks with small intensities on the red side of styrene's origin (-10 to –80 cm^{-1}) were assigned to the S_2E cluster. The two isomeric clusters of SE are distinguishable in the R2PI spectrum of SE mass channel. The first isomer (SE-I), with an origin at 50 cm^{-1}, has very loaded vdW progression. This van der Waals progression of SE-I cluster is located at 58.1, 64.8, 72.1, 83.0, 88.5 and 93.0 cm^{-1} (corresponding to the peaks marked with solid circles in SE mass channel in Figure 27). The R2PI mass spectrum that was obtained at a resonance wavelength corresponding to the assigned 0_0^0 origin of SE-I is displayed in Figure 28. The intensity gained by the SE_2 mass peak is in the order of the background intensity that was measured in SE_2 mass channel. The second isomer (SE-II) possesses a low frequency origin at 11.2 cm^{-1} with one vdW peak at 16.6 cm^{-1}.

The assigned absorption features of SE_2-I isomer are in close proximity and interfere with those assigned to SE-I isomer as shown in SE mass channel in Figure 27. The origin transition of SE_2-I was blue shifted by 36.9 cm^{-1} relative to the 0_0^0 origin of styrene molecule. The van der Waals structure built on the origin transition of the SE_2-I is

assigned to peaks 1-9 and extends over 55 wavenumbers as illustrated in Figure 27. The presence of rich van der Waals progression indicates that the geometry of the SE_2-I neutral cluster is changed significantly upon the electronic excitation.

In SE_2 mass channel, very congested spectral features are observed over the scan range (–100 to 180 cm^{-1}). Most of the major features could be assigned either by searching for fragmented clusters in the higher mass channels or by observing the dissociative proton transfer reaction within S_2E_n clusters as will be discussed later. A second isomer for SE_2 cluster (SE_2-II) is detected with an origin at 16.9 cm^{-1} and two vdW modes at 20.3 and 23.9 cm^{-1}. In contrast to the first isomer, SE_2-II isomer does not show fragmentation into SE mass channel. This means that the structure of SE_2-II isomer does not seem to be affected upon photoionization.

Two sets of interfered spectral features belonging to two neutral clusters are recognized to the blue side in SE_2 mass channel. One set is assigned to S_2E_2-I cluster with peaks at 111.0, 138.0, 145.4, 151.5, 154.9 and 156.7 cm^{-1} (marked with open circles in SE_2 mass channel in Figure 27). The other set was assigned to SE_3-I cluster and composed of an origin at 108.9 cm^{-1} and four-associated vdW modes at 114.0, 120.4, 128.6 and 133.5 cm^{-1} (corresponding to the peaks marked with ▲ in SE_2 mass channel in Figure 27). The remaining absorption features to the red side in the SE_2 mass channel was assigned to S_2E_2 and S_2E_n, where $n > 2$.

4.4.2 Spectra of SE_n Clusters, n = 3-5

The R2PI spectra obtained by monitoring the mass channels corresponding to BE_3, BE_4 and BE_5 clusters in the region of the styrene $S_1 \leftarrow S_0$ transition are illustrated in Figure 29. The R2PI spectrum of SE_3 mass channel exhibits envelope shape with several spectral features appearing in the base line. The envelope shape could be due to the fragmentation processes from higher styrene/ethanol clusters into SE_3 mass channel. However, several features could be identified as fragmentations from S_2E_3 and SE_4-I clusters as shown in SE_3 mass channel in Figure 29. A set of four peaks in the red side to the 0_0^0 of styrene molecule was assigned to a second isomer of SE_3 (SE_3-II). The 0_0^0 origin of SE_3-II cluster is located at –46.2 cm^{-1} with the associated vdW modes at –39.6, -32.9 and –26.6 cm^{-1}. The remaining features could not be assigned because of the interference problem arising from the fragmentation processes.

In SE_4 mass channel, three isomers of SE_4 cluster have been identified. The first isomer (SE_4-I) has a weak blue-shifted origin at 107.4 cm^{-1} followed by two vdW peaks at 120.1 and 123.8 cm^{-1}. The origin peak together with one vdW peak appears in SE_3 mass channel and they are obscured by the background intensity measured in that channel. The second isomer (SE_4-II) possesses a red-shifted origin at –65.2 cm^{-1} and three vdW peaks at –62.5, -51.9 and –43.2cm^{-1}. The third isomer (SE_4-III) is the most red-shifted cluster with strong origin at –118.4 cm^{-1} only one vdW mode at –99.8 cm^{-1}. Figure 30 displays the R2PI mass spectrum that obtained at the resonance wavelength corresponding to the origin of SE_4-III isomer.

The most predominant feature at –104.3 cm^{-1} in the SE_5 mass channel is assigned to the origin of SE_5 cluster. This origin is followed by a vdW triplet at –100.7, -88.9 and –80.8 cm^{-1}. The R2PI mass spectrum at the origin of SE_5 is displayed in Figure 31.

The overall R2PI spectra of SE_n clusters are shown in Figure 32. The relative frequencies and tentative assignments of the SE_n, where n = 1–5, cluster isomers are recorded in Table 10.

4.4.3 Intracluster Reactions following Photoionization

No ion-molecule chemistry is observed in SE_n cluster series. However, the dissociative proton transfer (DPT) reactions are noticed in S_2E_n clusters ($n \geq 2$). Figure 33 shows that the spectral features of E_2H are in resonance with those of S_2E. This means that E_2H and S_2E are coming from the same reaction precursor, which is S_2E_2. These features also appear in S_2 and SE_2 mass channels. This suggests that S_2E_n clusters undergo DPT reactions (Eq. 4-3) in competition with the fragmentation reactions by either evaporating a styrene molecule (Eq. 4-4) or evaporating one or two ethanol molecules (Eq. 4-8 and Eq. 4-9, respectively). Figure 34 illustrates the observation of DPT reaction initiating from S_2E_3 cluster.

$$C_{16}H_{16}^{+}(C_2H_5OH)_n \rightarrow H^{+}(C_2H_5OH)_n + C_{16}H_{15} \cdots n \geq 2 \qquad \text{Eq. 4-3}$$

$$C_{16}H_{16}^{+}(C_2H_5OH)_n \rightarrow C_8H_8^{+}(C_2H_5OH)_n + C_8H_8 \qquad \text{Eq. 4-4}$$

$$C_{16}H_{16}^{+}(C_2H_5OH)_n \rightarrow C_{16}H_{16}^{+}(C_2H_5OH)_{n-1} + C_2H_5OH \qquad \text{Eq. 4-5}$$

$$C_{16}H_{16}^{+}(C_2H_5OH)_n \rightarrow C_{16}H_{16}^{+}(C_2H_5OH)_{n-2} + 2C_2H_5OH \qquad \text{Eq. 4-6}$$

As mentioned before with respect to the styrene/methanol system (see section 4.3.6), the DPT reaction is only feasible if the proton affinity (PA) of the methanol trimer (or now ethanol dimer) is higher than that of the styrene dimer. The reported proton affinity value for the ethanol dimer is 220.4 kcal/mol.[120] This, in turn, lowers the estimated upper limit for the proton affinity of the styrene dimer to ≤ 220.4 kcal/mol.

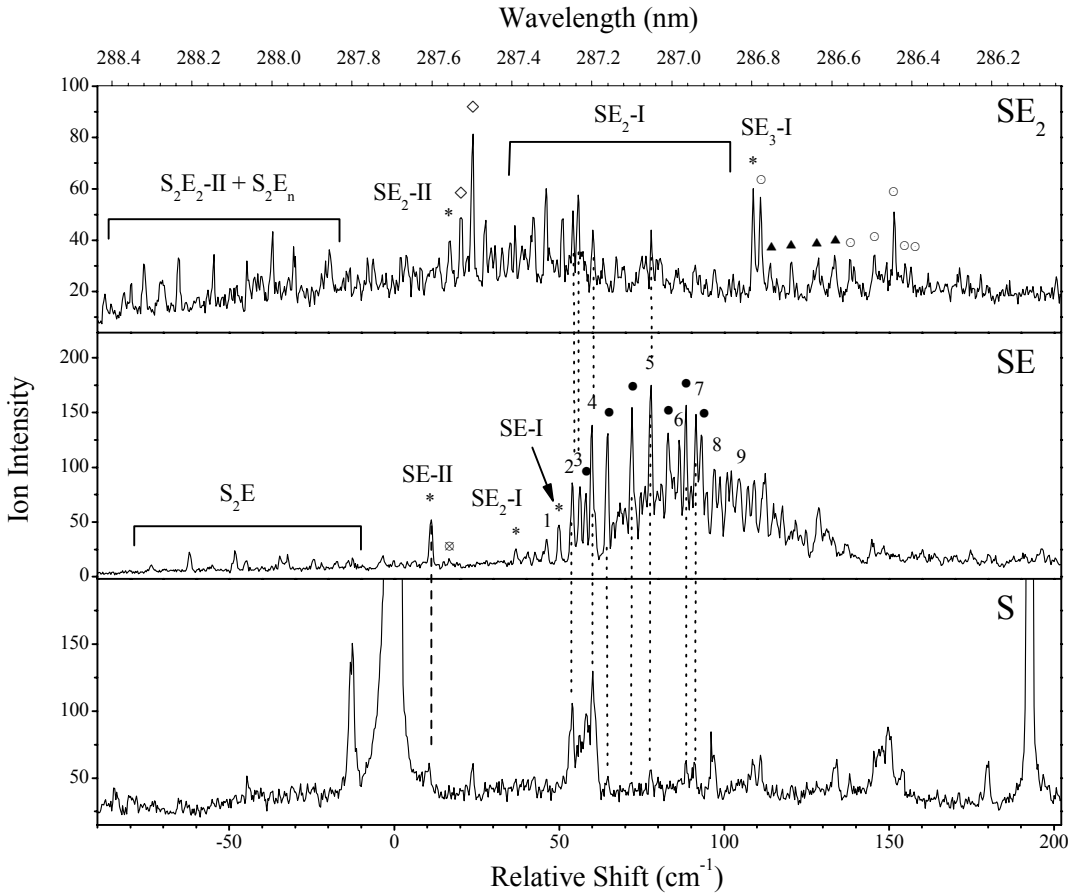

Figure 27: One-color R2PI spectra measured in styrene and styrene-(ethanol)$_n$ mass channels with n = 1-2, [S, SE and SE_2] relative to the electronic origin band of the $S_1 \leftarrow S_0$ transition of the styrene molecule at 34,758.79 cm^{-1}. The origin of each cluster isomer is marked with a (*). The peaks labeled with numbers, letters or symbols following each cluster's origin represent vdW bands associated with the cluster origin. The peaks labeled with (○) in SE_2 mass channel are assigned to S_2E_2-I isomer cluster (see Table 10).

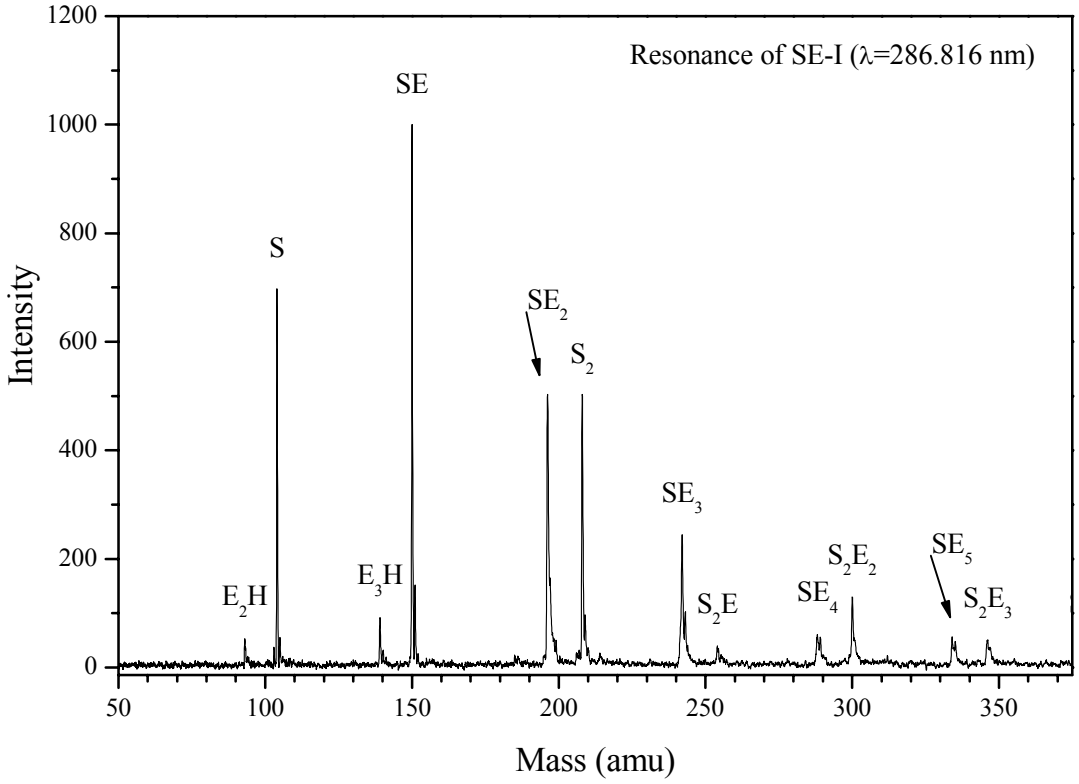

Figure 28: R2PI mass spectra of the styrene-ethanol (SE_n) cluster beam obtained at the resonance ionization assigned to the origin of SE-I cluster.

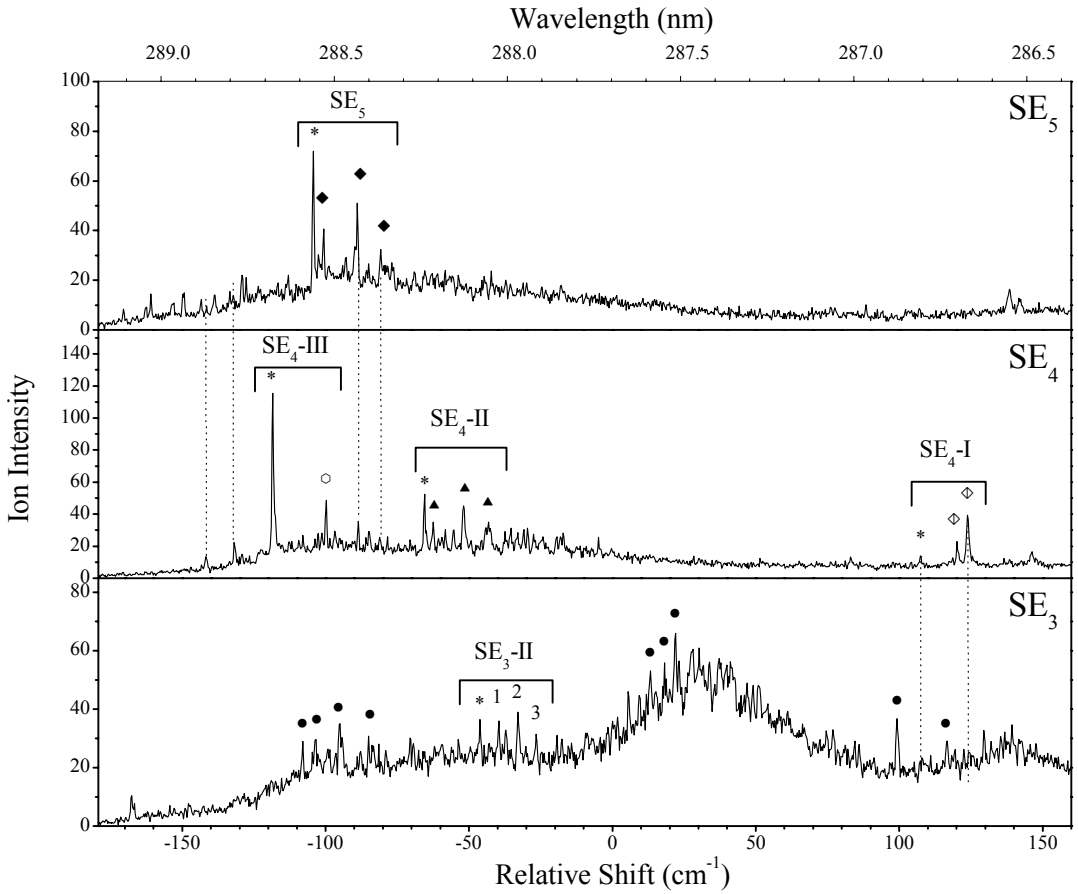

Figure 29: One-color R2PI spectra measured in the styrene-$(ethanol)_n$ mass channels with n = 3-5, [SE_3, SE_4 and SE_5] relative to the electronic origin band of the $S_1 \leftarrow S_0$ transition of the styrene molecule at 34,758.79 cm^{-1}. The origin of each cluster isomer is marked with a (*). The peaks labeled with numbers, letters or symbols following each cluster's origin represent vdW bands associated with the cluster origin. The peaks labeled with (●) in SE_3 mass channel are assigned to S_2E_3 cluster (see Table 10).

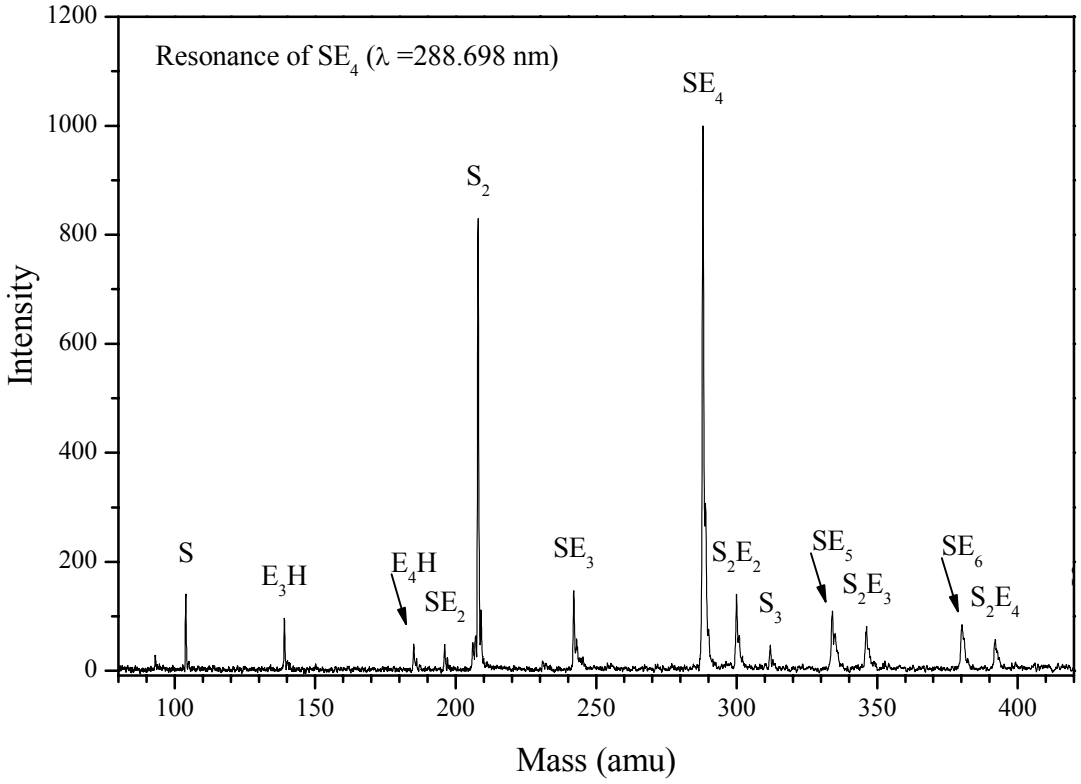

Figure 30: R2PI mass spectra of the styrene-ethanol (SE_n) cluster beam obtained at the resonance ionization assigned to the origin of SE_4 cluster.

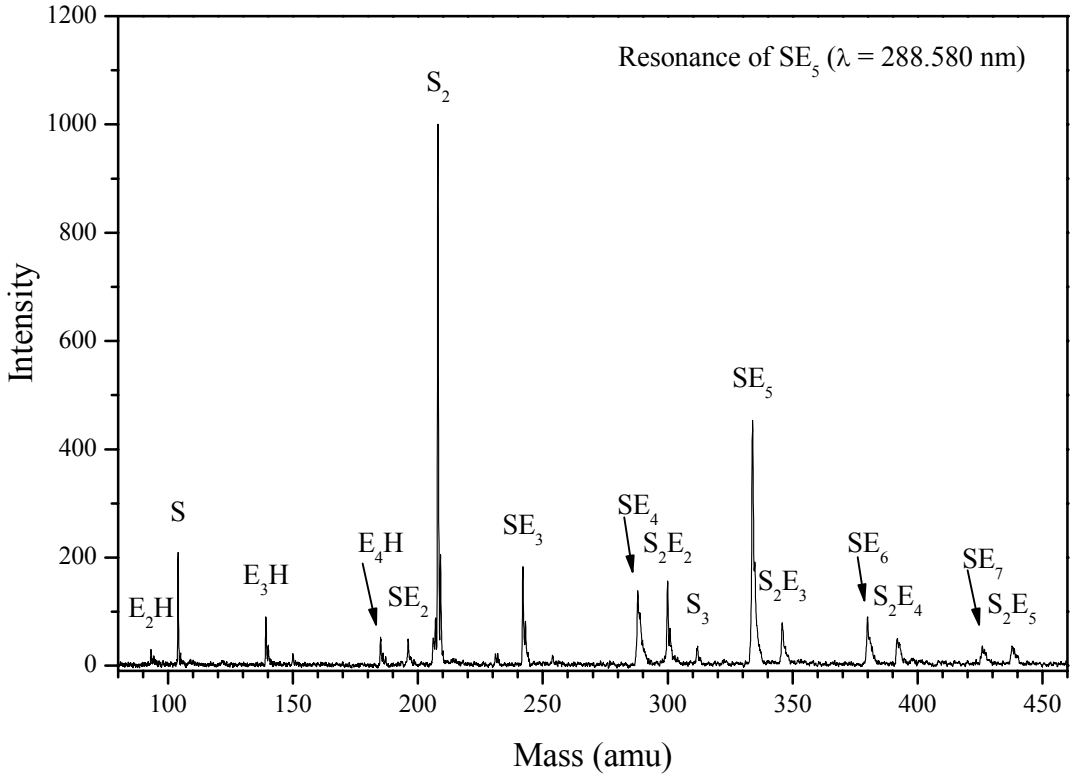

Figure 31: R2PI mass spectra of the styrene-ethanol (SE_n) cluster beam obtained at the resonance ionization assigned to the origin of SE_5 cluster.

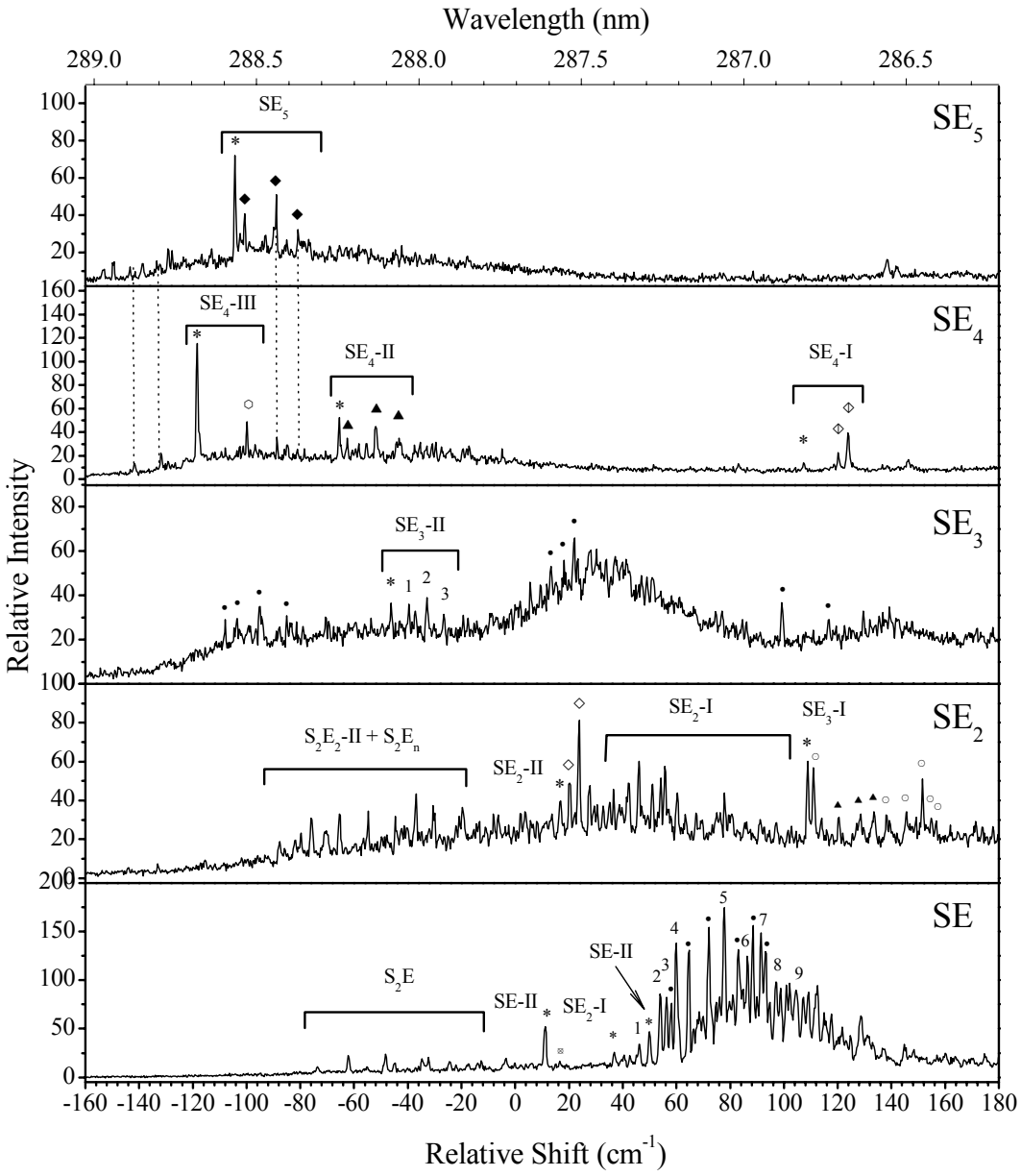

Figure 32: Overall R2PI spectra measured in the styrene-(ethanol)$_n$ mass channels (SE_n), n = 1-5, relative to the electronic origin band of the $S_1 \leftarrow S_0$ transition of the styrene molecule at 34,758.79cm^{-1}. The origin of each cluster isomer is marked with a (*). The peaks labeled with symbols following each cluster's origin represent vdW bands associated with the cluster origin (see Table 8). The peaks labeled with (●) and (○) in SE_2 and SE_3 mass channels are assigned to S_2E_2 and S_2E_3 clusters, respectively.

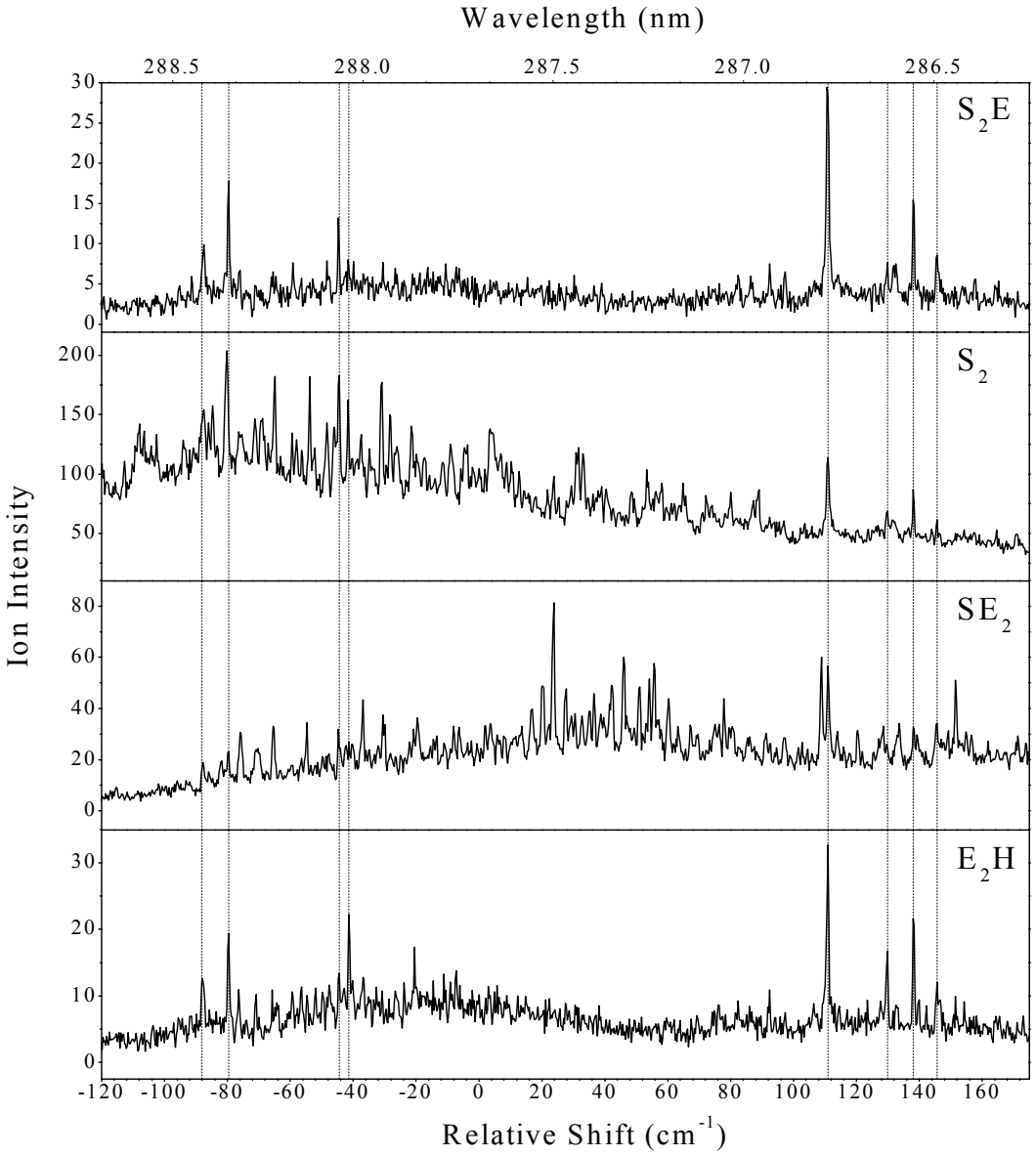

Figure 33: R2PI scans measured in E_2H, SE_2, S_2 and S_2E mass channels. The hashed lines point out the spectral features in resonance with those in the proton transfer product mass channel (E_2H). These features are assigned to S_2E_2 isomer clusters.

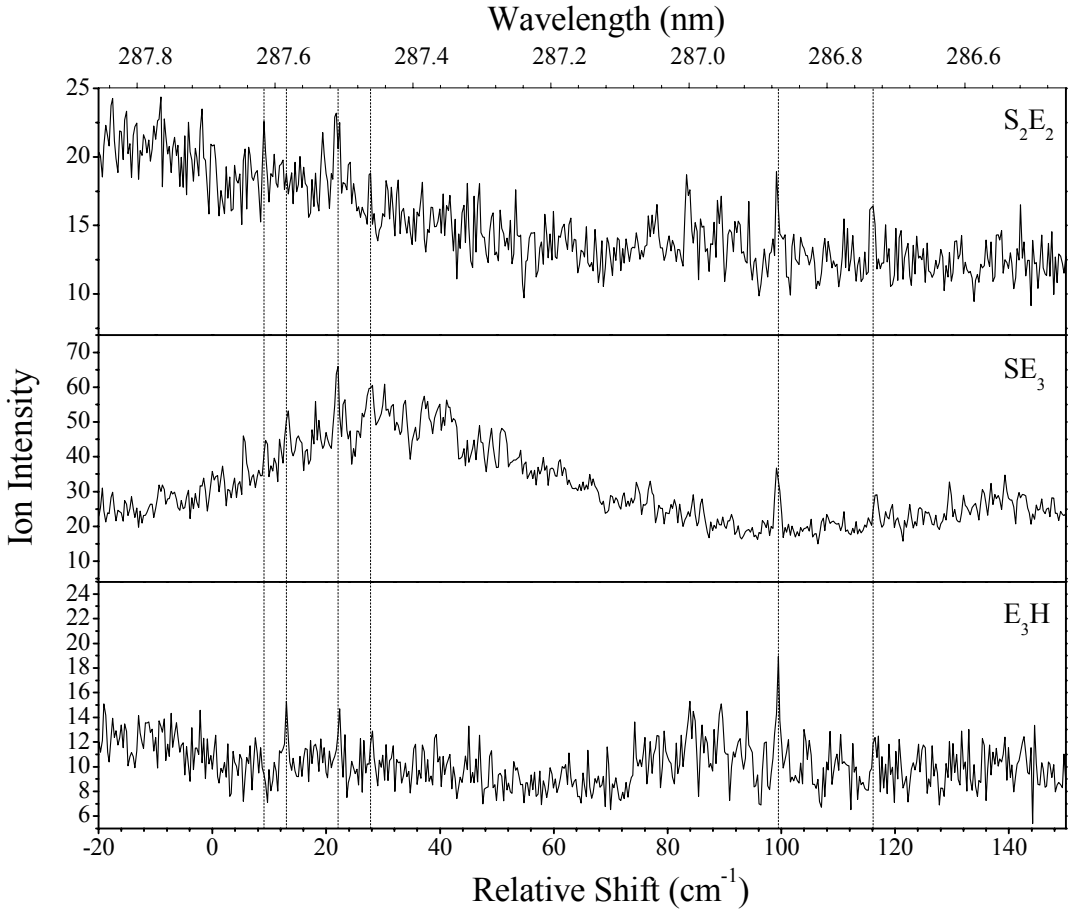

Figure 34: R2PI scans measured in E_3H, SE_3, and S_2E_2 mass channels. The hashed lines point out the spectral features in resonance with those in the proton transfer product mass channel (E_3H). These features are assigned to S_2E_3 cluster.

Table 10: Spectral features observed in the SE_n mass channels (S = styrene, E = ethanol, vdW = van der Waals mode).

Cluster	Shift (cm^{-1}) from the 0_0^0 of Styrene	Observed Mass Channel	Relative Intensity	Assignment	Shift (cm^{-1}) from Cluster's Origin
SE-I	50.0	SE	47	SE-I origin	0
	58.1	,,	76	vdW-1	8.1
	64.8	,,	131	vdW-2	14.8
	72.1	,,	155	vdW-3	22.1
	83.0	,,	131	vdW-4	33.0
	88.5	,,	157	vdW-5	38.5
	93.0	,,	129	vdW-6	43.0
SE-II	11.2	SE	52	SE-II origin	0
	16.6	,,	17	vdW	5.4
SE_2-I	36.9	SE	25	SE_2-I origin	0
	36.6	SE_2	47	,,	0
	46.3	SE	34	vdW-1	9.4
	46.0	SE_2	61	,,	9.4
	53.9	SE	86	vdW-2	17.0
	54.2	SE_2	51	,,	17.3
	56.3	SE	82	vdW-3	19.4
	56.0	SE_2	55	,,	19.4
	60.0	SE	138	vdW-4	23.7
	60.3	SE_2	44	,,	23.7
	77.9	SE	175	vdW-5	41.0
	77.9	SE_2	44	,,	41.3
	86.4	SE	125	vdW-6	49.5
	86.1	SE_2	29	,,	49.5
	91.5	SE	148	vdW-7	54.6
	91.2	SE_2	30	,,	54.6
	97.0	SE	98	vdW-8	60.1
	97.0	SE_2	28	,,	60.4
	104.6	SE	89	vdW-9	67.7
	104.6	SE_2	24	,,	68.0
SE_2-II	16.9	SE_2	40	SE_2-II origin	0
	20.3	,,	49	vdW-1	3.4

	23.9	,,	81	vdW-2	7.0
SE_3-I	108.9	SE_2	60	SE_3-I origin	0
	114.0	,,	31	vdW-1	5.1
	120.4	,,	31	vdW-2	11.5
	128.6	,,	33	vdW-3	19.7
	133.5	,,	34	vdW-4	24.6
SE_3-II	-46.2	SE_3	37	SE_3-II origin	0
	-39.6	,,	36	vdW-1	6.6
	-32.9	,,	39	vdW-2	13.3
	-26.6	,,	31	vdW-3	19.6
SE_4-I	107.4	SE_3	22	SE_4-I origin	0
	107.7	SE_4	13	,,	0
	120.1	,,	23	vdW-1	12.4
	124.1	SE_3	25	vdW-2	16.7
	123.8	SE_4	39	,,	16.1
SE_4-II	-65.2	SE_4	52	SE_4-II origin	0
	-62.5	,,	35	vdW-1	2.7
	-51.9	,,	45	vdW-2	13.3
	-43.2	,,	35	vdW-3	22.0
SE_4-III	-118.4	SE_4	115	SE_4-I origin	0
	-99.8	,,	49	vdW-1	18.6
SE_5	-104.3	SE_5	72	SE_5 origin	0
	-101.0	SE_4	28	vdW-1	3.3
	-100.7	SE_5	41	,,	3.6
	-88.6	SE_4	35	vdW-2	15.1
	-88.9	SE_5	51	,,	15.4
	-81.1	SE_4	26	vdW-3	23.2
	-80.8	SE_5	32	,,	23.5

4.5 R2PI of Styrene-Trifluoroethanol Clusters

4.5.1 Spectra of ST_n Clusters, n = 1-4

The binary mixed clusters of styrene and trifluoroethanol were investigated by using the R2PI technique. The R2PI spectra of the styrene-(trifluoroethanol)$_n$ clusters, C_8H_8-$(CF_3CH_2OH)_n$, were measured utilizing the $\tilde{A}^1A' \leftarrow \tilde{X}^1A'$ (0_0^0) transition of the styrene molecule, with n=1-4. The observed R2PI spectra of styrene-(trifluoroethanol)$_n$, ST_n, mass channels in Figure 35 reveal these spectral characterizations (1) the absence of the R2PI spectrum of ST ion cluster, (2) no evidence of cluster fragmentations was found in that system and (3) no intracluster ion products were obtained for that system under the given experimental conditions.

In liquid phase, reactions of styrene radical cation obtained by the laser excitation with 266 and 308 nm in neat trifluoroethanol alcohol have been observed.[121] Accordingly, one possible explanation for the absence of R2PI spectrum of ST^+ is that, upon photoexcitation of the ST cluster, radical reaction products are formed which are incapable of R2PI detection.

The observed spectral features in ST_2, ST_3 and ST_4 mass channels were assigned to 1:2, 1:3 and 1:4 neutral clusters, respectively. The most-red peaks in each mass channel could be assigned to the origins of the corresponding neutral cluster. The origins of 1:2, 1:3 and 1:4 neutral clusters are located at 53.92, 130.82 and 136.30 cm^{-1}, respectively. The small intensity peaks to the red side of 1:4 cluster's origin could be due another isomer. In each mass channel, several closely spaced features were observed following the cluster's

origin. The relative frequencies and the assignments of the ST_n clusters, with n =2-4, are tabulated in Table 11.

Shown in Figure 36 through Figure 38 are representative mass spectra measured at the origin of ST_n clusters. The mass spectra clearly show the mass peaks corresponding to (1) styrene clusters S_n, with n=1-3, (2) styrene-trifluoroethanol clusters ST_n, with n=1-5, and (3) styrene dimer-trifluoroethanol clusters S_2T_n, with n=1-3.

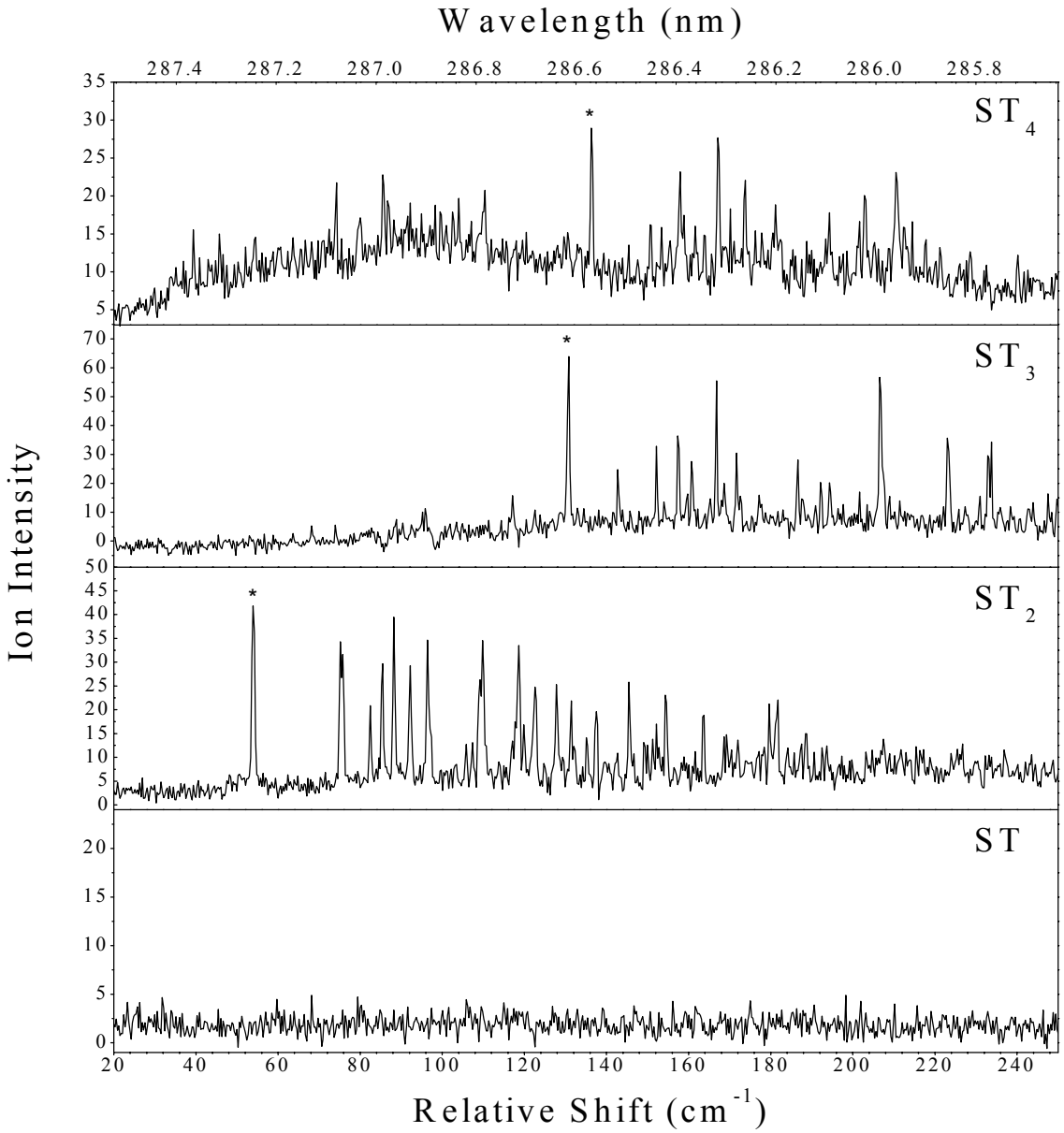

Figure 35: Overall R2PI spectra measured in the styrene-(trifluoroethanol)$_n$ mass channels (ST_n), n = 1-4, relative to the electronic origin band of the $S_1 \leftarrow S_0$ transition of the styrene molecule at 34,758.79 cm^{-1}. The origin of each cluster is marked with a (*).

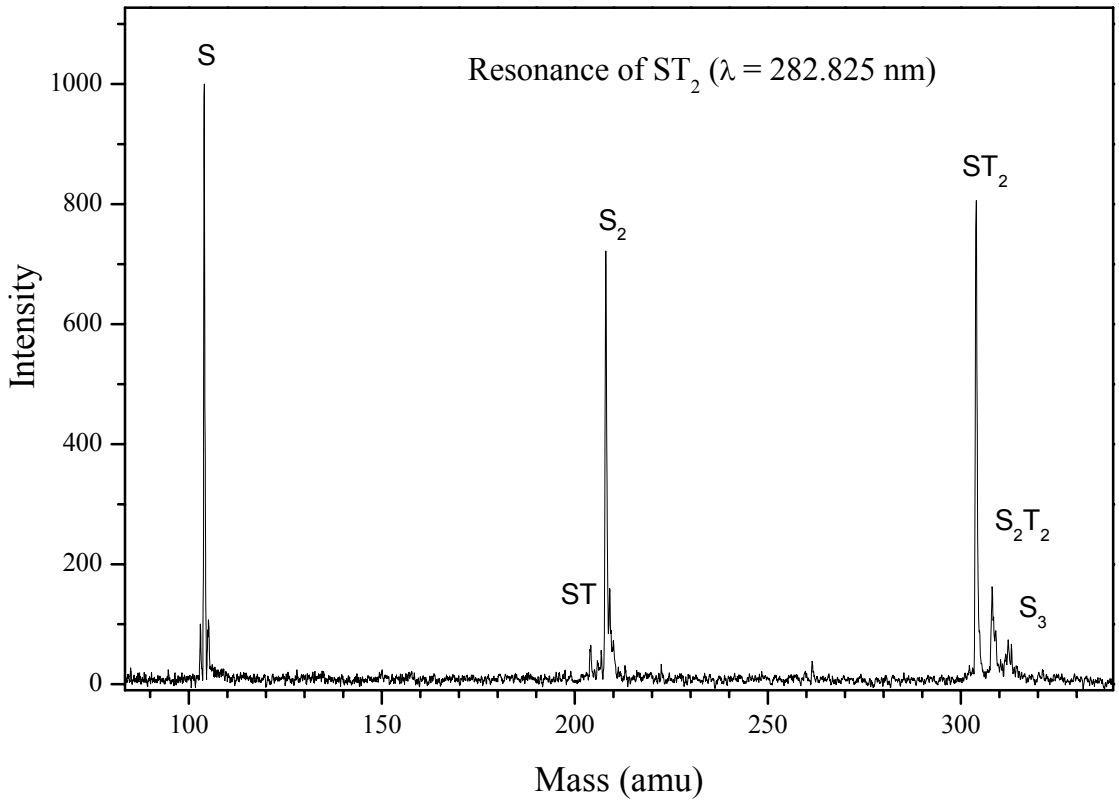

Figure 36: R2PI mass spectra of the styrene-trifluoroethanol (ST_n) cluster beam obtained at the resonance feature assigned to the origin of ST_2 cluster.

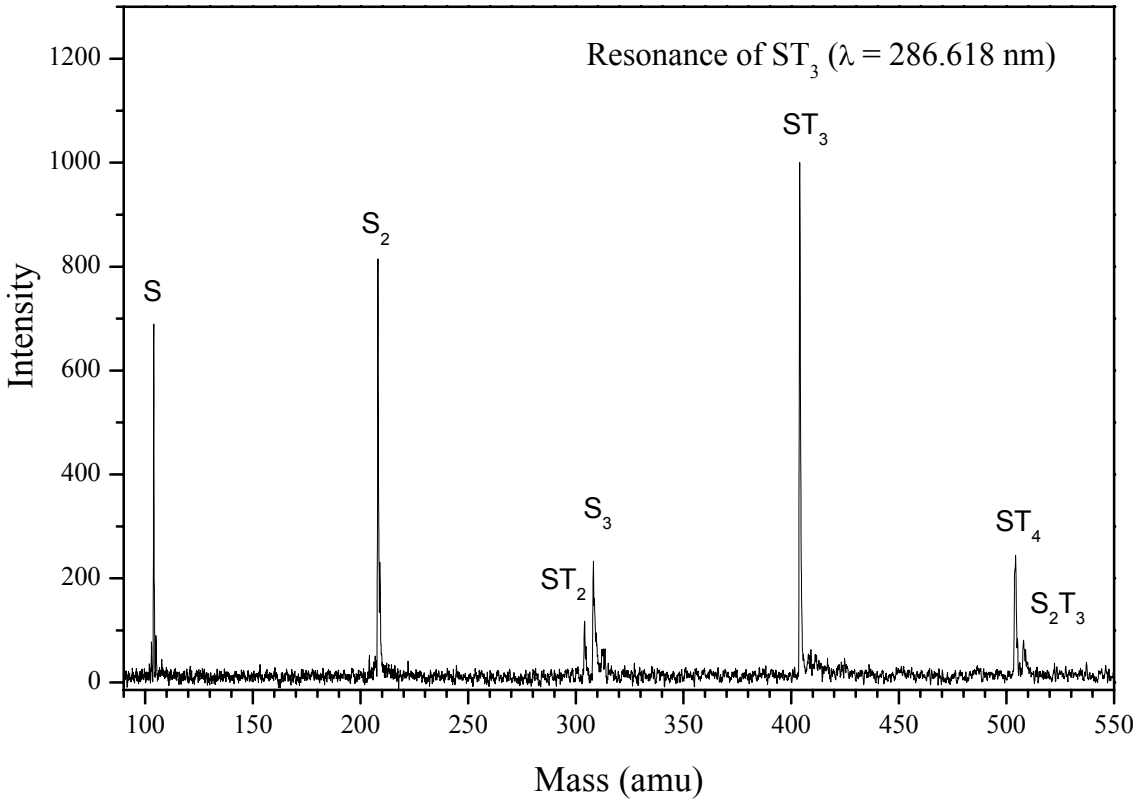

Figure 37: R2PI mass spectra of the styrene-trifluoroethanol (ST_n) cluster beam obtained at the resonance feature assigned to the origin of ST_3 cluster.

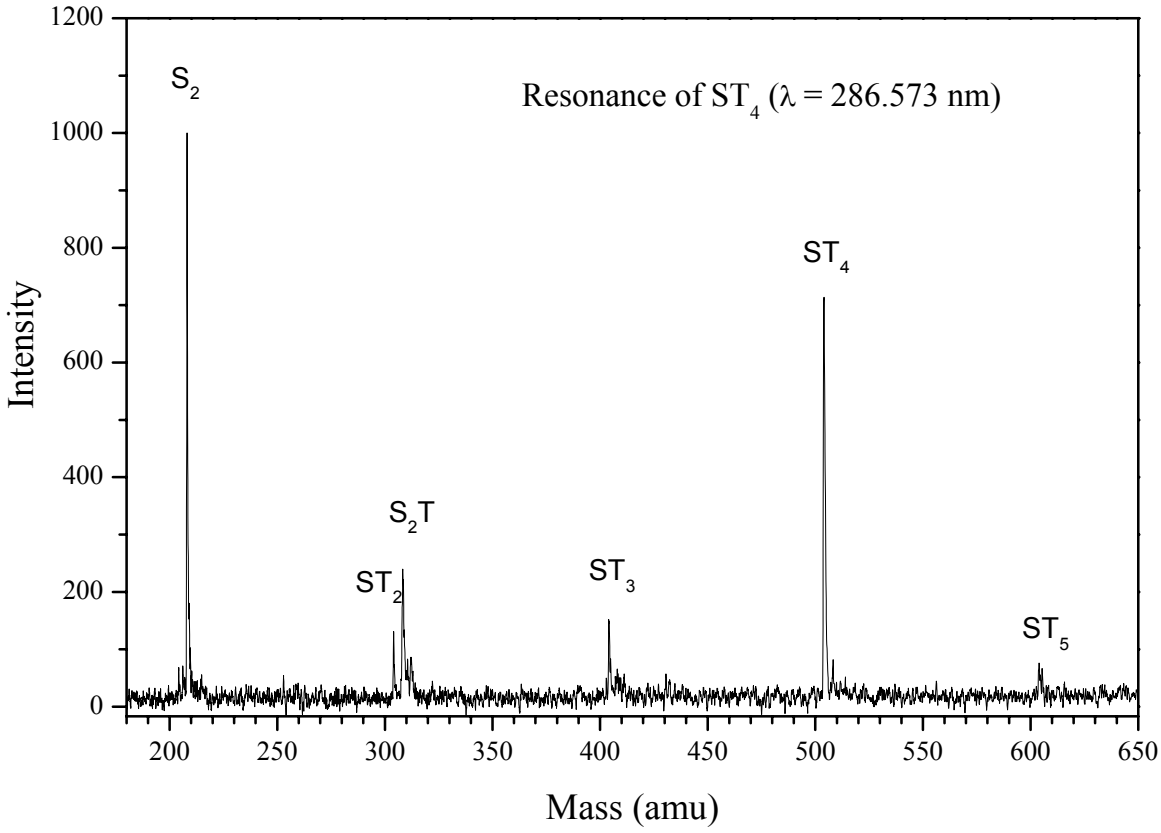

Figure 38: R2PI mass spectra of the styrene-trifluoroethanol (ST_n) cluster beam obtained at the resonance feature assigned to the origin of ST_4 cluster.

Table 11: Spectral features observed in the ST_n mass channels (S = styrene, T = trifluoroethanol)

Mass channel	Shift (cm^{-1}) from the 0_0^0 of styrene	Relative intensity	Assignments
ST_2	82.5	21	1:2 origin
	85.5	30	1:2
	88.2	39	1:2
	92.2	29	1:2
	96.4	35	1:2
	107.4	13	1:2
	109.8	35	1:2
	118.6	33	1:2
	119.9	17	1:2
	122.6	25	1:2
	127.8	25	1:2
	131.4	22	1:2
	135.1	14	1:2
	137.5	20	1:2
	145.4	26	1:2
	149.1	13	1:2
	154.3	23	1:2
	163.7	19	1:2
	169.2	15	1:2
ST_3	130.8	64	1:3 origin
	142.7	25	1:3
	152.1	33	1:3
	157.3	36	1:3
	160.7	28	1:3
	166.8	55	1:3
	171.7	30	1:3
	177.2	16	1:3
	186.6	28	1:3
	192.2	20	1:3
	206.5	57	1:3
	223.1	36	1:3
	233.8	34	1:3
	247.6	16	1:3
ST_4	136.3	29	1:4 origin
	145.4	14	1:4
	150.6	16	1:4

157.9	23	1:4
167.1	28	1:4
173.8	22	1:4
181.2	19	1:4
188.8	14	1:4
194.3	18	1:4
201.6	17	1:4
202.9	20	1:4
210.5	23	1:4

4.6 R2PI of Benzene-Ethanol and Benzene Deuterated Ethanol Clusters

The binary mixed clusters of benzene and ethanol were studied by using R2PI technique. The R2PI spectra for benzene-(ethanol)$_n$, C_6H_6-$(C_2H_5OH)_n$, were obtained via the $^1B_{2u} \leftarrow {}^1A_{1g}$ (6_0^1) transition of the benzene molecule, where n=1-5 (Figure 39). Ion-molecule chemistry yields were observed following the photoionization of benzene-(ethanol)$_n$ clusters. These are ionized ethanol clusters $(C_2H_5OH)_n$, where $n \geq 2$, the protonated ethanol clusters $(C_2H_5OH)_nH^+$, where $n \geq 3$, and the ionized products having the formula of $(C_2H_5OH)_n$-C_2H_5O, where n = 1 and 2. Same experiment was conducted on benzene-deuterated ethanol clusters, C_6H_6-$(C_2H_5OD)_n$, to further explore the ion-molecule reactions. The R2PI scan obtained in benzene-(deuterated ethanol)$_n$, C_6H_6-$(C_2H_5OD)_n$, where n = 1-6 is displayed in Figure 40. Also, well-resolved R2PI scans were obtained for $(C_6H_6)_2$-$(C_2H_5OD)_n$ and $(C_6H_6)_3$-$(C_2H_5OD)_n$ as shown in Figure 41 and Figure 42, respectively.

4.6.1 Intracluster Reactions following Photoionization

In one-color R2PI, the benzene molecule attains about 2730 cm^{-1} excess energy above the ionization threshold via its 6_0^1 transition. Following the photoionization of the neutral cluster, the ejected electron acquires most of this excess energy as a kinetic energy (Eq. 4-7). However, a considerable part of the excess energy is deposited in the cluster ion and thus increasing its internal energy. This, in turn, causes fragmentation of the cluster ion (Eq. 4-8) and initiates the molecule-ion chemistry. The precursors of the intracluster reactions are the neutral clusters of benzene-(ethanol)$_n$, C_6H_6-$(C_2H_5OH)_n$. The observed

intracluster reactions are dissociative electron transfer reaction DET (Eq. 4-9), dissociative proton transfer reaction DPT (Eq. 4-10) and hydrogen loss reaction. These reactions are in competition with the cluster fragmentation channel as shown in the following scheme:

R2PI:

$$C_6H_6-(C_2H_5OH)_n+2h\gamma_1 \rightarrow [C_6H_6-(C_2H_5OH)_n]^{+*}+e^- \qquad \text{Eq. 4-7}$$

Fragmentation:

$$[C_6H_6-(C_2H_5OH)_n]^{+*} \rightarrow [C_6H_6-(C_2H_5OH)_{n-1}]^{+}+C_2H_5OH \qquad \text{Eq. 4-8}$$

DET:

$$[C_6H_6-(C_2H_5OH)_n]^{+*} \rightarrow [(C_2H_5OH)_n]^{+}+C_6H_6 \qquad \text{Eq. 4-9}$$

DPT:

$$[C_6H_6-(C_2H_5OH)_n]^{+*} \rightarrow [H-(C_2H_5OH)_n]^{+}+C_6H_5 \qquad \text{Eq. 4-10}$$

The most efficient pathways for the cluster ions upon the ionization are the fragmentation channel and then the dissociative electron transfer channel. The dissociative electron transfer and dissociative proton transfer channel were observed for n ≥ 2 and n ≥ 3, respectively. The exothermicity of the proton transfer channel was tested. Unfortunately, not enough thermochemistry data was obtained to verify the energetic of the electron transfer channel. Assuming the following reaction, one can get the heat of reaction by knowing the heat of formations for $C_6H_6^+$, C_2H_5OH, C_6H_5 and $(C_2H_5OH)_nH^+$.

$$C_6H_6^+ + nC_2H_5OH \rightarrow (C_2H_5OH)_n H^+ + C_6H_5 \qquad \text{Eq. 4-11}$$

For protonated ethanol clusters $(C_2H_5OH)_nH^+$, only the heat of formations for n= 1-3 could be obtained. Since the heat of formations of protonated ethanol and protonated methanol clusters are very similar for n=1-3 (Table 12). Therefore, the heat of formation of

protonated methanol for n = 4 and 5, in very good approximation, was used to estimate the exothermicity of the DPT reactions in the analogous protonated ethanol clusters. Summarized in Table 13 is the thermochemical data that was used to calculate the heat of reaction in Eq. 4-11. The dissociative proton transfer DPT channel becomes apparently exothermic at protonated ethanol trimer by 30.3 kcal/mol (see Table 14). Although, the dissociative proton transfer DPT reaction is exothermic at protonated ethanol dimer (E_2H^+) by 8.9 kcal/mol, but it may not be enough to dissociate the intermediate complex [C_6H_5-$(C_2H_5OH)_2H^+$]. The formation of E_nH^+ becomes only possible if [$PA(C_6H_5)$ - $PA(E_n)$ + $D(C_6H_5\text{-}E_nH^+) < 0$], where PA and D are the proton affinity and the dissociation energy, respectively.[122] It seems that this condition is not fulfilled in the case of E_2H cluster ion but the dissociation energy was estimated for the intermediate complex [C_6H_5-$(C_2H_5OH)_2H^+$] to be $\geq$ 9.4 kcal/mol.

4.6.2 Spectra of Benzene Deuterated Ethanol (BD_n) Clusters, n = 1-5

Similar R2PI spectra were obtained for benzene/ethanol and benzene/deuterated ethanol clusters, therefore, only the results from the benzene/deuterated ethanol system were considered to avoid repetitive work.

The assignments for BD_n clusters, where 1:n is given for the number of benzene-to-deuterated ethanol in the neutral cluster responsible for the spectral features, are shown in Figure 40. The observation of intracluster reaction yields led to a clearly identifiable assignment of the neutral precursor cluster responsible for a particular spectral feature. The only exception is the 1:1 assignments in BD mass channel because there is no observable

ion-molecule chemistry products for n = 1. However, the fingerprints in the BD mass channel spectrum identical to those in D_2 (m/z = 94) and D_2-1 (m/z = 93) are assigned to 1:2 neutral cluster and the remaining features are assigned to 1:1 neutral cluster (see Figure 43). The mass spectrum obtained with the laser wavelength adjusted at 1:2 band shows masses 92, 93 and 94, corresponding to D_2-2, D_2-1 and D_2, respectively, arising from hydrogen loss and electron transfer reactions (Figure 44b). These masses confirm that the neutral precursor cluster must contain two C_2H_5OD molecules. On the other hand, these masses disappear when the laser is tuned to the feature of 1:1 as shown in Figure 44a.

Spectral characterizations of D_3 mass channel reveal that 1:3 neutral cluster possesses two isomers (Figure 45). Several bands toward the blue side in D_3 mass channel (starting from 123.04 to 161.78 cm^{-1}) are due to the first isomer 1:3 (I). While, the two most-red bands at –73.72 and –75.82 cm^{-1} are due to the second isomer 1:3 (II). The first isomer 1:3 (I) exhibits, unlike the red shifted isomer 1:3(II), efficient fragmentation into BD_2 mass channel and intense ion-molecule chemistry. The mass spectra obtained at the resonance features of the two isomers support the assignments. The mass spectrum obtained at the resonance feature of 1:3 (I) cluster is displayed in Figure 46a. The mass spectrum shows enhanced ion intensities for D_3-1 and D_3 masses. While, the mass spectrum recorded at the resonance feature of 1:3 (II) shows small ion intensity for D_3-1 mass and the BD_2 mass peak is almost disappear (Figure 46b).

As with the 1:2 and 1:3 clusters, the D_4 ion cluster is assigned to the electron transfer reaction taking place in 1:4 neutral precursor cluster. The fingerprints originating at 3.95 cm^{-1} in the D_4 mass channel spectrum, which are identical to those in BD_3 and BD_4

mass channels, are assigned to 1:4 cluster (as shown in Figure 47). The 1:4 cluster is showing a little fragmentation into BD_3 mass channel. The mass spectrum in Figure 48 obtained at the resonance feature of BD_4 shows enhanced intensity for BD_4 and D_4 mass peaks and small ion intensity for BD_3 peak.

D_5 ion cluster is the electron transfer product from the BD_5 neutral cluster. It has spectral features originating at –44.97 cm^{-1} and matching some features in BD_4 mass channel spectrum as clearly seen in Figure 49. These features are assigned to 1:5 cluster. The mass spectrum obtained at the resonance feature of 1:5 cluster is displayed in Figure 50. The relative frequencies and careful assignments of the BD_n clusters are recorded in Table 15.

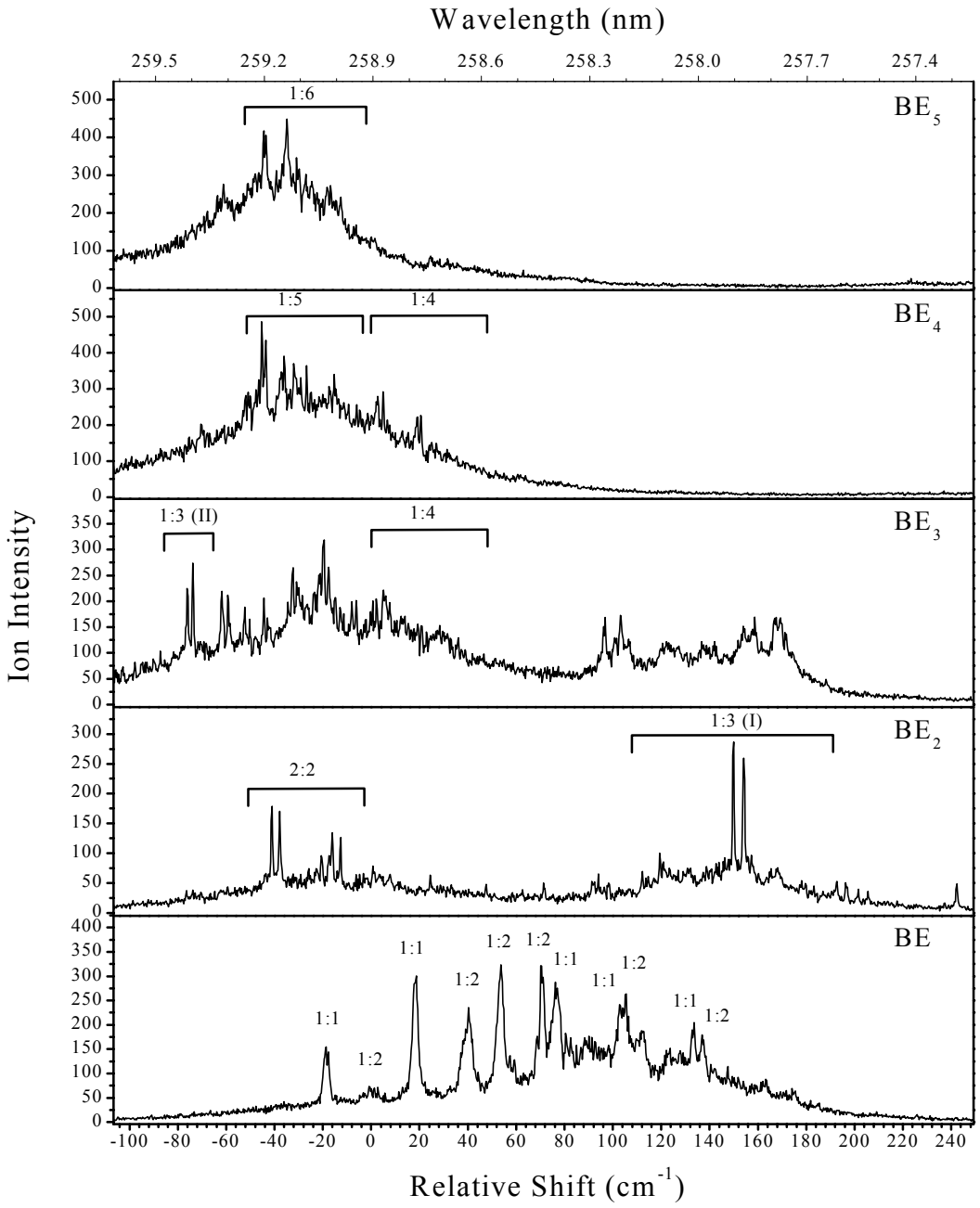

Figure 39 Overall R2PI spectra measured in the benzene (ethanol)$_n$ mass channels (BE$_n$), n = 1-5, relative to the 6_0^1 transition of the benzene molecule at 38,624.95 cm^{-1}. The peak labels (m:n) stand for the number of benzene:ethanol in the neutral cluster responsible for the spectral features.

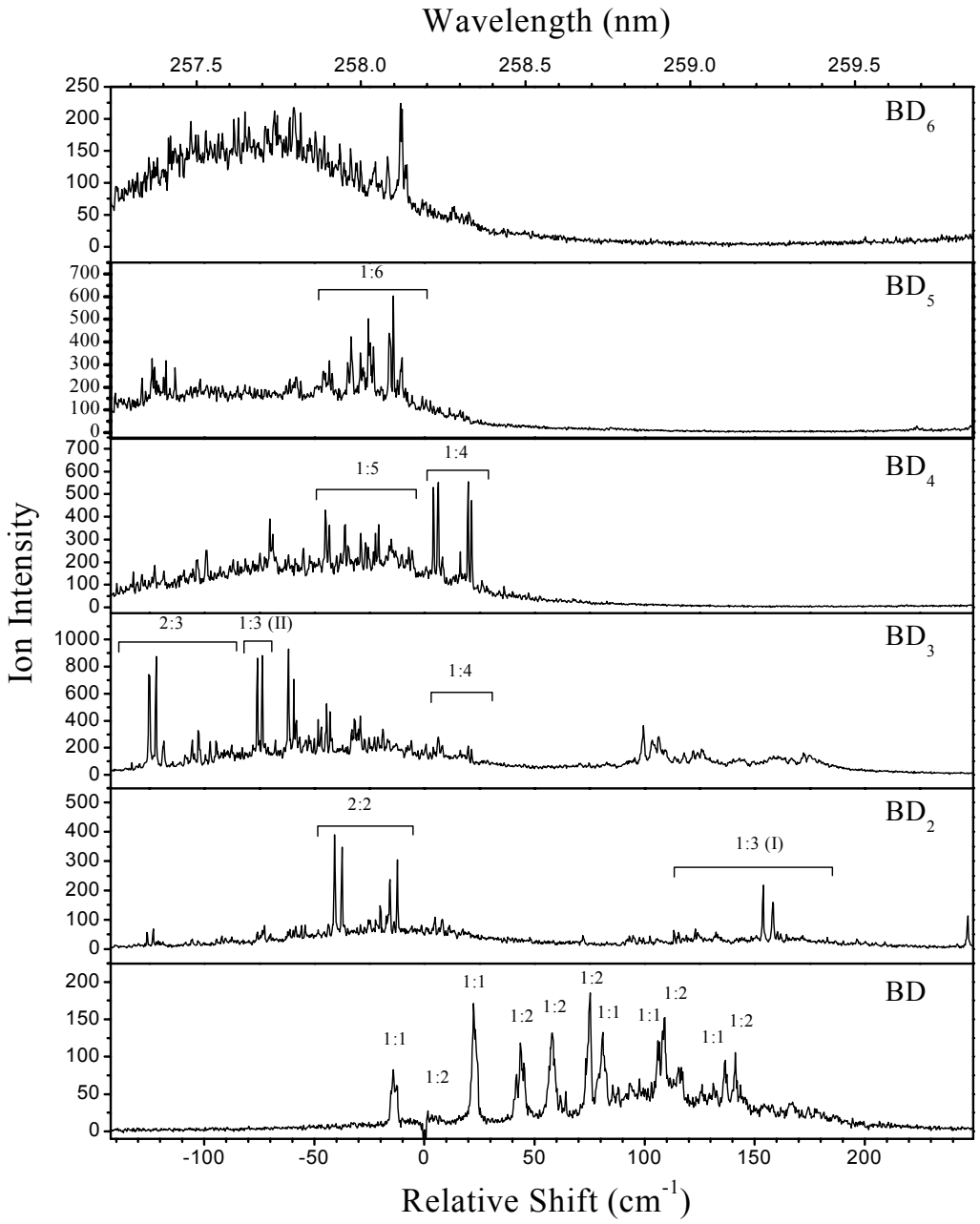

Figure 40: Overall R2PI spectra measured in the benzene (deuterated ethanol)$_n$ mass channels (BD_n), n = 1-6, relative to the 6_0^1 transition of the benzene molecule at 38,624.95 cm^{-1}. The peak labels (m:n) stand for the number of benzene:deuterated ethanol in the neutral cluster responsible for the spectral features (see Table 15).

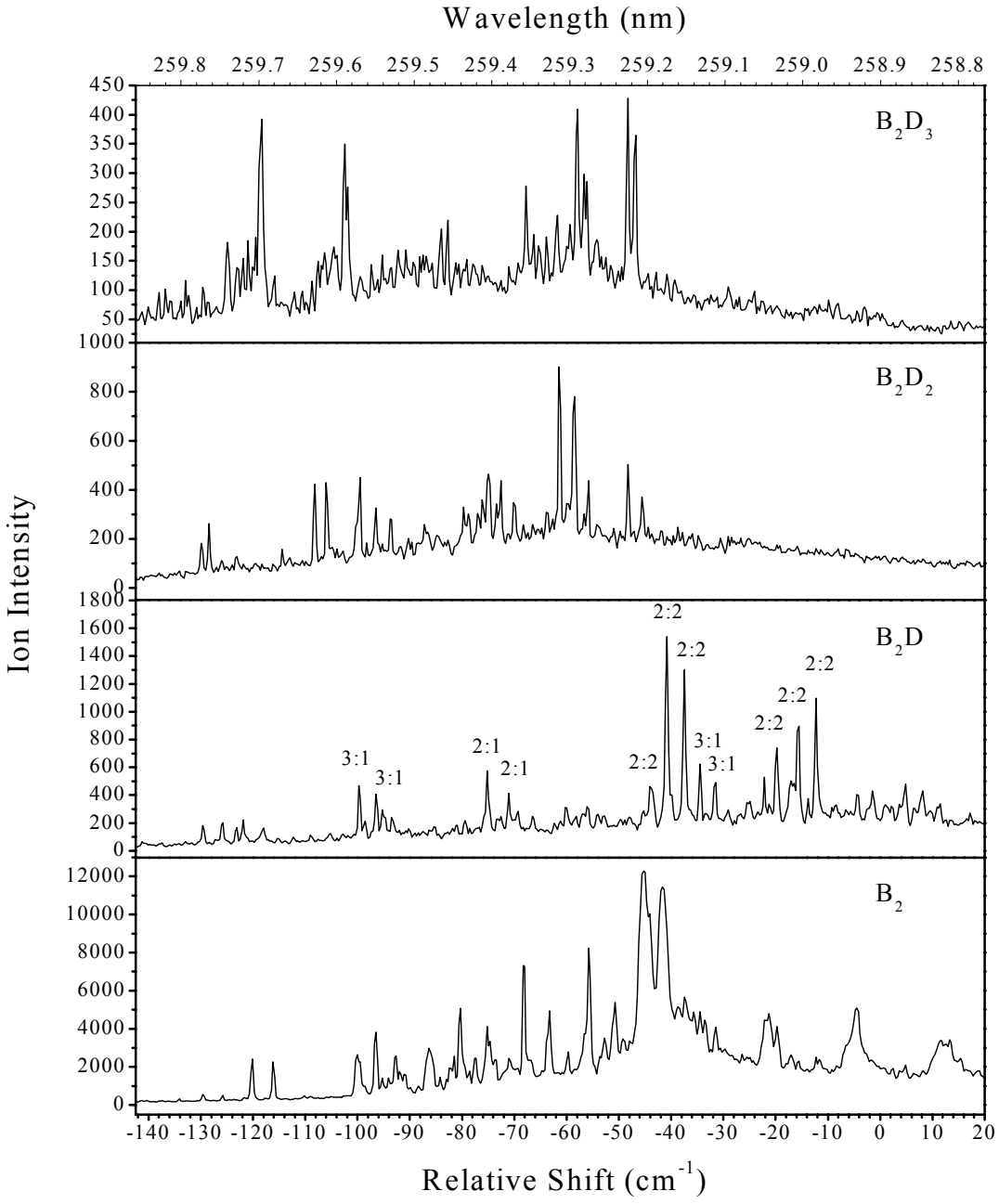

Figure 41: One-color R2PI spectra measured in $(benzene)_2$, B_2, and $(benzene)_2$ - $(deuterated\ ethanol)_n$ mass channels (B_2D_n), n = 1-3, relative to the 6_0^1 transition of the benzene molecule at 38,624.95 cm^{-1}.

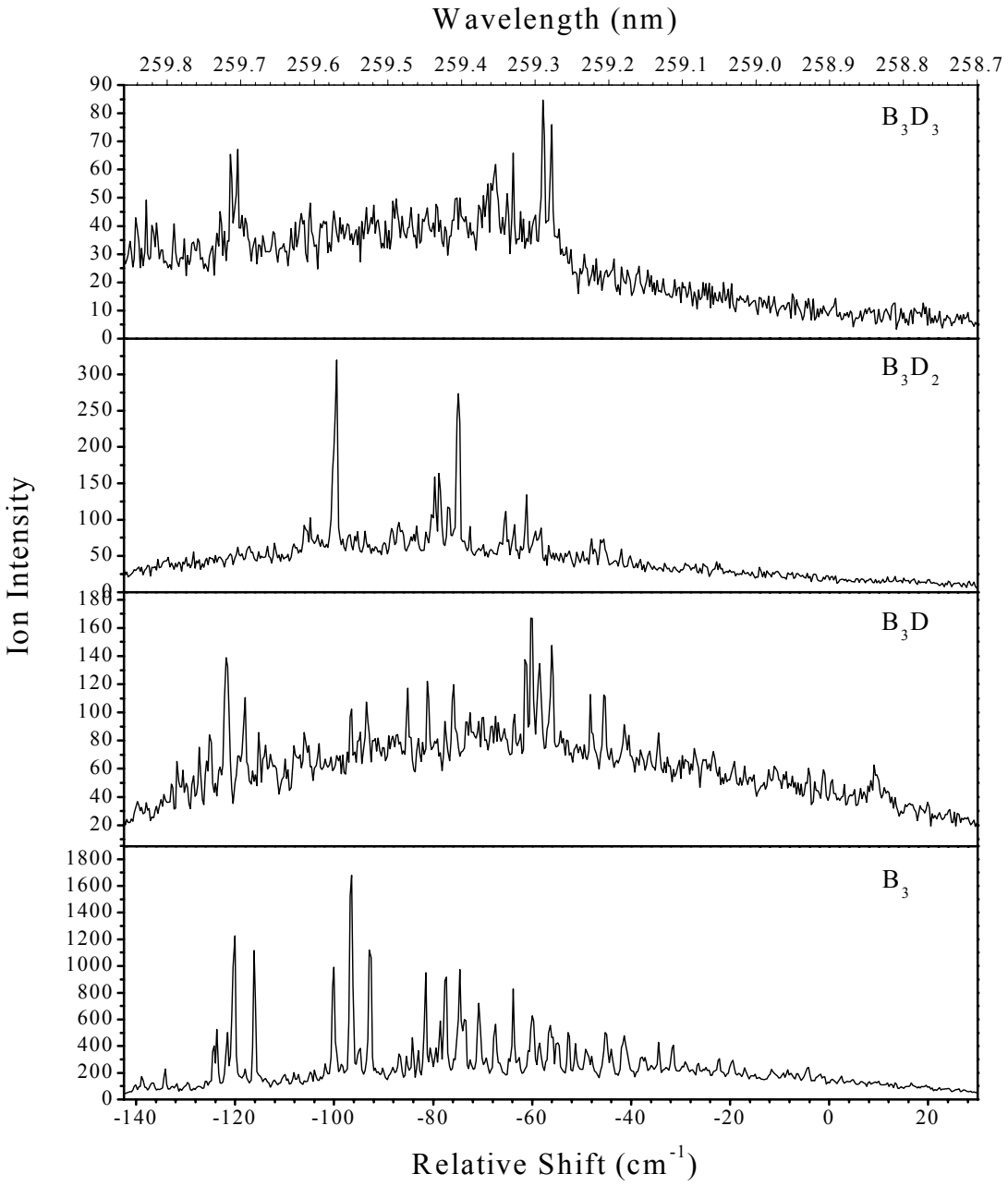

Figure 42: One-color R2PI spectra measured in $(benzene)_3$, B_3, and $(benzene)_3$-$(deuterated\ ethanol)_n$ mass channels (B_3D_n), n = 1-3, relative to the 6_0^1 transition of the benzene molecule at 38,624.95 cm^{-1}.

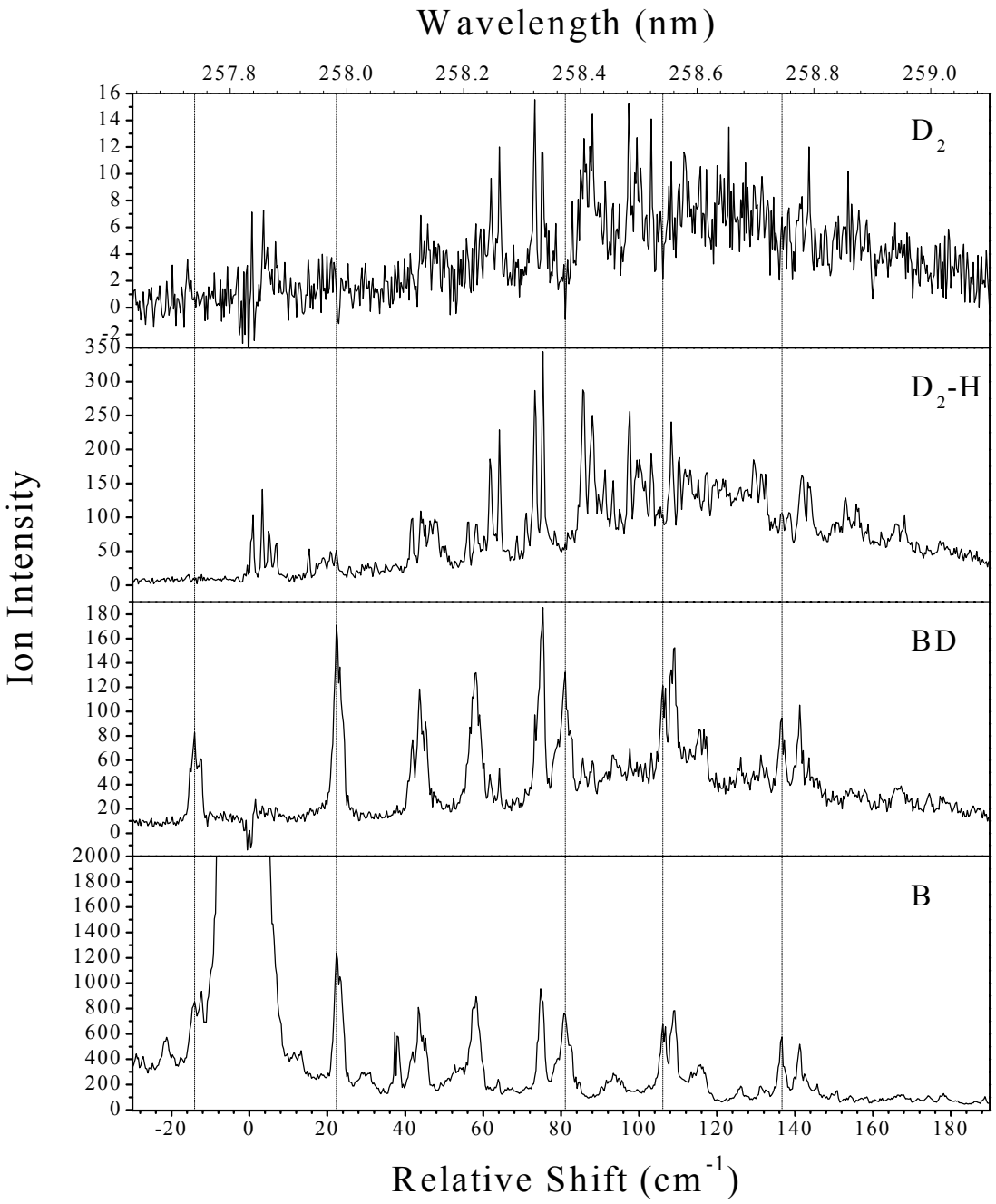

Figure 43: One-color R2PI spectra measured in benzene, B, deuterated ethanol, BD, $(C_2H_5OD)(C_2H_4OD)$, D_2-H, and $(C_2H_5OD)_2$, D_2, mass channels relative to the 6_0^1 transition of the benzene molecule at 38,624.95 cm^{-1}. The dashed lines indicate the peaks that assigned to 1:1 cluster. Notice the disappearance of these peaks from the D_2 and D_2-H mass channels (see the text).

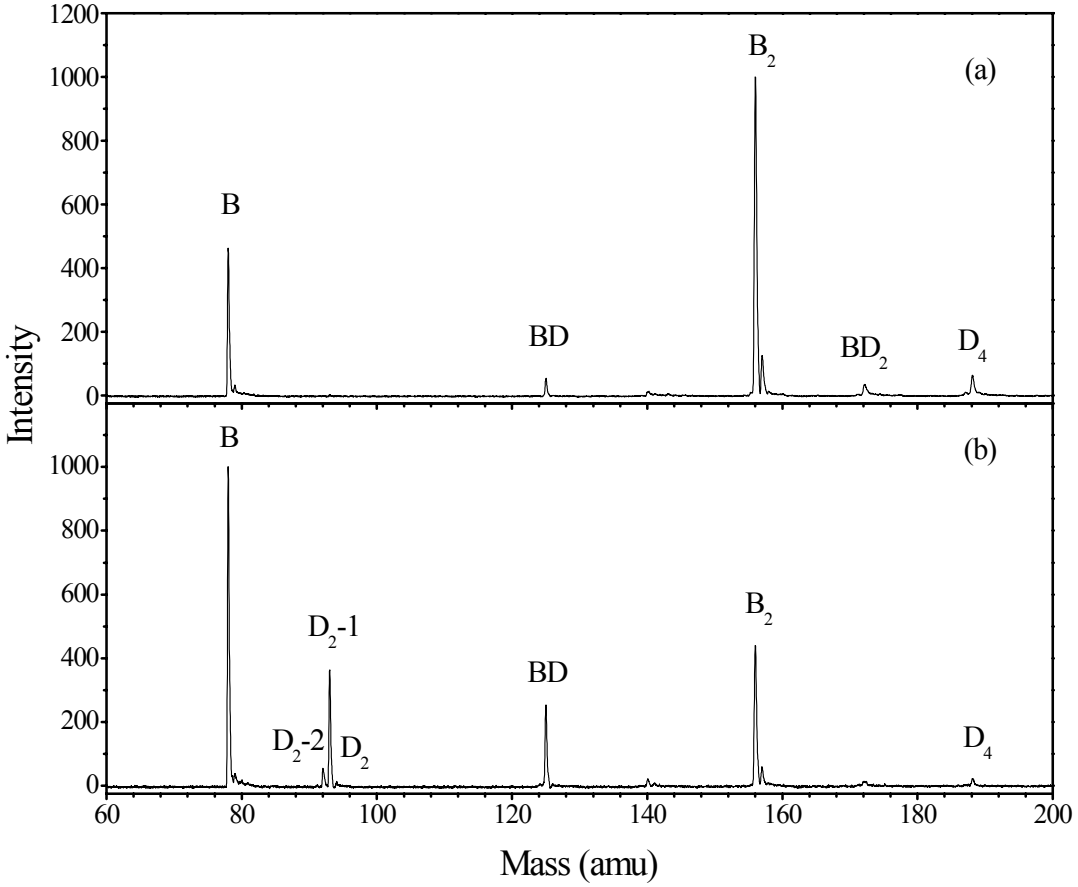

Figure 44: R2PI mass spectra of benzene-deuterated ethanol (BD) cluster beam obtained at the resonance wavelengths assigned to 1:1 and 1:2 neutral clusters at (a) 258.994 nm and (b) at 258.396 nm, respectively.

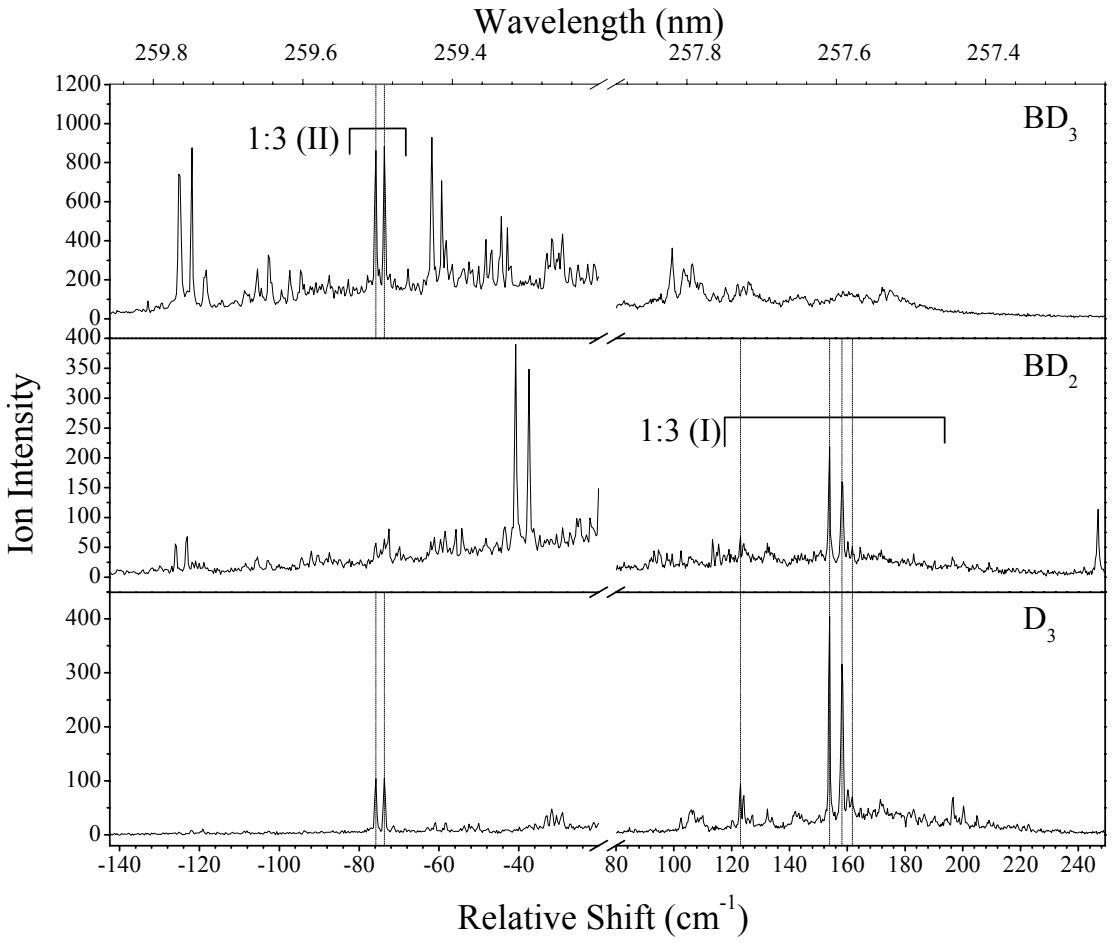

Figure 45: One-color R2PI spectra measured in $(C_2H_5OD)_3$, D_3, benzene-(deuterated ethanol)$_2$, BD_2, benzene-(deuterated ethanol)$_3$, BD_3, and mass channels relative to the 6_0^1 transition of the benzene molecule at 38,624.95 cm^{-1}. The dashed lines indicate the peaks that assigned to the blue shifted 1:3 (I) and the red shifted 1:3 (II) clusters in BD_2 and BD_3 mass channels, respectively.

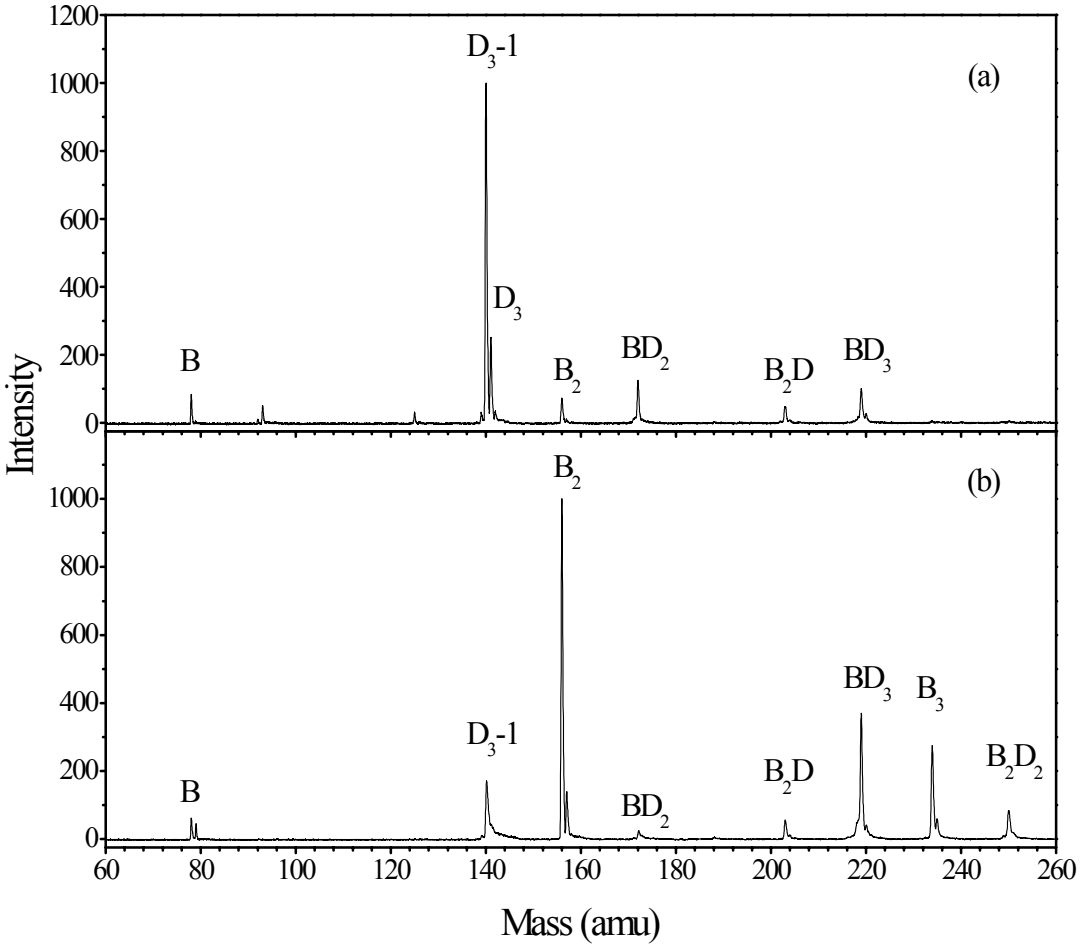

Figure 46: R2PI mass spectra of benzene-deuterated ethanol (BD) cluster beam obtained at the resonance wavelengths assigned to the 1:3 (I) and 1:3 (II) neutral clusters at (a) 257.842 nm and (b) at 259.395 nm, respectively.

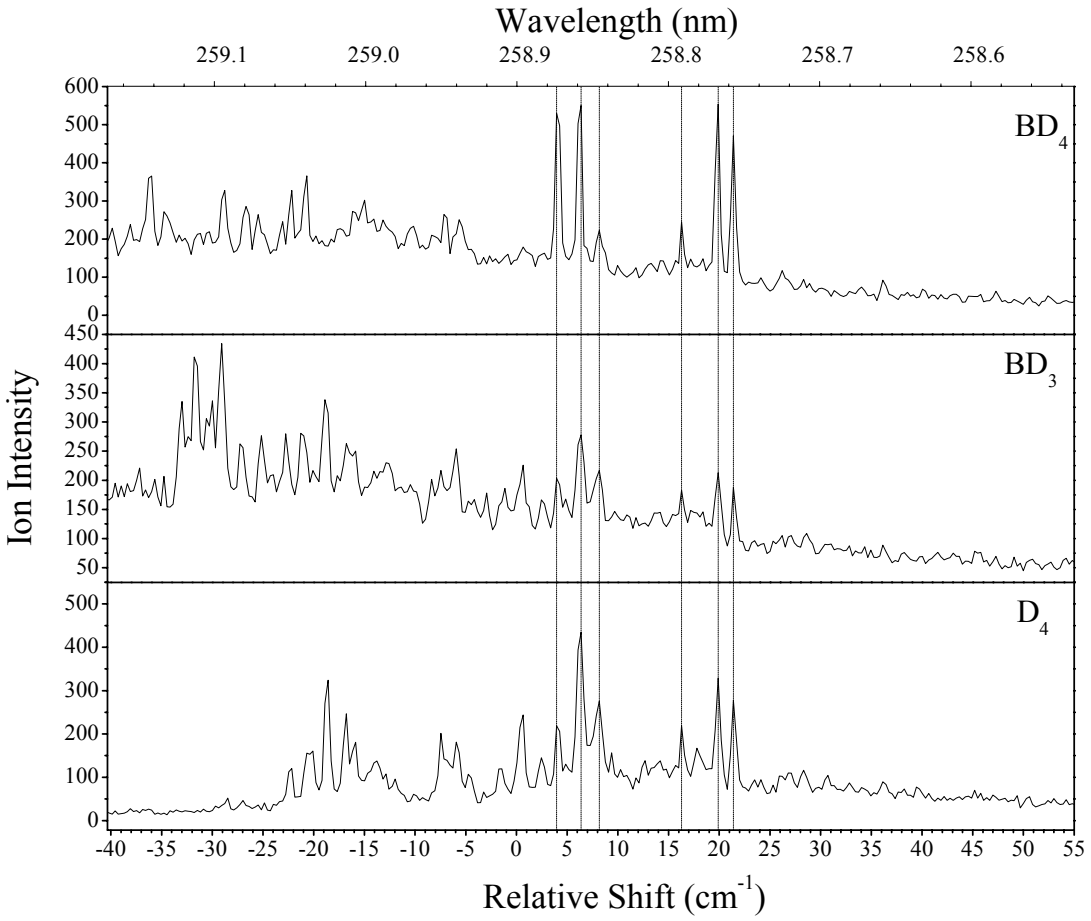

Figure 47: One-color R2PI spectra measured in $(C_2H_5OD)_4$, D_4, benzene-(deuterated ethanol)$_3$, BD_3, benzene-(deuterated ethanol)$_4$, BD_4, and mass channels relative to the 6_0^1 transition of the benzene molecule at 38,624.95 cm^{-1}. The dashed lines indicate the peaks that assigned to the spectral features of 1:4 neutral cluster in BD_3 and BD_4 mass channels.

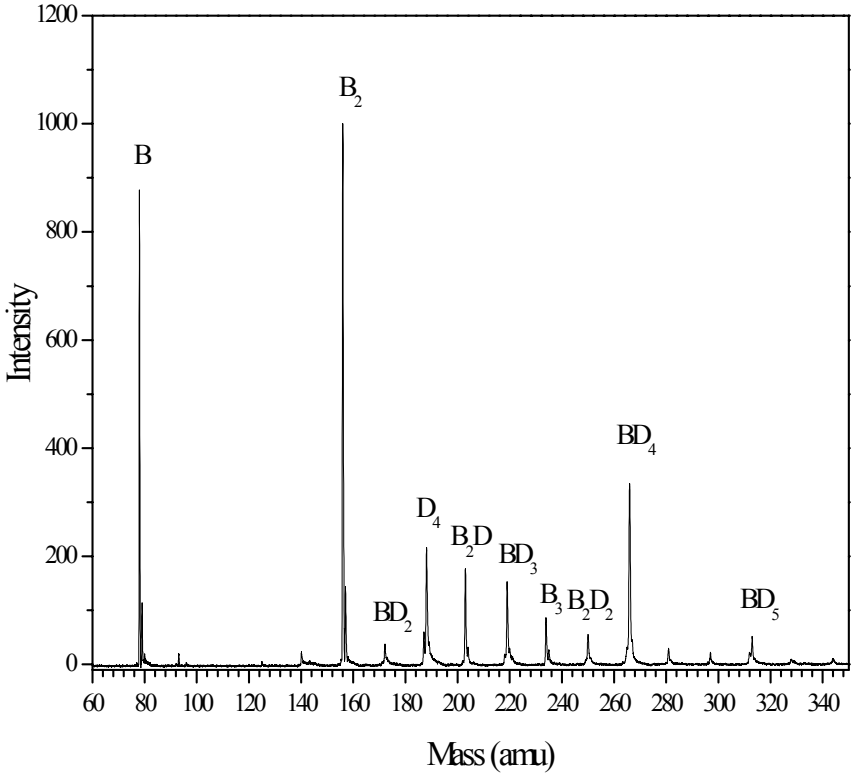

Figure 48: R2PI mass spectra of benzene-deuterated ethanol (BD) cluster beam obtained at the resonance wavelength assigned to the 1:4 neutral cluster at 258.857 nm.

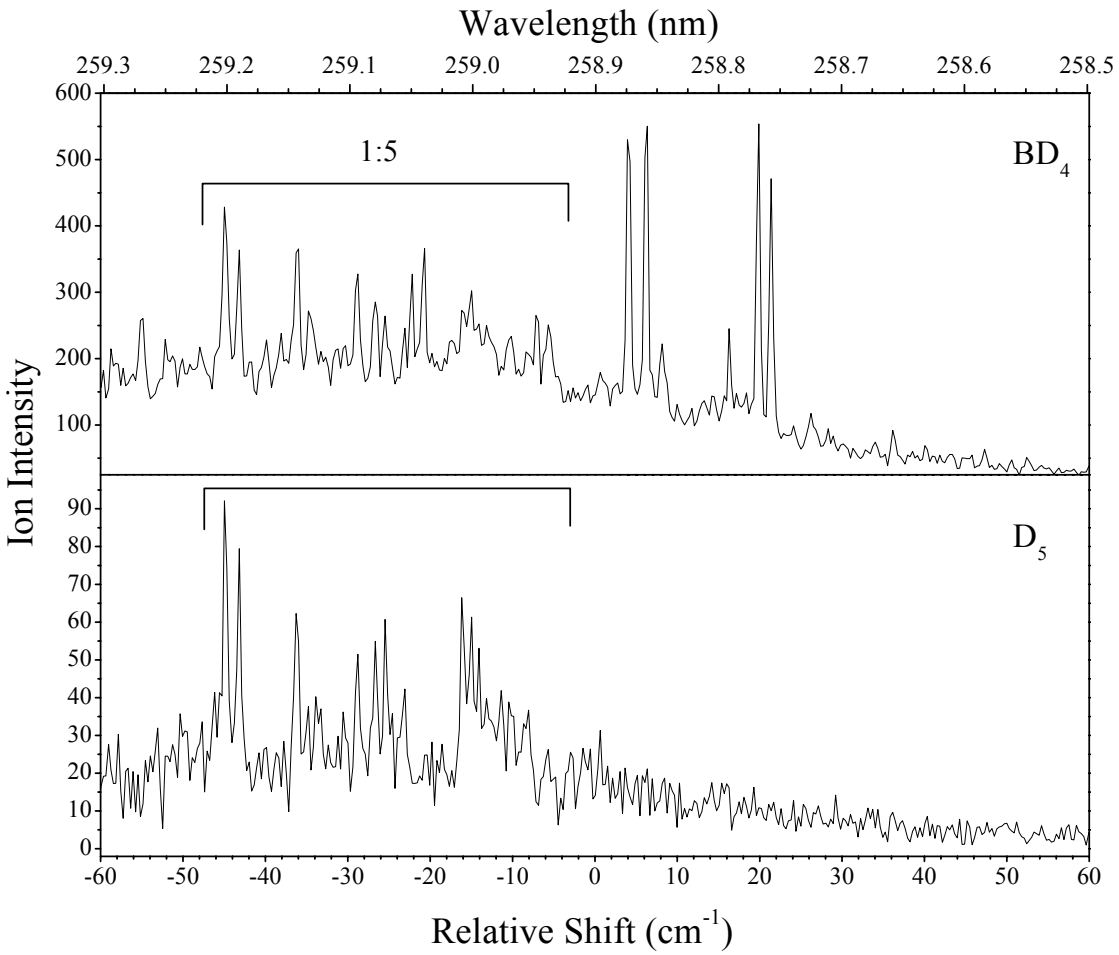

Figure 49: One-color R2PI spectra measured in $(C_2H_5OD)_5$, D_5, and benzene-(deuterated ethanol)$_4$, BD_4, mass channels relative to the 6_0^1 transition of the benzene molecule at 38,624.95 cm^{-1}. The same spectral features that are in resonance in both channels assigned to 1:5 cluster.

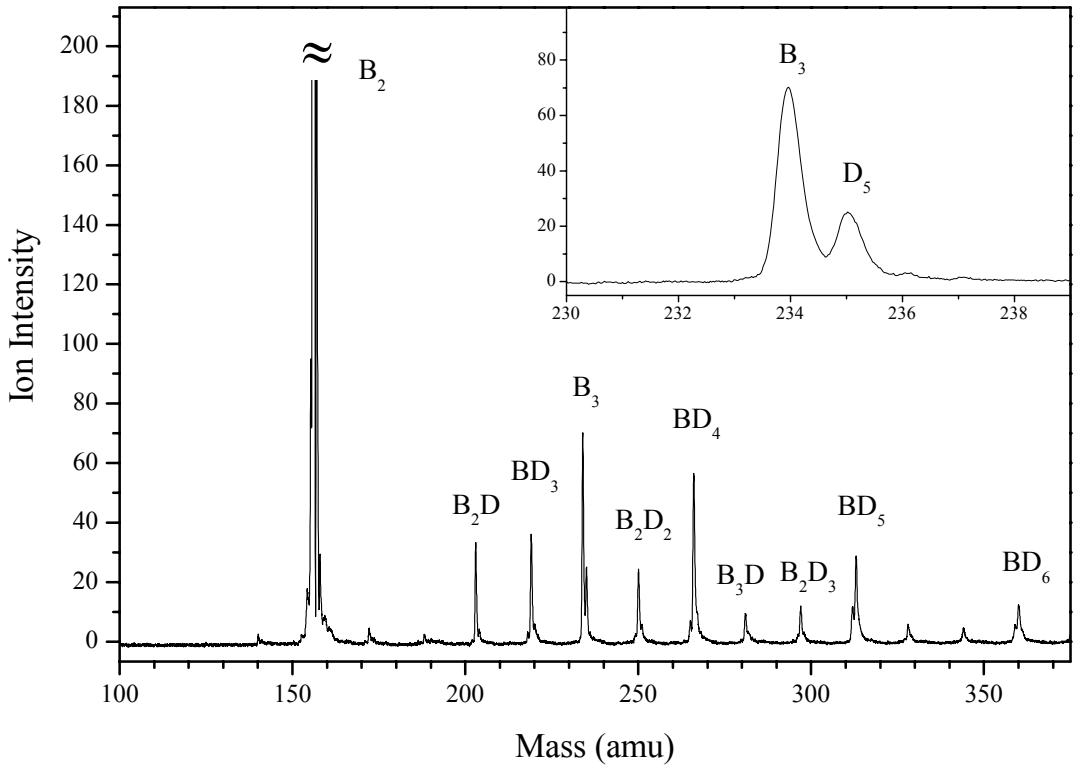

Figure 50: R2PI mass spectra of benzene-deuterated ethanol (BD) cluster beam obtained at the resonance wavelength assigned to the 1:5 neutral cluster at 259.202 nm.

Table 12: Thermochemistry of the clustering reactions: $(ROH)_{n-1} + H^+ + ROH \rightarrow (ROH)_nH^+$

(n-1), n	Heat of reaction,[a] kcal/mol R=CH_3	Heat of reaction,[b] kcal/mol R=C_2H_5
0, 1	-180.3 (-182)	-188.3
1, 2	-32.6	-32.1
2, 3	-21.2	-21.4
3, 4	-14.0	
4, 5	-11.3	

[a] Ref [82, 123]
[b] Ref [120]

Table 13: Thermochemical data relevant to the BE_n clusters (B = C_6H_6, E = C_2H_5OH)

Species	Heat of formation kcal/mol	Proton affinity kcal/mol
H^+	356.7	
B^+	233.2	
C_6H_5	79	211
E	-56.2	188.3
E_2H^+	32.9[a]	220.4
E_3H^+	-44.7[a]	241.8
E_4H^+	-114.9[a]	
E_5H^+	-182.4[a]	

[a] Calculated from the thermochemical data in Table 12.
[b] Ref [120].

Table 14: Exothermicity of the proton transfer reactions (PT)

n	ΔH^0 kcal/mol
1	87.6
2	-8.9
3	-30.3
4	-44.3
5	-55.6

Table 15: Spectral features observed in the BD_n mass channels (B = benzene, D = deuterated ethanol, n = 1-5).

Mass channel	Shift (cm^{-1}) from the 6_0^1 of benzene	Relative intensity	Assignments
BD	141.20	105.27	1:2
	136.66	94.80	1:1
	108.22	134.36	1:2
	106.11	121.33	1:1
	81.06	132.39	1:1
	75.32	185.42	1:2
	58.14	131.85	1:2
	43.67	118.51	1:2
	22.30	170.84	1:1
	3.36	22.52	1:2
	-14.06	82.60	1:1
BD_2	161.78	51.27	1:3 (I)
	160.28	59.39	1:3 (I)
	158.16	159.78	1:3 (I)
	153.92	218.29	1:3 (I)
	124.25	56.34	1:3 (I)
	123.04	68.92	1:3 (I)
	-12.26	304.62	2:2
	-15.57	236.80	2:2
	-20.07	148.16	2:2
	-22.17	99.21	2:2
	-37.47	348.47	2:2
	-40.77	389.97	2:2
	-73.72	63.90	1:3 (II)
	-75.82	57.06	1:3 (II)
BD_3	21.39	187.81	1:4
	19.90	212.86	1:4
	16.28	182.98	1:4
	8.16	216.95	1:4
	6.36	277.58	1:4
	3.95	203.55	1:4
	-73.72	883.01	1:3 (II)
	-75.82	860.96	1:3 (II)
	-77.91	221.81	2:3
	-82.71	201.65	2:3
	-87.49	222.30	2:3

	-89.29	177.58	2:3
	-94.67	249.66	2:3
	-97.37	247.54	2:3
	-102.74	327.15	2:3
	-105.43	256.09	2:3
	-118.29	249.82	2:3
	-121.86	876.17	2:3
	-125.15	741.25	2:3
BD_4	21.39	470.97	1:4
	19.90	553.93	1:4
	16.28	245.23	1:4
	8.16	222.28	1:4
	6.36	550.34	1:4
	3.95	529.97	1:4
	-5.65	250.97	1:5
	-7.16	265.03	1:5
	-14.97	302.24	1:5
	-20.67	366.00	1:5
	-26.67	285.52	1:5
	-28.77	327.53	1:5
	-34.77	271.97	1:5
	-35.98	365.34	1:5
	-44.97	428.52	1:5
BD_5	-10.16	329.85	1:6
	-29.07	351.10	1:6
	-41.97	260.77	1:6
	-43.17	317.29	1:6
	-56.06	227.09	1:6
	-61.15	235.40	1:6

4.7 R2PI of Benzene-Trifluoroethanol

The binary mixed clusters of benzene and trifluoroethanol were investigated by using the R2PI method. The R2PI spectra for benzene-(trifluoroethanol)$_n$, C_6H_6-$(CF_3CH_2OH)_n$, were achieved by utilizing the $^1B_{2u} \leftarrow {}^1A_{1g}$ (6_0^1) transition of benzene molecule, where n=1-7 (Figure 51). Well-resolved R2PI scans were obtained for $(C_6H_6)_2$-$(CF_3CH_2OH)_n$, where n = 1-5, as shown in Figure 52. Intracluster reactions were observed following the photoionization of benzene-(trifluoroethanol)$_n$ clusters. The protonated triflurorethanol clusters $(CF_3CH_2OH)_nH^+$, where $n \geq 2$, were detected. The R2PI technique was carried out on deuterated benzene-trifluoroethanol clusters, C_6D_6-$(CF_3CH_2OH)_n$, to investigate the proton transfer reactions. The R2PI scan measured in C_6D_6-$(CF_3CH_2OH)_n$, where n = 1-7, with respect to the 6_0^1 of C_6D_6 molecule is shown in Figure 53. The frequency of the 6_0^1 transition was detected at 38,805.64 cm^{-1}. The spectral characterization of the R2PI scans obtained of the C_6D_6/trifluoroethanol system revealed identical spectral features as those of C_6H_6/trifluoroethanol system.

In the following sections, the spectral assignments of benzene-trifluoroethanol $(BT)_n$ clusters, where n = 1-5, and the intracluster reactions upon photoionization of BT_n neutral clusters are discussed.

4.7.1 Spectra of Benzene Trifluoroethanol (BT_n) Clusters, n = 1-2

The R2PI absorption spectra obtained by monitoring the benzene, B, and benzene-$(CF_3CH_2OH)_n$, BT_n, (n = 1 and 2) mass channels are represented in Figure 54. The assignments have been carefully given in BT and BT_2 mass channels to the observed

spectral features considering the possible fragmentations from higher mass channels. The BT mass channel shows several features, which appear in the BT_2 mass channel with very small ion intensities (as indicated by dashed lines in Figure 54). These features are originating at 109.25 cm^{-1} relative to the 6_0^1 transition of benzene and assigned to 1:2 cluster. Three peaks are found in the mass channel corresponding to BW (m/z = 96) at the same frequencies as they appear in the BT channel (as shown in Figure 55). These features are assigned to the multi-component cluster (BTW) and they appear in BT channel as a result of the fragmentations of BTW cluster upon photoionization into B^+T and B^+W. The observation of benzene-trifluoroethanol-water clusters could be attributed to the contamination of traces of water in the gas line. Several weak features in BT channel could be assigned to 1:1 cluster with no traces in the higher mass channels. The 6_0^1 origin of 1:1 cluster is blue-shifted by 65.47 cm^{-1}. The mass spectra obtained at the resonance features of 1:1 and 1:2 are displayed in Figure 56. The remaining features in BT mass could not be assigned due to their complexity.

4.7.2 Spectra of Benzene Trifluoroethanol (BT_n) Clusters, n = 3-5

Besides the spectral features described above in BT_2 channel, two clusters were identified to be responsible for the remaining features. Four peaks are present in BT_2 channel arising from the fragmentation of B^+T_2W [$B^+T_2W \rightarrow B^+T_2 + W$]; these peaks were assigned to the BT_2W neutral cluster (as indicated by dashed lines in Figure 57). The bands assigned to 1:3 in BT_2 mass channel arise from the fragmentation of B^+T_3 cluster are clearly seen in Figure 57. The spectral shift for the first band is a blue-shift by 179.48 cm^{-1}.

This cluster was the most blue shifted cluster, which is indicative of the extent of the hydrogen bonding between the OH group of trifluoroethanol and the styrene π-system.. The efficient fragmentation exhibited by the 1:3 cluster is consistent with the π-hydrogen bonding that may be incorporated in the 1:3 structure. The TOF mass spectrum when the laser is tuned to the resonance feature of BT_3 cluster is shown in Figure 58. It is interesting to see how the fragmentation process affects the shape of the BT_2 mass peak. Since B^+T_3 breaks up in the acceleration region, in a time scale of sub-microsecond, the B^+T_2 peak will have a tail toward B^+T_3 mass peak.

The assignments of both 1:4 and 1:5 clusters were afforded by the observation of their fingerprints in T_2H mass channel. The peaks marked with the dashed lines in T_2H channel and linked with those in either BT_4 or BT_5 channels were designated to 1:4 or 1:5, respectively, as illustrated in Figure 59. The mass spectrum recorded at the resonance feature of BT_4 cluster has a T_2H mass peak, which is the product of intracluster reaction (Figure 60). The 6_0^1 origins of 1:4 and 1:5 are located at 78.14 and 35.94 cm^{-1}, respectively. Although, the spectral shift reverses direction in the 1:4 cluster, all BT_n clusters (n = 1-5) possess blue-shifted 6_0^1 origins relative to that of benzene molecule. The relative frequencies and careful assignments of the BT_n clusters are tabulated in Table 16.

4.7.3 Intracluster Reactions following Photoionization

The T_nH^+ intracluster products were observed for $n \geq 2$. The R2PI spectrum of T_2H channel carries signatures for 1:4 and 1:5 neutral clusters, while the R2PI spectrum of T_3H channel (in poor resolution) has bands from 1:n, where n = 5-7. To examine the

mechanism of the intracluster reactions, the R2PI experiments were carried out using C_6D_6. Only the reaction products of protonated trifluoroethanol clusters T_nH^+ ($n \geq 2$) were observed. The R2PI spectra of these products have similar spectral features as those obtained using C_6H_6 (for example, compare Figure 61 with Figure 59). The observation of the T_nH^+ protonated trifluoroethanol clusters (not T_nD^+ clusters) in the R2PI experiments using C_6D_6 suggests that the dissociative proton transfer reactions DPT are taking place in the trifluoroethanol sub-clusters. The proposed mechanism involves a dissociative electron transfer reaction via the neutral precursor 1:n, where $n \geq 4$, to produce T_n^+ cluster followed by an evaporative loss (or losses) of trifluoroethanol monomer to form either T_3^+ or T_4^+, and then the later undergo a dissociative proton transfer reaction to form T_2H^+ or T_3H^+, respectively. The proposed mechanism is the following:

$$C_6H_6^+ - T_n \xrightarrow{\text{DET}} T_n^+ + C_6H_6 \qquad \text{Eq. 4-12}$$

$$T_n^+ \xrightarrow{\text{evaporative loss(es)}} T_3^+ \xrightarrow{\text{DPT}} T_2H^+ + CF_3CH_2O \quad n = 4\text{-}5 \qquad \text{Eq. 4-13}$$

or

$$T_n^+ \xrightarrow{\text{evaporative loss(es)}} T_4^+ \xrightarrow{\text{DPT}} T_3H^+ + CF_3CH_2O \quad n \geq 5 \qquad \text{Eq. 4-14}$$

The proposed mechanism is supported by these facts: first, the ionization potential of the trifluoroethanol molecule is about 2.25 ev above that of the benzene molecule and it is reasonably to deduce that the DET channel is endothermic for 1:1, 1:2 and 1:3 clusters. It seems that three trifluoroethanol molecules are involved in stabilizing the $(CF_3CH_2OH)^+$ and hence lowering the ionization potential of the $(CF_3CH_2OH)_4^+$ cluster to be equal or less

than that of the benzene molecule (IP of benzene is 9.24 ev). Compared that with the benzene/ethanol system, the DET channel is exothermic for 1:2 cluster and the IP(ethanol) is above that of benzene by 1.24 ev. Second, no fragmentation processes were observed for the cluster ions above the 1:3 ion cluster. Third, the evaporative loss of the monomer constituents is the preferential process for cluster fragmentation in many clusters.[124]

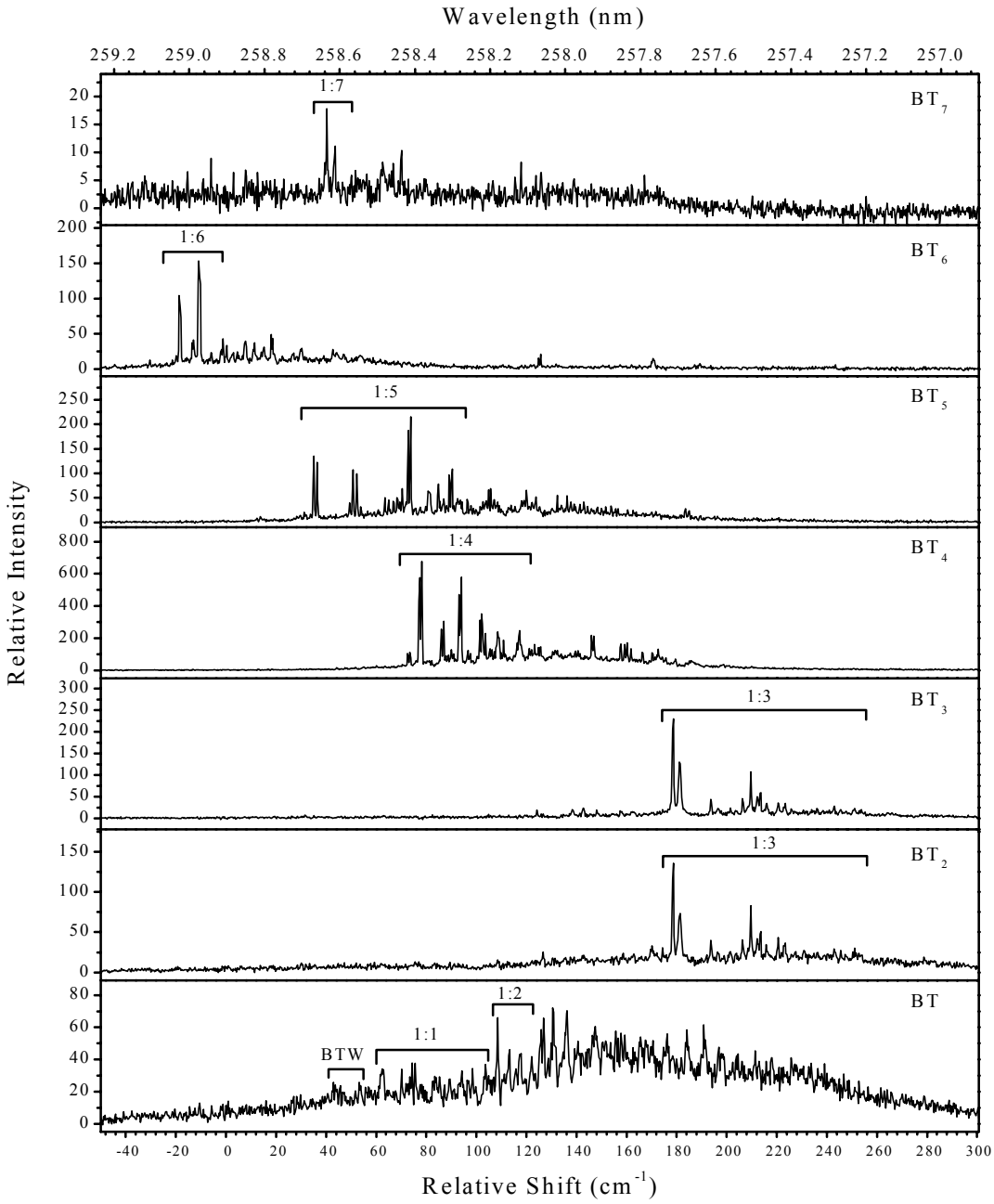

Figure 51: Overall R2PI spectra measured in the benzene (trifluoroethanol)$_n$ mass channels (BT_n), n = 1-6, relative to the 6_0^1 transition of the benzene molecule at 38,624.95 cm^{-1}. The peak designations (m:n) stand for the number of benzene:trifluoroethanol in the neutral cluster which is responsible for the spectral features.

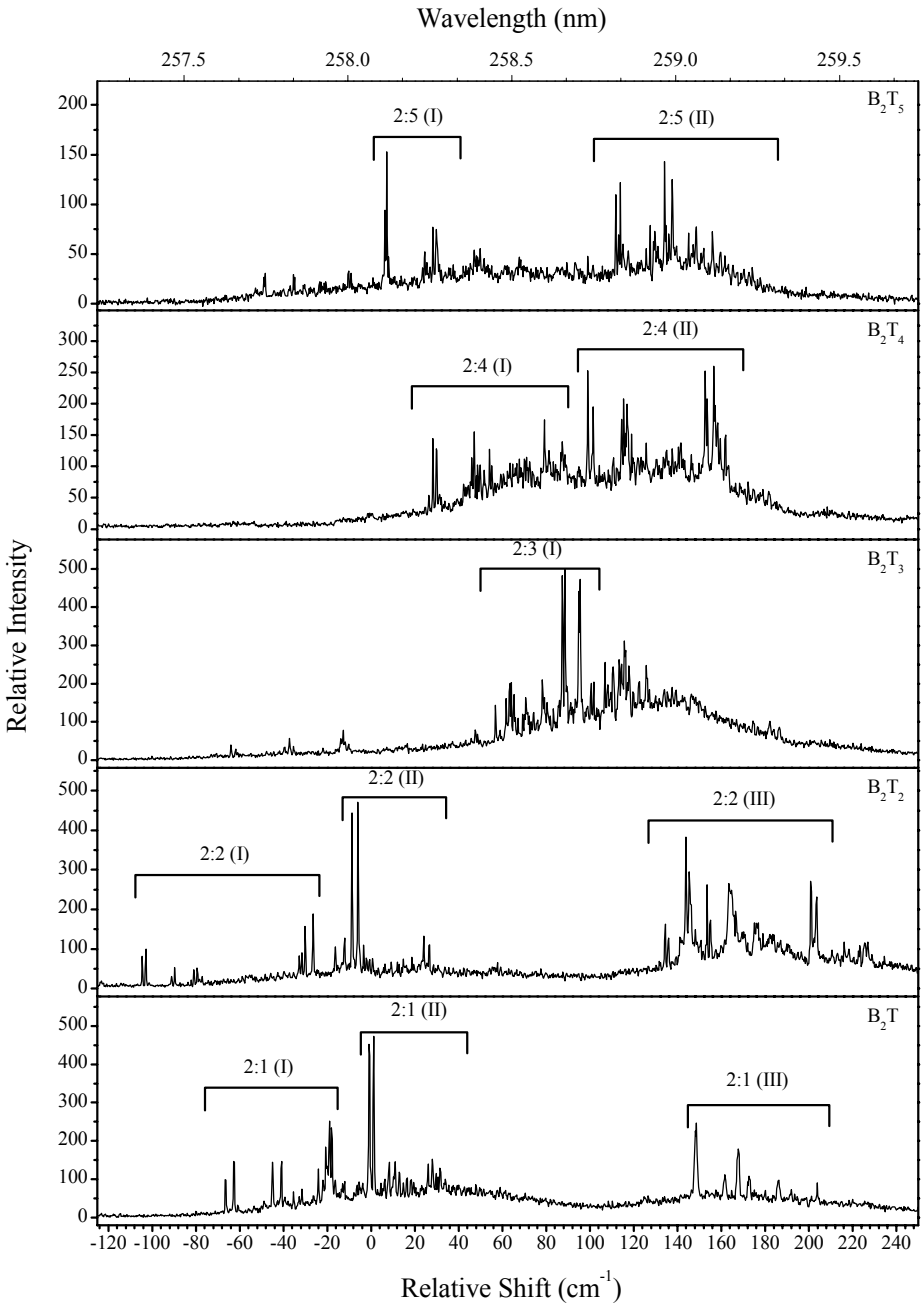

Figure 52: One-color R2PI spectra measured in and $(benzene)_2$-$(trifluoroethanol)_n$ mass channels (B_2T_n), n = 1-5, relative to the 6_0^1 transition of the benzene molecule at 38,624.95 cm^{-1}.

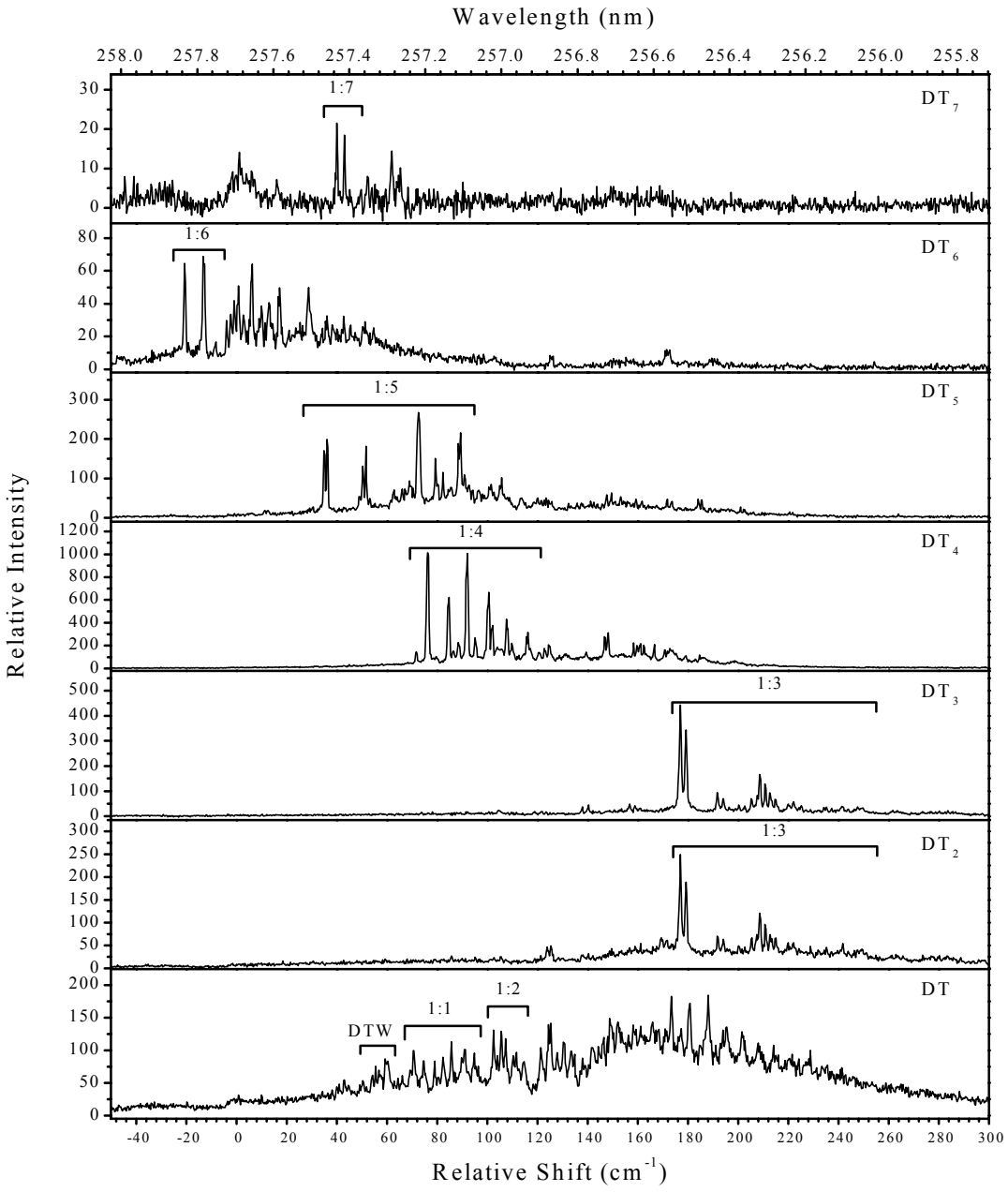

Figure 53: Overall R2PI spectra measured in the C_6D_6-(trifluoroethanol)$_n$ mass channels (DT_n), n = 1-7, relative to the 6_0^1 transition of C_6D_6 molecule at 38,805.64 cm^{-1}. The peak designations (m:n) stand for the number of C_6D_6:trifluoroethanol in the neutral cluster which is responsible for the spectral features.

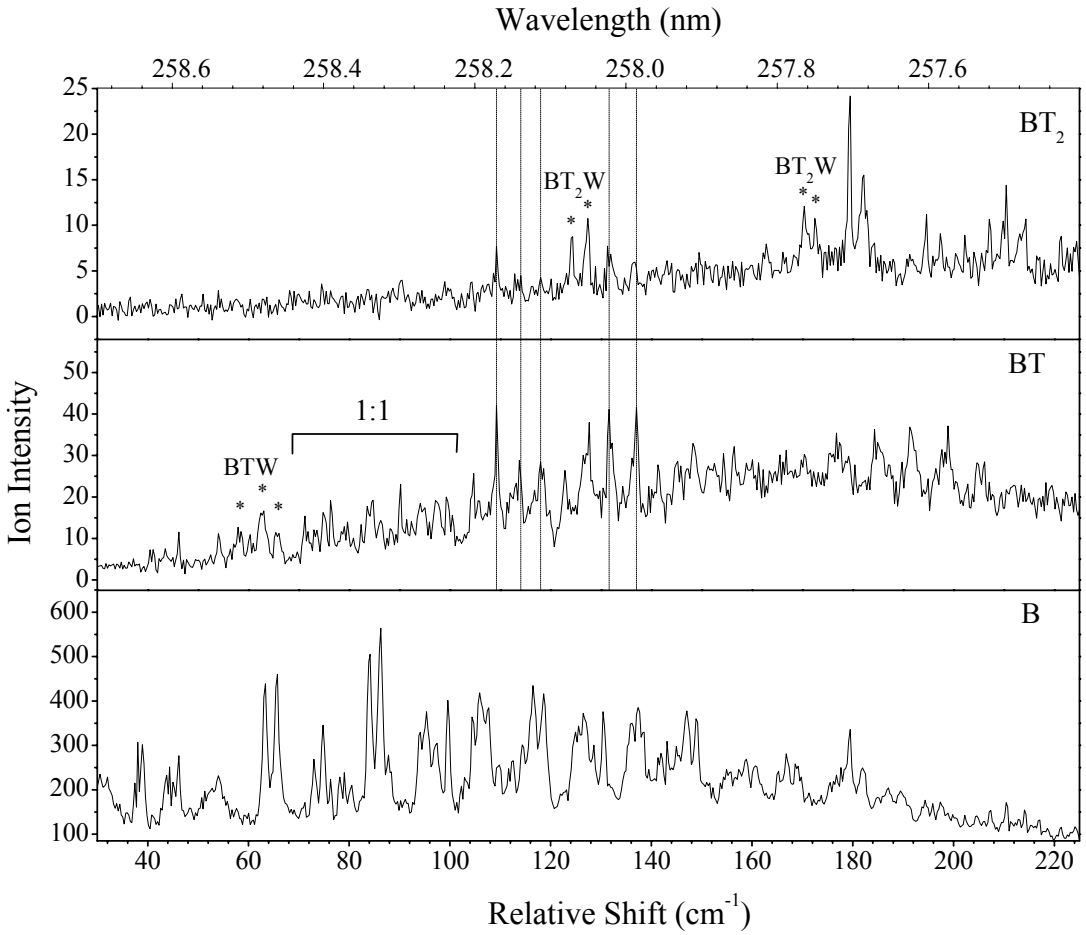

Figure 54: One-color R2PI spectra measured in benzene, B, benzene-trifluoroethanol, BT, and benzene-(trifluoroethanol)$_2$, BT_2, mass channels relative to the 6_0^1 transition of the benzene molecule at 38,624.95 cm^{-1}. The dashed lines indicate the peaks that assigned to 1:2 cluster. BT_nW donate to ternary clusters of benzne-(trifluoroethanol)$_n$-water.

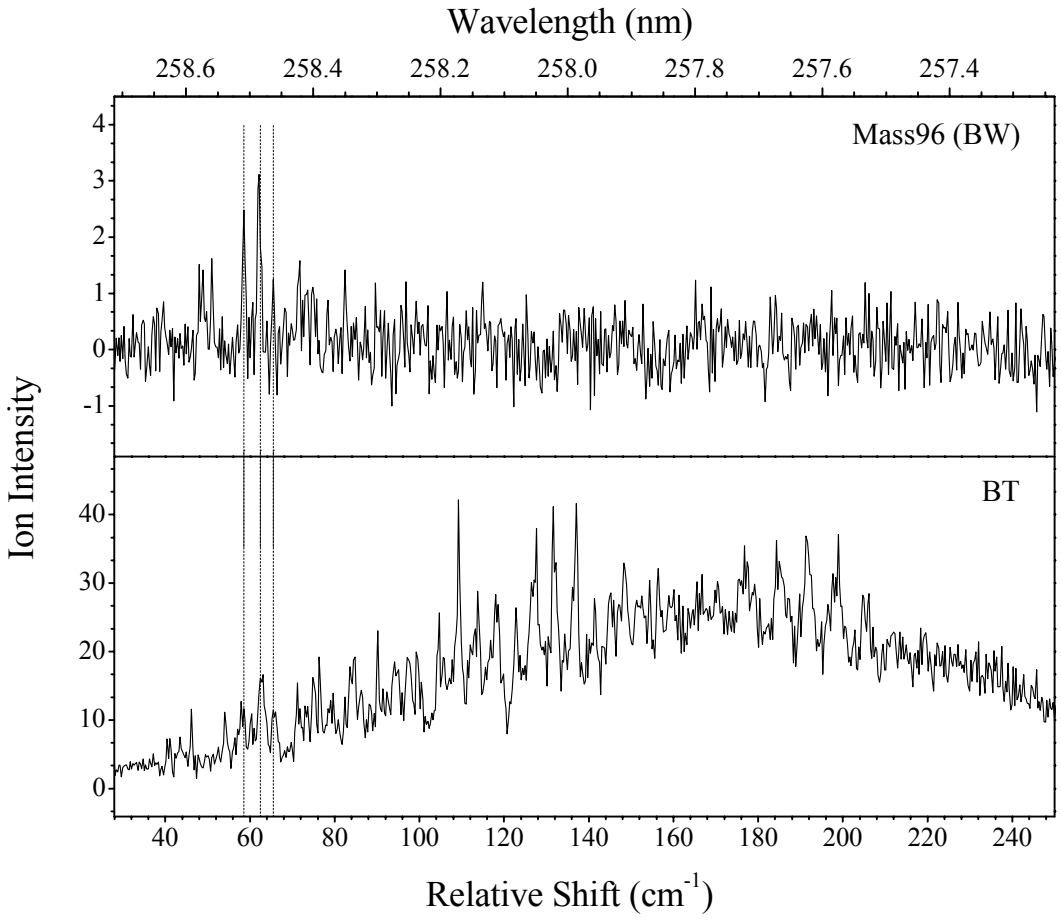

Figure 55: One-color R2PI spectra measured in benzene-trifluoroethanol, BT, and benzene-water, BW, mass channels relative to the 6_0^1 transition of the benzene molecule at 38,624.95 cm^{-1}. The dashed lines indicate the peaks that assigned to the ternary BTW cluster.

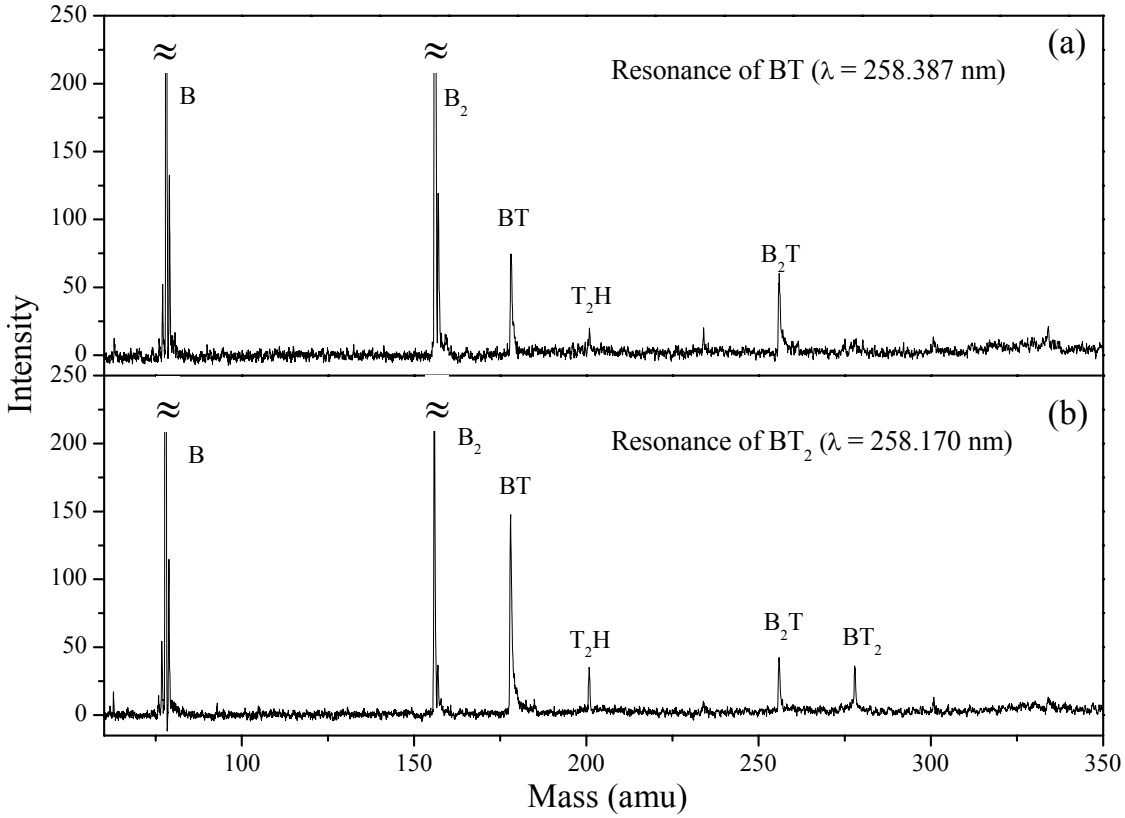

Figure 56: R2PI mass spectra of the benzene-trifluorothanol (BT_n) cluster beam obtained at the resonance features assigned to (a) BT and (b) BT_2 clusters.

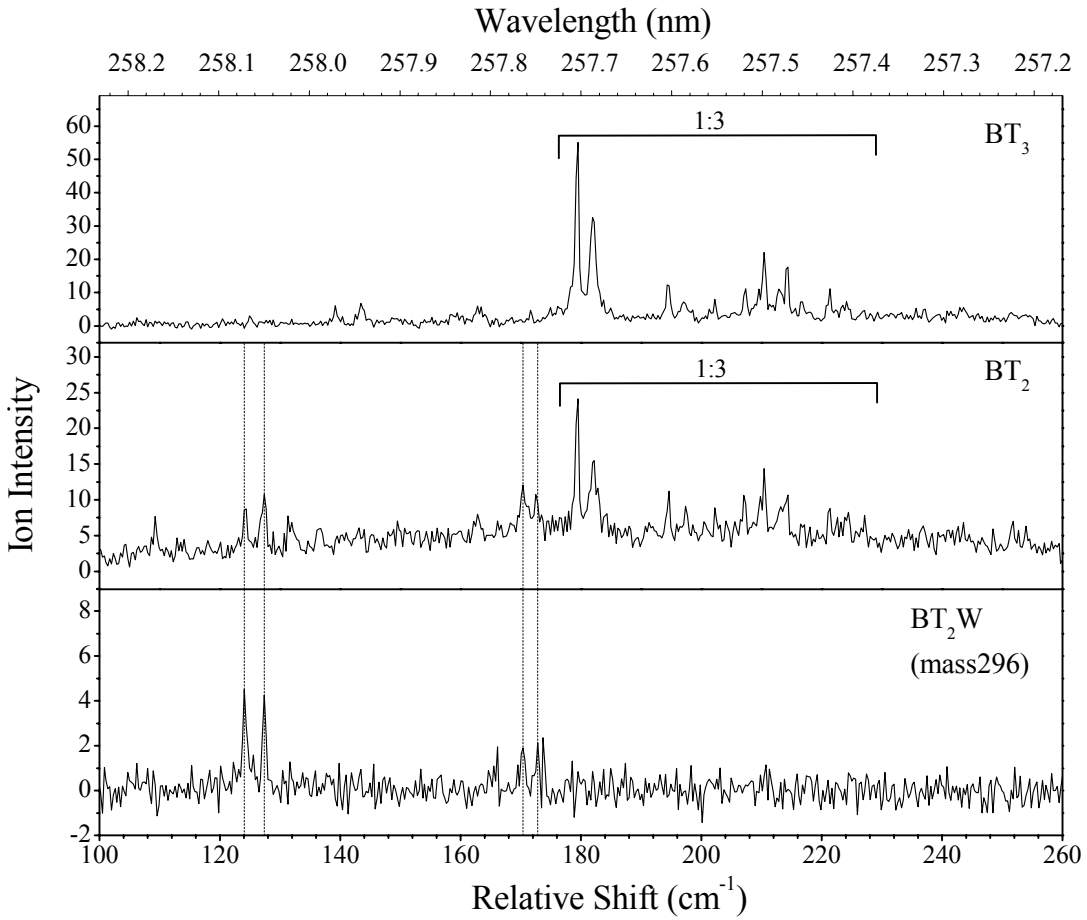

Figure 57: One-color R2PI spectra measured in benzene-(trifluoroethanol)$_2$-water, BT_2W, benzene-(trifluoroethanol)$_2$, BT_2, and benzene-(trifluoroethanol)$_3$, BT_3, mass channels relative to the 6_0^1 transition of the benzene molecule at 38,624.95 cm^{-1}. The dashed lines indicate the peaks that assigned to the ternary BT_2W cluster.

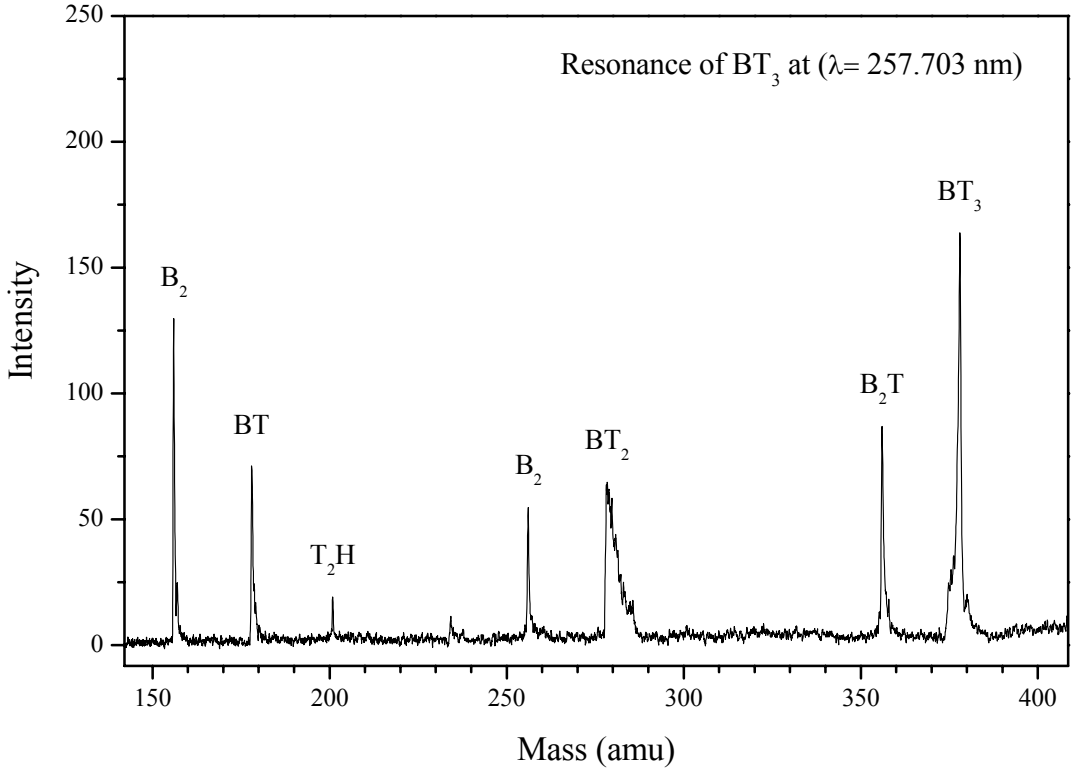

Figure 58: R2PI mass spectra of the benzene-trifluorothanol (BT_n) cluster beam obtained at the resonance feature assigned to BT_3 cluster.

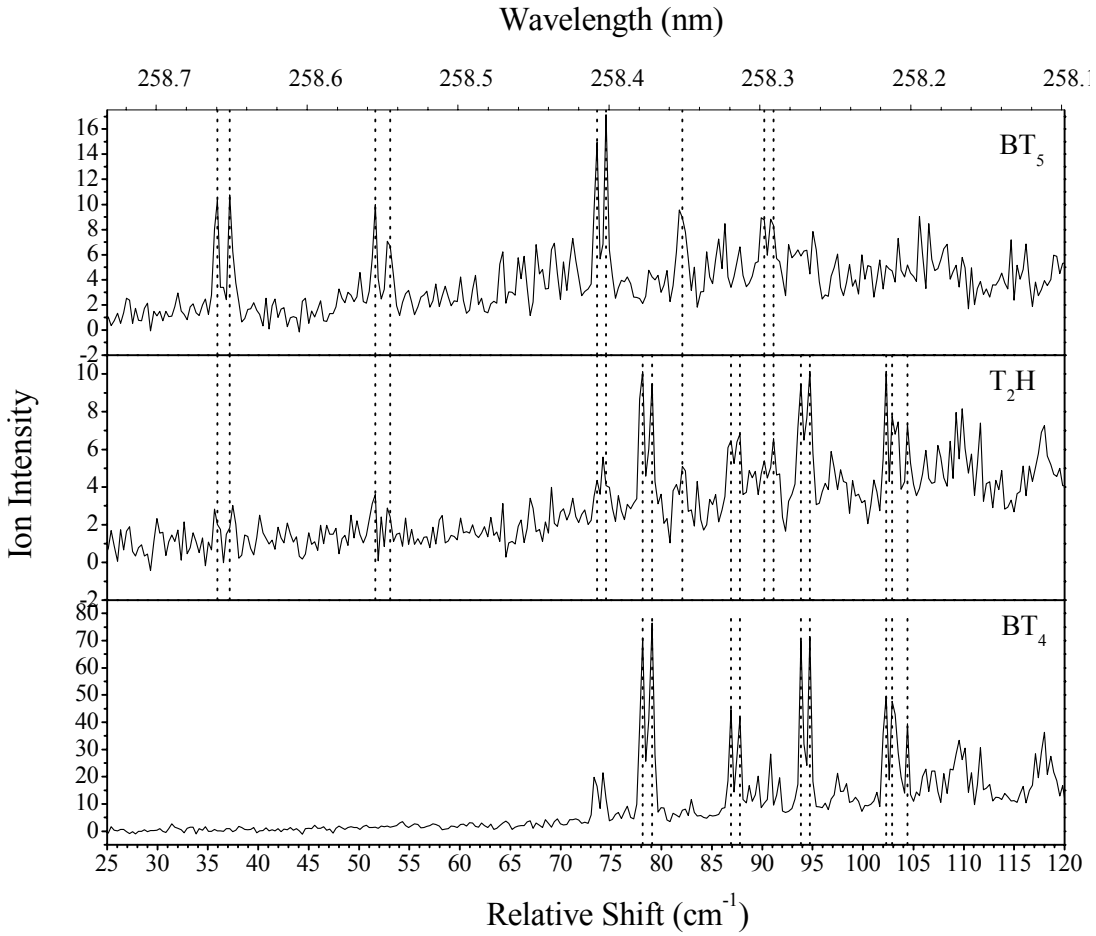

Figure 59: One-color R2PI spectra measured in benzene-(trifluoroethanol)$_4$, BT_4, (trifluoroethanol)$_2$H, T_2H, and benzene-(trifluoroethanol)$_5$, BT_5, mass channels relative to the 6_0^1 transition of the benzene molecule at 38,624.95 cm^{-1}.

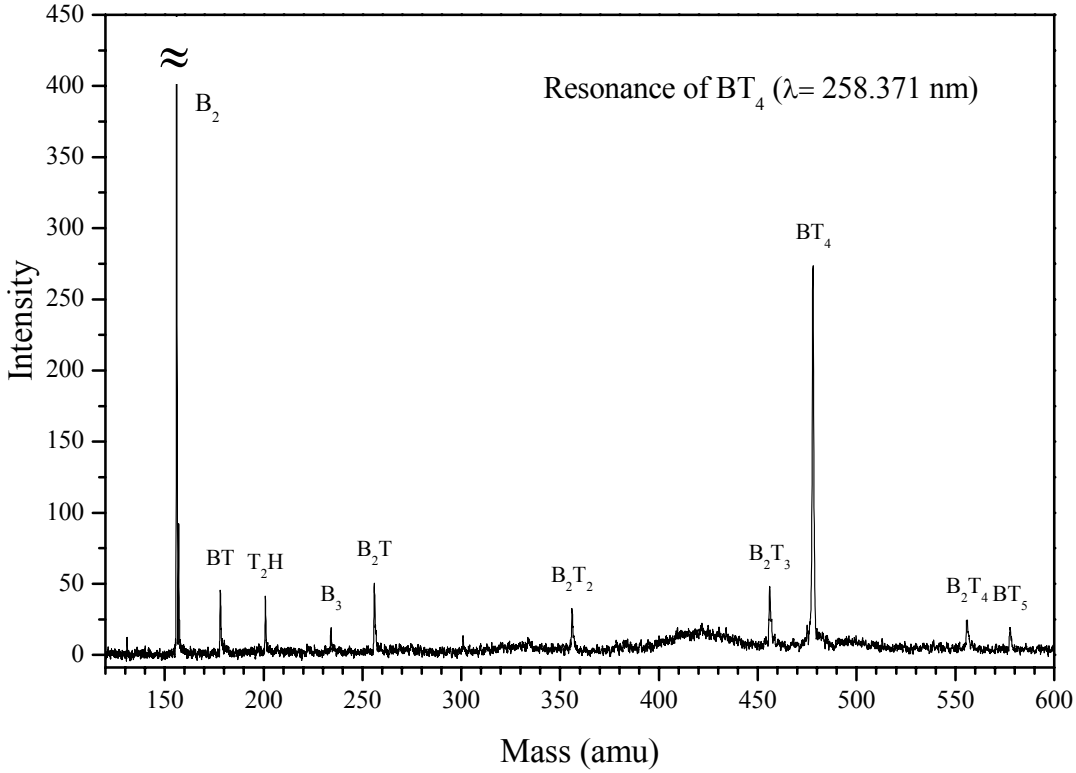

Figure 60: R2PI mass spectra of the benzene-trifluorothanol (BT_n) cluster beam obtained at the resonance feature assigned to BT_4 cluster.

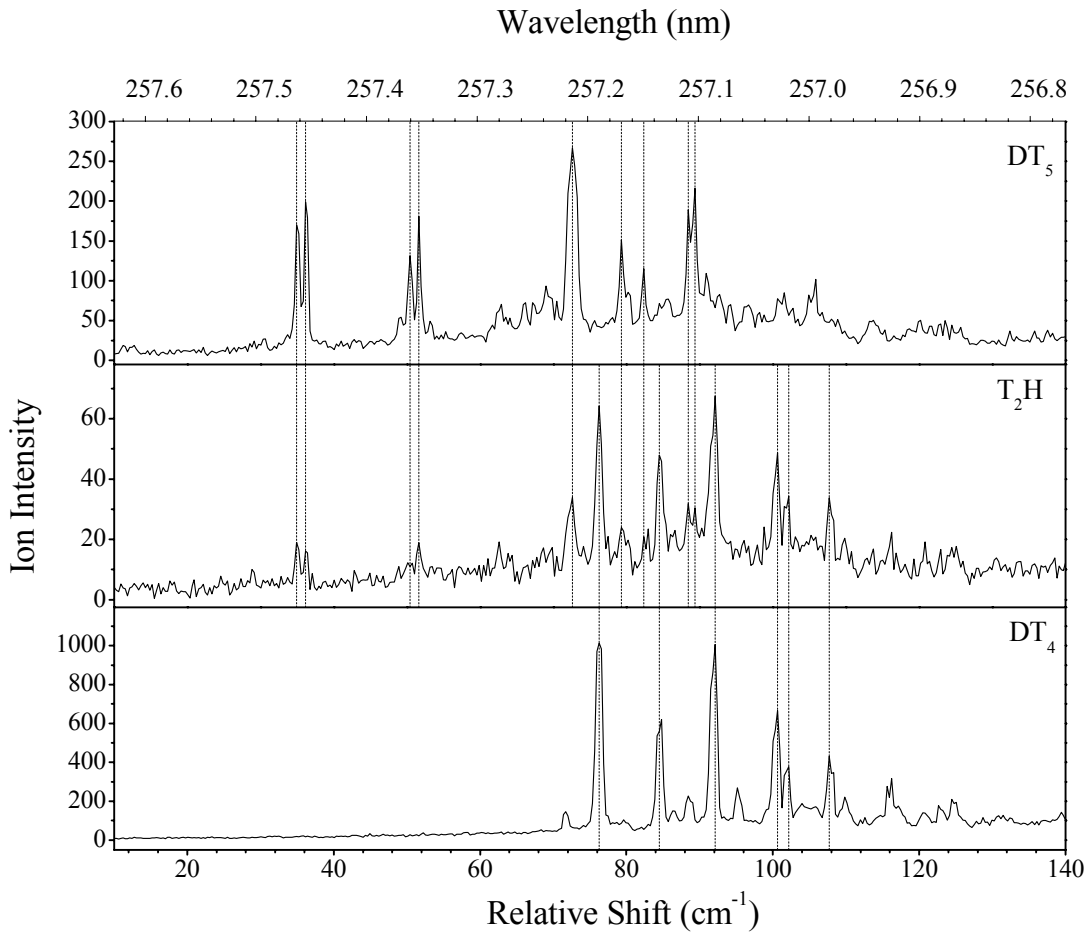

Figure 61: One-color R2PI spectra measured in C_6D_6-(trifluoroethanol)$_4$, DT_4, (trifluoroethanol)$_2$H, T_2H, and C_6D_6-(trifluoroethanol)$_5$, DT_5, mass channels relative to the 6_0^1 transition of the C_6D_6 molecule at 38,805.64 cm^{-1}.

Table 16: Spectral features observed in the BT_n mass channels (B = benzene, T = trifluoroethanol, n = 1-5).

Mass channel	Shift (cm^{-1}) from the 6_0^1 of benzene	Relative intensity	Assignments
BT	137.07	41.61	1:2
	131.61	41.14	1:2
	118.01	28.34	1:2
	113.78	28.80	1:2
	109.25	42.14	1:2
	99.27	19.97	1:1
	97.16	19.16	1:1
	94.14	18.51	1:1
	86.29	14.32	1:1
	84.78	19.22	1:1
	83.58	17.74	1:1
	78.44	11.66	1:1
	76.33	19.20	1:1
	74.83	16.21	1:1
	73.02	12.06	1:1
	71.20	15.42	1:1
	65.47	11.45	1:1
	63.06	16.65	BTW
	57.94	12.73	BTW
BT_2	221.37	17.13	1:3
	214.39	21.66	1:3
	210.44	30.06	1:3
	207.41	20.16	1:3
	202.23	14.07	1:3
	197.98	11.23	1:3
	194.34	16.83	1:3
	182.21	32.52	1:3
	179.48	47.92	1:3
	172.50	11.69	BT_2W
	170.38	13.36	BT_2W
	136.77	5.97	1:2
	131.31	7.01	1:2
	127.38	11.45	BT_2W
	124.96	7.68	1:2
	124.36	9.25	BT_2W

	118.10	4.29	1:2
	112.86	6.65	1:2
	109.25	7.06	1:2
BT_3	221.37	15.82	1:3
	214.09	22.35	1:3
	210.44	28.39	1:3
	207.41	14.67	1:3
	202.23	12.22	1:3
	197.38	9.62	1:3
	194.65	16.84	1:3
	181.91	42.29	1:3
	179.48	70.21	1:3
	163.41	8.18	1:3
BT_4	104.40	39.47	1:4
	102.90	47.64	1:4
	102.29	49.57	1:4
	94.74	71.55	1:4
	93.83	70.01	1:4
	87.80	41.60	1:4
	86.89	44.73	1:4
	79.05	76.45	1:4
	78.14	70.93	1:4
BT_5	92.63	6.80	1:5
	90.82	8.82	1:5
	81.76	9.57	1:5
	74.51	17.13	1:5
	73.62	14.95	1:5
	52.81	7.07	1:5
	51.61	10.00	1:5
	37.15	10.76	1:5
	35.94	10.33	1:5

Chapter 5 Conclusions

Well-resolved R2PI spectra of the styrene-methanol clusters were described. The spectra reveal a rapid increase in complexity with the number of methanol molecules in the cluster, associated with van der Waal modes and isomeric forms. While only single cluster origins were found for the SM, SM_4 and SM_8 clusters, two distinct isomers were identified for each of the SM_n clusters with n = 2, 3, 5-7, and 9. The progressive addition of methanol molecules to the SM complex led to the formation of stable cyclic and bicyclic methanol sub-clusters within the SM_4 and SM_8 clusters, respectively. The spectral shifts of the cluster origins reflect the nature of the intermolecular interactions within the binary clusters. Blue shifts were observed for the SM, SM_2 and SM_3 clusters consistent with hydrogen bonding interactions between the OH groups and the styrene π-system. A remarkable switch in the spectral shift from blue to red was observed at the SM_4 cluster consistent with the ring structure of the methanol tetramer. Evidence was provided for intracluster dissociative proton transfer reactions within the $S_2M_n^+$ clusters with $n \geq 3$ to generate protonated methanol clusters. It was proposed that the interaction of the methanol molecules with the olefin center of styrene promotes the proton transfer from the styrene dimer to the hydrogen-bonded methanol cluster. These reactions may explain the strong inhibition effects exerted by small concentrations of methanol on the cationic polymerization of styrene.

Well-resolved R2PI spectra of the small styrene-water clusters were reported, and compared with the spectra of the analogous benzene containing clusters. The styrene-water complex exhibited very different spectral shift and structure as compared to the benzene-water complex. The small blue shift of 21.5 cm^{-1}, relative to the styrene 0_0^0 transition, was consistent with the predominant interaction between water and the ethylene group of styrene. The favorable interactions of water and methanol with the olefin group of styrene may explain the strong inhibition effects of exerted by small concentrations of water on the cationic polymerization of styrene. It was proposed that water molecules tend to aggregate around the olefin center, which promotes the transfer of the charge from the propagating chain to the hydrogen-bonded water cluster.

The R2PI spectra of the styrene-ethanol clusters (SE_n) were obtained in the region of the S_1-S_0 transition of styrene molecule. The spectra showed an increase in complexity with the number of ethanol molecules in the cluster, associated with intermolecular vibration modes and isomeric structures. Two distinct isomers were recognized for each of the SE_n clusters with n = 1, 2, 3 and 5, and three isomers were identified for SE_4 cluster. Evidence was provided for the dissociative proton transfer reactions within the $S_2E_n^+$ clusters with n≥2 to generate protonated ethanol clusters.

The binary mixed clusters of styrene and trifluoroethanol were investigated by using the R2PI technique. The R2PI spectra of the ST_n clusters (with n = 1-4) reveal these spectral characterizations (1) the absence of the R2PI spectrum of ST ion cluster, (2) no evidence of cluster fragmentations is found in that system and (3) No intracluster

reaction was observed for styrene-trifluoroethanol (ST_n) system under the experimental condition. One isomer was identified for ST_2, ST_3 and ST_4 clusters.

The binary mixed clusters of benzene and ethanol were studied by using R2PI technique. The R2PI spectra for benzene-$(ethanol)_n$, BE_n, clusters were obtained through the 6_0^1 transition of the benzene molecule, where n=1-5. Both the dissociative electron transfer and the dissociative proton transfer reactions were observed within the BE_n clusters and intracluster ion products were detected following the photoionization of BE_n clusters. These products were the ionized ethanol clusters $(C_2H_5OH)_n$, where $n \geq 2$, and the protonated ethanol clusters $(C_2H_5OH)_nH^+$, where $n \geq 3$. The thermochemistry of the intracluster reactions was discussed.

The R2PI spectra of the benzene-trifluoroethanol clusters (BT_n) were obtained in the region of the 6_0^1 transition of the benzene molecule. The R2PI have been analyzed and the assignments for (BT_n) clusters have been given, where n = 1-5. This system showed different ion-molecule chemistry. Proton transfer reactions were observed following dissociative electron transfer reactions within (BT_n) clusters, where n = 4. The mechanisms for the ion-molecule reactions involved evaporative losses of neutral trifluoroethanol molecules.

Literature Cited

Literature Cited

1. Jeffrey, G.A. and W. Saenger, *Hydrogen Bonding in Biological Structures*. 1991: Springer-Verlag Berlin and Heidelberg GmbH & Co. KG. 569.

2. Israelachvili, J.N., *Intermolecular and Surface Forces*. 1991. 291 pp.

3. Stone, A.J. and Editor, *The Theory of Intermolecular Forces*. 1996. 272 pp.

4. Scheiner, S. and Editor, *Molecular Interactions: From van der Waals to Strongly Bound Complexes*. 1997. 359 pp.

5. Weber, A. and Editor, *NATO Advanced Science Institutes Series, Series C: Mathematical and Physical Sciences, Vol. 212: Structure and Dynamics of Weakly Bound Complexes. [Proceedings of the NATO Advanced Workshop Held in Acquatredda di Marqtea, Italy, September 21-16, 1986]*. 1987. 633 pp.

6. Bernstein, E.R. and Editor, *Studies in Physical and Theoretical Chemistry, Vol. 68: Atomic and Molecular Clusters*. 1990. 806 pp.

7. Shang, Q.Y. and E.R. Bernstein, *Energetics, dynamics, and reactions of Rydberg state molecules in van der Waals clusters.* Chem. Rev., 1994. **94**(7): p. 2015-25.

8. Castleman, A.W., Jr. and S. Wei, *Cluster reactions.* Annual Review of Physical Chemistry, 1994. **45**: p. 685-719.

9. Castleman, A.W., Jr. and K.H. Bowen, Jr., *Clusters: Structure, Energetics, and Dynamics of Intermediate States of Matter.* J. Phys. Chem., 1996. **100**(31): p. 12911-12944.

10. Zwier, T.S., *The spectroscopy of solvation in hydrogen-bonded aromatic clusters.* Annual Review of Physical Chemistry, 1996. **47**: p. 205-241.

11. Fung, K.H., H.L. Selzle, and E.W. Schlag, *Study of isotope effects in benzene dimers in a seeded supersonic jet.* J. Phys. Chem., 1983. **87**(25): p. 5113-16.

12. Law, K.S., M. Schauer, and E.R. Bernstein, *Dimers of aromatic molecules: $(benzene)_2$, $(toluene)_2$, and benzene-toluene.* J. Chem. Phys., 1984. **81**(11): p. 4871-82.

13. Schauer, M. and E.R. Bernstein, *Calculations of the geometry and binding energy of aromatic dimers: benzene, toluene, and toluene-benzene.* J. Chem. Phys., 1985. **82**(8): p. 3722-7.

14. Boernsen, K.O., H.L. Selzle, and E.W. Schlag, *Spectra of isotopically mixed benzene dimers: details on the interaction in the vdW bond.* J. Chem. Phys., 1986. **85**(4): p. 1726-32.

15. Wanna, J., J.A. Menapace, and E.R. Bernstein, *Hydrogen bonded and non-hydrogen bonded van der Waals clusters: comparison between clusters of pyrazine, pyrimidine, and benzene with various solvents.* J. Chem. Phys., 1986. **85**(4): p. 1795-805.

16. Hopkins, J.B., D.E. Powers, and R.E. Smalley, *Mass-selective two-color photoionization of benzene clusters.* J. Phys. Chem., 1981. **85**(25): p. 3739-42.

17. Easter, D.C., M.S. El-Shall, M.Y. Hahn, and R.L. Whetten, *Spectroscopic manifestations of structural shell filling in $(benzene)_n$ clusters, n = 1-20.* Chem. Phys. Lett., 1989. **157**(4): p. 277-82.

18. Li, X., M.Y. Hahn, M.S. El-Shall, and R.L. Whetten, *Nonbulk convergence of solvent spectral shifts in doped molecular clusters.* J. Phys. Chem., 1991. **95**(22): p. 8524-8.

19. Henson, B.F., G.V. Hartland, V.A. Venturo, R.A. Hertz, and P.M. Felker, *Stimulated Raman spectroscopy in the n1 region of isotopically substituted benzene dimers: evidence for symmetrically inequivalent benzene moieties.* Chem. Phys. Lett., 1991. **176**(1): p. 91-8.

20. Gotch, A.J. and T.S. Zwier, *The spectroscopy and dynamics of π hydrogen-bonded complexes: benzene-hydrogen chloride/deuterium chloride and toluene-hydrogen chloride/deuterium chloride.* J. Chem. Phys., 1990. **93**(10): p. 6977-86.

21. Gord, J.R., A.W. Garrett, R.E. Bandy, and T.S. Zwier, *REMPI fragmentation as a probe of hydrogen bonding in aromatic-X clusters.* Chem. Phys. Lett., 1990. **171**(5-6): p. 443-50.

22. Gotch, A.J., A.W. Garrett, and T.S. Zwier, *The Ham bands revisited: spectroscopy and photophysics of the benzene-carbon tetrachloride complex.* J. Phys. Chem., 1991. **95**(24): p. 9699-707.

23. Gotch, A.J., A.W. Garrett, D.L. Severance, and T.S. Zwier, *The structure and photophysics of clusters of immiscible liquids: benzene-water (C_6H_6-$(H_2O)_n$).* Chem. Phys. Lett., 1991. **178**(1): p. 121-9.

24. Gotch, A.J. and T.S. Zwier, *Multiphoton ionization studies of clusters of immiscible liquids. I. Benzene-$(water)_n$ clusters (C_6H_6-$(H_2O)_n$, n = 1, 2).* J. Chem. Phys., 1992. **96**(5): p. 3388-401.

25. Garrett, A.W., D.L. Severance, and T.S. Zwier, *Multiphoton ionization studies of benzene-methanol(C_6H_6-$(CH_3OH)_n$) clusters. I. Comparisons with benzene-water(C_6H_6-$(H_2O)_n$) clusters.* J. Chem. Phys., 1992. **96**(10): p. 7245-58.

26. Menapace, J.A. and E.R. Bernstein, *Van der Waals modes of solute/solvent clusters: benzene-methane, -deuteriomethane, and -carbon tetrafluoride.* J. Phys. Chem., 1987. **91**(11): p. 2843-8.

27. Hobza, P. and R. Zahradnik, *Intermolecular Complexes: Role of van der Waals Complexes in Physical Chemistry and Bio Disciplines*. 1989. 375 pp.

28. Pribble, R.N. and T.S. Zwier, *Size-specific infrared spectra of benzene-$(H_2O)_n$ clusters (n = 1 through 7): evidence for noncyclic $(H_2O)_n$ structures.* Science (Washington, DC, United States), 1994. **265**(5168): p. 75-9.

29. Gruenloh, C.J., J.R. Carney, C.A. Arrington, T.S. Zwier, S.Y. Fredericks, and K.D. Jordan, *Infrared spectrum of a molecular ice cube: the S4 and D2d water octamers in benzene-(water)$_8$.* Science (Washington, D. C.), 1997. **276**(5319): p. 1678-1681.

30. Germanenko, I.N. and M.S. El-Shall, *Clustering of Acetic Acid by Association of Hydrogen-Bonded Dimers: Spectroscopic Observation of Multicomponent (Ne).(C_6H_6).(CH_3COOH)$_n$ Clusters.* J. Phys. Chem. A, 1999. **103**(30): p. 5847-5851.

31. Daly, G.M., D. Wright, and M.S. El-Shall, *Spectroscopy of acetonitrile-(benzene)$_n$ clusters, n=1-3. Comparison with benzene clusters.* Chem. Phys. Lett., 2000. **331**(1): p. 47-56.

32. El-Shall, M.S., G.M. Daly, and D. Wright, *Experimental and theoretical study of benzene-(acetonitrile)$_n$ clusters, n=1-4.* J. Chem. Phys., 2002. **116**(23): p. 10253-10266.

33. Gruenloh, C.J., J.R. Carney, F.C. Hagemeister, C.A. Arrington, T.S. Zwier, S.Y. Fredericks, J.T. Wood, and K.D. Jordan, *Resonant ion-dip infrared spectroscopy of the S-4 and D-2d wafer octamers in benzene-(water)$_8$ and (benzene)$_2$-(water)$_8$.* J. Chem. Phys., 1998. **109**(16): p. 6601-6614.

34. Carney, J.R., F.C. Hagemeister, and T.S. Zwier, *The hydrogen-bonding topologies of indole-(water)$_n$ clusters from resonant ion-dip infrared spectroscopy.* J. Chem. Phys., 1998. **108**(9): p. 3379-3382.

35. Tanford, C., *The Hydrophobic Effect: Formation of Micelles and Biological Membranes. 2nd Ed*. 1980. 233 pp.

36. Privalov, P.L. and S.J. Gill, *Stability of protein structure and hydrophobic interaction.* Advances in Protein Chemistry, 1988. **39**: p. 191-234.

37. Kennedy, J.P. and E. Marechal, *Carbocationic Polymerization*. 1982, New York: John Wiley & Sons. 510 pp.

38. Odian, G., *Principles of Polymerization*. 1970, New York: McGraw-Hill. 652 pp.

39. Silverman, J., S. Tagawa, H. Kobayashi, Y. Katsumura, M. Washio, and Y. Tabata, *Pulse radiolysis studies on short-lived intermediates in radiation-induced polymerization of bulk styrene and methanol-styrene solutions.* Radiat. Phys. Chem., 1983. **22**(6): p. 1039-42.

40. Tagawa, S. and W. Schnabel, *Laser flash photolysis studies on excited singlet states of benzene, toluene, p-xylene, polystyrene, and poly(a-methylstyrene).* Chem. Phys. Lett., 1980. **75**(1): p. 120-2.

41. Hollas, J.M., E. Khalilipour, and S.N. Thakur, *Vibrational assignments in the 288 nm $\tilde{A}^1A'$-X^1A' electronic absorption spectrum of styrene: new information on the C(1)-C(α) torsional vibrational levels in the ground electronic state of styrene, styrene-β-D_2, and p-fluorostyrene.* J. Mol. Spectrosc., 1978. **73**(2): p. 240-65.

42. Man Him, H. and S.A. Rice, *Intramolecular energy transfer in cis-trans isomerization. Fluorescence from single vibronic levels of styrene, trans-b-styrene-d_1, styrene-d_8, and ethynylbenzene.* J. Chem. Phys., 1974. **61**(3): p. 833-42.

43. Carreira, L.A. and T.G. Towns, *Determination of the torsional potential function for styrene.* J. Chem. Phys., 1975. **63**(12): p. 5283-6.

44. Hollas, J.M. and T. Ridley, *The C(1)-C(α) torsional potential function in the ground electronic state of styrene obtained from the single vibronic level fluorescence and other spectra.* Chem. Phys. Lett., 1980. **75**(1): p. 94-8.

45. Hollas, J.M. and T. Ridley, *The $\tilde{A}^1A'$-X^1A' single vibronic level fluorescence spectrum of styrene vapor.* J. Mol. Spectrosc., 1981. **89**(1): p. 232-53.

46. Syage, J.A., F. Al Adel, and A.H. Zewail, *Jet-cooled styrene: spectra and isomerization.* Chem. Phys. Lett., 1983. **103**(1): p. 15-22.

47. Dimopoulou-Rademann, O., U. Even, A. Amirav, and J. Jortner, *Binding energy of the styrene-argon van der Waals molecule.* J. Phys. Chem., 1988. **92**(19): p. 5371-3.

48. Jortner, J., U. Even, S. Leutwyler, and Z. Berkovitch-Yellin, *Large van der Waals ions.* J. Chem. Phys., 1983. **78**(1): p. 309-11.

49. Dyke, J.M., H. Ozeki, M. Takahashi, M.C.R. Cockett, and K. Kimura, *A study of phenylacetylene and styrene, and their argon complexes PA-Ar and ST-Ar with laser threshold photoelectron spectroscopy.* J. Chem. Phys., 1992. **97**(12): p. 8926-33.

50. Consalvo, D., A. van der Avoird, S. Piccirillo, M. Coreno, A. Giardini-Guidoni, A. Mele, and M. Snels, *The intermolecular vibrations of argon-styrene and argon-4-fluorostyrene complexes.* J. Chem. Phys., 1993. **99**(11): p. 8398-406.

51. Zensen, T.A., P. Jarski, and J.G. Eaton, *A REMPI study of styrene(Ar)$_n$, n=4-12 clusters.* Chem. Phys. Lett., 2000. **326**(5-6): p. 389-394.

52. Ziegler, L.D. and B.S. Hudson, *The vibronic spectroscopy of benzene: old problems and new techniques.* Excited States, 1982. **5**: p. 41-140.

53. Spears, K.G. and S.A. Rice, *Lifetimes of individual vibronic states of the isolated benzene molecules.* J. Chem. Phys., 1971. **55**(12): p. 5561-81.

54. Knight, A.E.W., C.S. Parmenter, and M.W. Schuyler, *Extended view of the benzene 260-nm transition via single vibronic level fluorescence. I. General aspects of benzene single vibronic level fluorescence.* J. Am. Chem. Soc., 1975. **97**(8): p. 1993-2005.

55. Knight, A.E.W., C.S. Parmenter, and M.W. Schuyler, *Extended view of the benzene 260-nm transition via single vibronic level fluorescence. II. Single vibronic level fluorescence as a probe in the assignment of the absorption spectrum.* J. Am. Chem. Soc., 1975. **97**(8): p. 2005-13.

56. Johnson, P.M., *Multiphoton ionization spectroscopy. New state of benzene.* J. Chem. Phys., 1975. **62**(11): p. 4562-3.

57. Johnson, P.M., *The multiphoton ionization spectrum of benzene.* J. Chem. Phys., 1976. **64**(10): p. 4143-8.

58. Wunsch, L., H.J. Neusser, and E.W. Schlag, *Two photon excitation spectrum of benzene and benzene-d_6 in the gas phase. Assignment of inducing modes by hot band analysis.* Chem. Phys. Lett., 1975. **31**(3): p. 433-40.

59. Fischer, G. and S. Jakobson, *Band intensities in the absorption spectrum of benzene vapor.* Mol. Phys., 1979. **38**(1): p. 299-308.

60. Zandee, L. and R.B. Bernstein, *Laser ionization mass spectrometry: extensive fragmentation via resonance-enhanced multiphoton ionization of a molecular benzene beam.* J. Chem. Phys., 1979. **70**(5): p. 2574-5.

61. Zandee, L. and R.B. Bernstein, *Resonance-enhanced multiphoton ionization and fragmentation of molecular beams: nitric oxide, iodine, benzene, and butadiene.* J. Chem. Phys., 1979. **71**(3): p. 1359-71.

62. Atkinson, G.H. and C.S. Parmenter, *The 260 nm absorption spectrum of benzene: remeasured band positions and refined assignments.* J. Mol. Spectrosc., 1978. **73**(1): p. 20-30.

63. Atkinson, G.H. and C.S. Parmenter, *The 260 nm absorption spectrum of benzene: selection rules and band contours of vibrational angular momentum components.* J. Mol. Spectrosc., 1978. **73**(1): p. 31-51.

64. Atkinson, G.H. and C.S. Parmenter, *The 260 nm absorption spectrum of benzene: vibronic analysis.* J. Mol. Spectrosc., 1978. **73**(1): p. 52-95.

65. Beck, S.M., M.G. Liverman, D.L. Monts, and R.E. Smalley, *Rotational analysis of the $^1B_{2u}(\pi\pi^*) \leftarrow {}^1A_{1g}(6^1_0)$ band of benzene and helium-benzene van der Waals complexes in a supersonic jet.* J. Chem. Phys., 1979. **70**(1): p. 232-7.

66. Callomon, J.H., T.M. Dunn, and I.M. Mills, *Rotational analysis of the 2600-A. absorption system of benzene.* Philosophical Transactions of the Royal Society of London, Series A: Mathematical, Physical and Engineering Sciences, 1966. **259**(1104): p. 499-532.

67. Boesl, U., H.J. Neusser, and E.W. Schlag, *Visible and UV multiphoton ionization and fragmentation of polyatomic molecules.* J. Chem. Phys., 1980. **72**(8): p. 4327-33.

68. Aron, K., C. Otis, R.E. Demaray, and P. Johnson, *Linewidths and high resolution structure of the benzene $^1B_{2u} \leftarrow {}^1A_{1g}$ two photon transition by multiphoton ionization-supersonic beam techniques.* J. Chem. Phys., 1980. **73**(9): p. 4167-74.

69. Wunsch, L., H.J. Neusser, and E.W. Schlag, *Fluorescence from high vibronically excited benzene: a \"channel three\" problem.* Zeitschrift fuer Naturforschung, Teil A: Astrophysik, Physik und Physikalische Chemie, 1981. **36A**(12): p. 1340-3.

70. Rettner, C.T. and J.H. Brophy, *Resonance-enhanced laser ionization mass spectrometry of four aromatic molecules.* Chem. Phys., 1981. **56**(1): p. 53-61.

71. Riedle, E., H.J. Neusser, and E.W. Schlag, *Sub-Doppler high-resolution spectra of benzene: anomalous results in the \"channel three\" region.* J. Phys. Chem., 1982. **86**(25): p. 4847-50.

72. Sur, A., J. Knee, and P. Johnson, *The $^1B_{2u} \leftarrow {}^1A_{1g}$ two-photon spectra of several isotopes of benzene by supersonic beam-multiphoton ionization spectroscopy.* J. Chem. Phys., 1982. **77**(2): p. 654-68.

73. Stephenson, T.A., P.L. Radloff, and S.A. Rice, *$^1B_{2u} \leftrightarrow {}^1A_{1g}$ spectroscopy of jet-cooled benzene: single vibronic level fluorescence studies.* J. Chem. Phys., 1984. **81**(3): p. 1060-72.

74. Stephenson, T.A. and S.A. Rice, *Relaxation dynamics of photoexcited benzene-rare gas van der Waals complexes.* J. Chem. Phys., 1984. **81**(3): p. 1083-101.

75. Langridge-Smith, P.R.R., D.V. Brumbaugh, C.A. Haynam, and D.H. Levy, *Ultraviolet spectra of benzene clusters.* J. Phys. Chem., 1981. **85**(25): p. 3742-6.

76. Mons, M., A. Courty, M. Schmidt, J. Le Calve, F. Piuzzi, and I. Dimicoli, *New assignments in the UV spectroscopy of the small benzene-argonn clusters: The*

effects of a structure-selective vibrational predissociation. J. Chem. Phys., 1997. **106**(5): p. 1676-1686.

77. Weber, T., E. Riedle, H.J. Neusser, and E.W. Schlag, *Van der Waals bond lengths and electronic spectral shifts of the benzene-krypton and benzene-xenon complexes.* Chem. Phys. Lett., 1991. **183**(1-2): p. 77-83.

78. Weast, R.C. and Editor, *CRC Handbook of Chemistry and Physics. 64th Ed*. 1984. 2320 pp.

79. Carrasquillo M, E., T.S. Zwier, and D.H. Levy, *The multiphoton ionization spectrum of complexes of benzene and acetylene.* J. Chem. Phys., 1985. **83**(10): p. 4990-9.

80. Schauer, M. and E.R. Bernstein, *Molecular jet study of the solvation of benzene by methane, ethane, and propane.* J. Chem. Phys., 1985. **82**(2): p. 726-35.

81. Atkins, P.W., *Physical Chemistry. 3rd Ed*. 1986. 880 pp.

82. Lias, S.G., J.E. Bartmess, J.F. Liebman, J.L. Holmes, R.D. Levin, and W.G. Mallard, *Gas-phase ion and neutral thermochemistry.* Journal of Physical and Chemical Reference Data, Supplement, 1988. **17**(1): p. 861 pp.

83. El-Shall, M.S. and R.L. Whetten, *Ultraviolet spectroscopy of benzene in cyclohexane clusters. Further evidence for structural shells and resonance interactions.* Chem. Phys. Lett., 1989. **163**(1): p. 41-7.

84. Schauer, M., K.S. Law, and E.R. Bernstein, *Molecular jet study of the solvation of toluene by methane, ethane, and propane.* J. Chem. Phys., 1985. **82**(2): p. 736-46.

85. Stert, V., W. Radloff, H.H. Ritze, and T. Freudenberg, *Resonant two-photon ionization spectroscopy of small benzene-(sulfur hexafluoride)$_m$ clusters.* Chem. Phys. Lett., 1993. **204**(3-4): p. 287-95.

86. Stert, V., W. Radloff, H.H. Ritze, and T. Freudenberg, *Resonant two-photon ionization spectroscopy of benzene-sulfur hexafluoride clusters(C_6H_6-$(SF_6)_{1,2}$).*

Zeitschrift fuer Physik D: Atoms, Molecules and Clusters, 1993. **26**(1-4): p. 213-16.

87. Nowak, R., J.A. Menapace, and E.R. Bernstein, *Benzene clustered with molecular nitrogen, carbon dioxide, and carbon monoxide: energy levels, vibrational structure, and nucleation.* J. Chem. Phys., 1988. **89**(3): p. 1309-21.

88. Weber, T., A.M. Smith, E. Riedle, H.J. Neusser, and E.W. Schlag, *High-resolution UV spectrum of the benzene-molecular nitrogen van der Waals complex.* Chem. Phys. Lett., 1990. **175**(1-2): p. 79-83.

89. Menapace, J.A. and E.R. Bernstein, *Calculation of the vibronic structure of solute solvent van der Waals clusters.* J. Phys. Chem., 1987. **91**(10): p. 2533-44.

90. Daly, G.M., C. Schultz, C. Castevens, D.D. Shillady, and M.S. El-Shall, *Spectroscopy and structure of van der Waals complexes of benzene and acetonitrile.* Proceedings of the Science and Technology of Atomically Engineered Materials, Richmond, Oct. 30-Nov. 4, 1995, 1996: p. 251-256.

91. Garrett, A.W. and T.S. Zwier, *Multiphoton ionization studies of benzene-methanol(C_6H_6-$(CH_3OH)_n$) clusters. II. Intracluster ion-molecule reactions.* J. Chem. Phys., 1992. **96**(10): p. 7259-67.

92. Keesee, R.G. and A.W. Castleman, Jr., *Atomic and Molecular Clusters*, E.R. Bernstien, Editor. 1990, Elsevier Science Publishers B.V. p. 507.

93. Wiley, W.C. and I.H. McLaren, *Time-of-flight mass spectrometer with improved resolution.* Rev. Sci. Instr., 1955. **26**: p. 1150-7.

94. Pithawalla, Y.B., J. Gao, Z. Yu, and M.S. El-Shall, *Even/Odd Alternation in Styrene Cluster Ions. Evidence for Multiple Cyclization during the Early Stages of Polymerization and the Inhibition Effect of Water.* Macromolecules, 1996. **29**(26): p. 8558-8561.

95. Groenewold, G.S., E.K. Chess, and M.L. Gross, *Structure of the intermediate formed in the reaction of the styrene radical cation and neutral styrene.* J. Am. Chem. Soc., 1984. **106**(3): p. 539-43.

96. El-Shall, M.S. and Z. Yu, *Concerted Reactions of Charge Transfer and Covalent Bond Formation in Ionized Alkylbenzene-Isobutene Clusters. Copolymerization of Styrene-Isobutene and a-Methylstyrene-Isobutene Clusters.* J. Am. Chem. Soc., 1996. **118**(51): p. 13058-13068.

97. Chia, L., L. Goodman, and J.G. Philis, *Two-photon Ã← X spectra of benzonitrile and styrene vapors: tests of perturbation rules.* J. Chem. Phys., 1983. **79**(2): p. 593-602.

98. Kendler, S. and Y. Haas, *A Rempi Study of Styrene and Trans-Beta-Methylstyrene Clusters in a Supersonic Jet.* Chem. Phys. Lett., 1995. **236**(3): p. 324-335.

99. El-Shall, M.S., D. Wright, Y. Ibrahim, and H. Mahmoud, *Theoretical Study of Styrene (Methanol)$_n$ Clusters, n = 1-9. Comparison with Methanol Clusters.* J. Phys. Chem. A, 2003. **107**(31): p. 5933-5940.

100. Shalev, E., N. Ben-Horin, U. Even, and J. Jortner, *Electronic spectral shifts of aromatic molecule-rare gas heteroclusters.* J. Chem. Phys., 1991. **95**(5): p. 3147-66.

101. Shalev, E., N. Ben-Horin, and J. Jortner, *Radiative lifetimes of van der Waals heteroclusters.* J. Chem. Phys., 1991. **94**(12, Pt. 1): p. 7757-68.

102. Longuet-Higgins, H.C. and J.A. Pople, *Electronic spectral shifts of nonpolar molecules in nonpolar solvents.* J. Chem. Phys., 1957. **27**: p. 192-4.

103. Bach, A. and S. Leutwyler, *Water-chain clusters: vibronic spectra of 7-hydroxyquinoline.(H_2O)$_n$, n=1-4.* Chem. Phys. Lett., 1999. **299**(5): p. 381-388.

104. Mahmoud, H., I.N. Germanenko, Y. Ibrahim, and M.S. El-Shall, *Spectroscopy and structure of styrene (water)$_n$ and styrene (methanol)$_n$ clusters, n=1, 2.* Chem. Phys. Lett., 2002. **356**(1-2): p. 91-100.

105. Kendler, S. and Y. Haas, *Styrene clusters in a supersonic jet: Reactive and nonreactive systems.* J. Phys. Chem. A, 1997. **101**(14): p. 2578-2588.

106. Zingher, E., S. Kendler, and Y. Haas, *The photophysics of a photoreactive system in a supersonic jet. Styrene-trimethylamine.* Chem. Phys. Lett., 1996. **254**(3,4): p. 213-222.

107. Zilberg, S. and Y. Haas, *Ab initio study of styrene and b-methyl styrene in the ground and in the two lowest excited singlet states.* J. Chem. Phys., 1995. **103**(1): p. 20-36.

108. Foltin, M., G.J. Stueber, and E.R. Bernstein, *Dynamics of neutral cluster growth and cluster ion fragmentation for toluene/water, aniline/argon, and 4-fluorostyrene/argon clusters: Covariance mapping of the mass spectral data.* J. Chem. Phys., 1998. **109**(11): p. 4342-4360.

109. Douin, S., S. Piccirillo, and P. Brechignac, *Solvation of charge in aromatic/noble gas Van der Waals clusters.* Chem. Phys. Lett., 1997. **273**(5,6): p. 389-396.

110. Piccirillo, S., D. Consalvo, M. Coreno, A. Giardini-Guidoni, S. Douin, P. Parneix, and P. Brechignac, *Isomeric structures, van der Waals frequencies and spectral shifts of cold 4-fluorostyrene-(argon)$_n$ clusters (n = 1 to 4).* Chem. Phys., 1994. **187**(1-2): p. 97-106.

111. Piccirillo, S., M. Coreno, A. Giardini-Guidoni, G. Pizzella, M. Snels, and R. Teghil, *Spectroscopy of 4-fluorostyrene clusters.* J. Mol. Struct., 1993. **293**: p. 197-200.

112. Kendler, S. and Y. Haas, *A REMPI study of styrene and trans-b-methylstyrene clusters in a supersonic jet.* Chem. Phys. Lett., 1995. **236**(3): p. 324-35.

113. Sim, F., A. St. Amant, I. Papai, and D.R. Salahub, *Gaussian density functional calculations on hydrogen-bonded systems.* J. Am. Chem. Soc., 1992. **114**(11): p. 4391-400.

114. Wright, D. and M.S. El-Shall, *A Monte Carlo study of methanol clusters $(CH_3OH)_n$, n = 5-256.* J. Chem. Phys., 1996. **105**(24): p. 11199-11208.

115. Mo, O., M. Yanez, and J. Elguero, *Study of the methanol trimer potential energy surface.* J. Chem. Phys., 1997. **107**(9): p. 3592-3601.

116. Buck, U., J.-G. Siebers, and R.J. Wheatley, *Structure and vibrational spectra of methanol clusters from a new potential model.* J. Chem. Phys., 1998. **108**(1): p. 20-32.

117. Hagemeister, F.C., C.J. Gruenloh, and T.S. Zwier, *Density functional theory calculations of the structures, binding energies, and infrared spectra of methanol clusters.* J. Phys. Chem. A, 1998. **102**(1): p. 82-94.

118. Machi, S., J. Silverman, and D.J. Metz, *Radiation-induced polymerization of pure styrene at low temperature.* Proc. Tihany Symp. Radiat. Chem., 3rd, 1972. **1**: p. 573-88.

119. Gotoh, T., M. Yamamoto, and Y. Nishijima, *Radiation-induced cationic dimerization and polymerization of styrene in methylene chloride solution. I.* Journal of Polymer Science, Polymer Chemistry Edition, 1981. **19**(5): p. 1047-60.

120. Feng, W.Y. and C. Lifshitz, *The reactivity of neat and mixed proton-bound ethanol clusters.* Int. J. Mass Spectom. Ion Process., 1995. **149/150**: p. 13-25.

121. Johnston, L.J. and N.P. Schepp, *Reactivities of radical cations: characterization of styrene radical cations and measurements of their reactivity toward nucleophiles.* J. Am. Chem. Soc., 1993. **115**(15): p. 6564-71.

122. Brutschy, B., *Ion-molecule reactions within molecular clusters.* Chem. Rev., 1992. **92**(7): p. 1567-87.

123. Hush, N.S., *Distance dependence of electron transfer rates.* Coordination Chemistry Reviews, 1985. **64**: p. 135-57.

124. Castleman, A.W., Jr. and R.G. Keesee, *Ionic clusters.* Chem. Rev., 1986. **86**(3): p. 589-618.

VITA

Hatem A. Mahmoud was born on December 12, 1966, in Sohag, Egypt, and is an Egyptian citizen. He graduated from Al-Baliana High School, Sohag, Egypt in 1985. He received his Bachelor of Science in Chemistry from South Valley University, Sohag, Egypt in 1989. He received a Master of Science in Chemistry from South Valley University, Sohag, Egypt in 1995.